

The Gibbs Free Energy of mixing of natural silicate liquids; an expanded regular solution approximation for the calculation of magmatic intensive variables

Mark S. Ghiorso¹, Ian S.E. Carmichael², Mark L. Rivers², and Richard O. Sack^{2,3}

¹ Department of Geological Sciences, University of Washington, Seattle, WA, 98195 and the Lawrence Berkeley Laboratory, University of California, Berkeley, CA, 94720, USA

² Department of Geology and Geophysics and the Lawrence Berkeley Laboratory, University of California, Berkeley, CA, 94720, USA

Abstract. The compositions of liquids coexisting with experimentally grown crystals of olivine, plagioclase, clinopyroxene, orthopyroxene, leucite, spinel, rhombohedral oxide, melilite and potassium feldspar are used to define, through mass action expressions of liquid/solid equilibrium, compositional derivatives of the Gibbs free energy of mixing of naturally occurring silicate liquids as a function of temperature, pressure and the fugacity of oxygen. The available experimental data describe these derivatives over a range of compositions which includes basic magmas. Therefore, for silicate liquids in this composition range, the topology of the Gibbs free energy of mixing can be approximated from experimental determinations of its derivatives. The majority of the existing thermodynamic data on the liquid phase is consistent with the application of regular solution theory to model the free energy of mixing. Strictly symmetric, temperature and pressure independent, regular solution interaction parameters are calibrated from this phase equilibrium data using regression techniques which have their basis in inverse theory. These techniques generate numerically stable interaction parameters which incorporate inter-variable correlation and account for experimental uncertainty. The regular solution model fits the available data on anhydrous silicate liquids to within the accuracy of the thermodynamic database (± 550 cal). Extensions to regular solution theory allow water solubility in more silica rich liquids to be modelled somewhat less accurately (± 750 cal).

The topology of the excess free energy of mixing surface is strongly asymmetric, possessing a single multicomponent saddle point which defines a spinodal locus. Given this prediction of a multicomponent spinode, a mathematical procedure based upon minimisation of the Gibbs free energy of mixing is developed for the calculation of the compositions of coexisting immiscible liquids. Predicted binodal compositions substantially agree with elemental liquid/liquid partitioning trends observed in lavas. Calculations suggest that an immiscible dome, in temperature-composition space, intersects the liquidus field of the magma type tholeiite. Immiscible phenomena are predicted at sub-liquidus

temperatures for the bulk compositions of more basic or alkalic lavas, but are absent in more siliceous rock types for temperatures of the metastable liquid down to 900 K.

The regular solution model is used in four petrological applications. The first concerns a prediction of the *binary* olivine-liquid phase diagram. The calculated geometry exhibits a minimum near Fa_{75} , which, though not in accord with experimental results on the pseudobinary system, compares quite favorably with olivine-liquid phase equilibria interpreted from rhyolites, namely that the olivine phenocrysts of rhyolites are more iron rich than their coexisting liquids. The second petrological example concerns estimating the depth of the source regions of several basic lavas whose compositions cover a range from ugandite to basaltic andesite. The third application is a calculation of the saturation temperatures and compositions of plagioclase and olivine in four experimental basaltic liquids and a prediction of the liquidus temperatures and first phenocryst compositions of the Thingmuli lava series of Eastern Iceland. Lastly, enthalpies of fusion are computed for a variety of stoichiometric compounds of geologic interest. These demonstrate good agreement with calorimetrically measured quantities.

Introduction

Magmatic processes such as differentiation, assimilation and fractionation are fundamental concepts in the interpretation of the origin and cooling history of igneous rocks. The compositions of coexisting minerals and, in the case of volcanic rocks, glass, provide evidence for these phenomena, documenting changes in thermodynamic intensive variables (T, P and chemical potentials) as the rock crystallized and later cooled below the solidus. The interpretation of these compositional relationships is a complicated problem which petrologists have attempted to tackle in three ways: 1) simplification, through the use of phase diagrams, 2) experimentation, usually in the form of the determination of equilibrium phase relations in naturally occurring compositions, and 3) extrapolation and approximation using thermodynamic data and modelling.

The projection of multicomponent compositional

³ *Current address:* Department of Geosciences, Purdue University, West Lafayette, IN, 47907, USA

Offprint requests to: I.S.E. Carmichael

trends into two-, three- or four-component phase diagrams is an attempt to simplify igneous phase relations in such a manner that the salient concepts can be appreciated graphically. This visual approach comes at the expense of ignoring certain compositional variables, and as such phase diagrams cannot uniquely or completely interpret multicomponent compositional trends in igneous liquids.

Melting and crystal growth experiments on igneous rocks constitute a direct and purely empirical approach to the study of igneous phase relations. The basic data provided by these experiments suffers from one serious limitation; it pertains specifically to the narrow compositional space spanned by the rock types investigated. What is lacking in this approach is the ability to extrapolate to all igneous rocks the phase relations gleaned from a limited study of just a few. To do so one must know the physiochemical properties of the phases involved. In particular, the thermodynamic functions of the minerals of igneous rocks and the liquids from which they were derived must be characterized.

All attempts to quantitatively understand igneous phase relations incorporate efforts to describe the compositions of those solid and liquid phases which define the minimum total Gibbs free energy of the system at a particular temperature, pressure and bulk composition. It follows that efforts to numerically simulate equilibrium crystallization in igneous systems should, to a large degree, have a thermodynamic basis. This becomes evident when empirical or "statistical" approaches to computing mineral/melt equilibria are critically examined. For example, the multivariate linear regression approach taken by French (1971), Hostetler and Drake (1980) and French and Cameron (1981) adequately expresses certain mineral/melt equilibria, but fails to provide any insight into phenomena such as liquid immiscibility or the crystallization of a mineral phase not used in the calibration of their models. To be fair, these empirical procedures were not meant to provide such information, but a liquid/solid model which is thermodynamically based has the potential to make predictions considerably beyond its database. This is because the crystallization temperatures and liquidus compositions of all igneous minerals as well as the compositions of any coexisting immiscible liquids are all dependent upon the Gibbs free energy of the liquid. A thermodynamic formulation which is calibrated upon enough data to approximate the shape of the Gibbs free energy in temperature, pressure and composition space, has the potential to predict all the equilibrium properties of the system.

The most serious difficulty that has been encountered in defining a Gibbs free energy function for igneous systems concerns modelling the thermodynamic solution properties of natural silicate liquids. Microscopic approaches based upon statistical mechanical consideration of structural models involving cation association and polymerization (Toop and Samis 1962; Masson 1968; Hess 1971, 1980) have met with limited success, due primarily to the paucity and contradictory nature of the available data (see Bottinga et al. 1981 or Gaskell 1982 for a recent review). In addition, such models have been tested and calibrated on two- and three-component silica-metal oxide systems, and their

success in predicting the behavior of multicomponent natural silicate liquids is largely qualitative. Moreover, any structural or lattice model for the thermodynamic properties of the liquid makes certain assumptions about the extent of long range order in solution. Thus, "although lattice models have occasionally suggested forms of equations that were useful empirically for liquid systems, this empirical success did not establish the correctness of the model. Indeed, alternate models frequently lead to the same expression for a thermodynamic property of a complex liquid" (Pitzer 1981).

Macroscopic formulations of the Gibbs free energy of silicate liquids (Nicholls and Carmichael 1972; Barron 1972; Carmichael et al. 1977; Bottinga and Richet 1978; Mukherjee and Bhattacharya 1980; Barron 1981) have suffered from incomplete characterization of the thermodynamic properties of end-member components and compositionally restricted experimental data necessary to the definition of solution properties. Despite these limitations the work of Ghiorso and Carmichael (1980) has been quite successful in accounting for igneous phase relations involving olivine and plagioclase in basaltic liquids. This was due primarily to two factors: 1) The available experimental data on the thermodynamic properties of multicomponent silicate liquids (c.f. Carmichael et al. 1977; Nelson and Carmichael 1979), coupled with consideration of natural phenomena such as immiscibility, allowed the adoption of a very simple thermodynamic model for the liquid, and 2) The approach treated seventeen variables simultaneously and utilized twenty-one liquid component interactions in assessing olivine- and plagioclase-liquid phase relations as a function of T and P . In applying the regular solution model of Ghiorso and Carmichael (1980) however, several limitations have become apparent. Firstly, the model contains no mechanism for defining ferric/ferrous equilibria as a function of oxygen fugacity. Secondly, it was calibrated from a relatively small number of experimental data, which for the most part reflect phase relations in basalts. The calibration procedure was implemented by stepwise linear regression of the binary regular solution interaction parameters from mass action expressions describing four compositional derivatives of the free energy of mixing surface (i.e. $\text{CaAl}_2\text{Si}_2\text{O}_8$, $\text{NaAlSi}_3\text{O}_8$, Mg_2SiO_4 and Fe_2SiO_4). Subsequent computations have revealed that this least squares technique is not the best method of accounting for correlations between the interaction parameters, since the inherent numerical instability in the parameter values distorts the actual shape of the free energy of mixing surface. Thus compositional derivatives in directions other than those used for calibration may be incorrectly computed. In petrological terms this means that phase relations for minerals other than olivine and plagioclase in basalts and mineral stabilities in non-basaltic liquids, as well as compositions of coexisting immiscible liquids, may not be correctly predicted by the Ghiorso and Carmichael (1980) model.

The purpose of the present paper is to expand the scope of the thermodynamic model of Ghiorso and Carmichael (1980) to 1) cover a much broader compositional range of silicate liquids, essentially including all basic lavas, 2) utilize as many phases as possible in

calibrating the free energy of mixing surface – thereby more accurately describing its topology, 3) perform this calculation using regression techniques which explicitly account for parameter correlation and generate values for these parameters which are numerically stable to minor perturbations in the database, 4) utilize the empirical expressions of Sack et al. (1981) to account for ferrous/ferric equilibria as a function of oxygen fugacity and 5) demonstrate these improvements by calculating liquid immiscibility and phase stabilities of clino- and orthopyroxenes, olivines and plagioclases in lavas of widely varying composition.

It is not our intention to produce a comprehensive model for silicate liquids that is capable of calculating the thermodynamic properties of all intermediate compositions from the simple two-component systems to that of basalt. We are concerned here with approximating the Gibbs free energy surface only in that small fraction of the total compositional volume occupied by naturally occurring liquids. It is a simple matter to calculate just how restricted this volume fraction is. If we consider the eleven oxides which describe the major element compositions of igneous rocks¹ and recast bulk wt. % analyses into mole fractions of these oxides, the volume fraction which natural liquids occupy in this eleven component space is on the order of 10^{-10} . Now a great deal of experimental data are available within this restricted “natural liquid” volume as is the case for many of the two- or three-component constituent sub-systems, but certainly phase diagrams for all 55 binaries have not been determined let alone all 165 ternaries. It might be argued that the appropriate petrological simple phase diagrams have been determined for this space, however the relevance of the equilibrium relations gleaned from a study of these simple systems is uncertain. One need only consider the dissimilarity of the phase relations depicted in the system $\text{NaAlSi}_3\text{O}_8 - \text{CaAl}_2\text{Si}_2\text{O}_8$ compared with plagioclase liquid relations found in synthetic liquids saturated with diopside and plagioclase (Morse 1980, p.93) or plagioclase liquid relations derived from experiments on basaltic liquids, to recognise this discrepancy. Alternatively, the phase relations in the system $\text{Mg}_2\text{SiO}_4 - \text{Fe}_2\text{SiO}_4$ predict that all olivines should be more Mg-rich (higher $\text{Mg}/(\text{Mg}+\text{Fe})$ ratio) than the liquids from which they crystallize, but the exact opposite is observed in studying the fayalitic olivines of rhyolitic liquids (Carmichael 1967a). Unfortunately, there is a compositional gulf in the experimental data on silicate liquids which lies between simple systems and magmas, across which the thermodynamic properties of the liquid change in interesting and mysterious ways. A thermodynamic model for the liquid that successfully reproduces the phase relations in the simple systems as well as magmas must bridge this gulf, and in our opinion, would probably be very complex. However, it is our contention that much simpler formulations may be applicable over sufficiently small fractions of the total composition space, much in the same way that the shape of a complex curve can be locally approximated by a simple polynomial. In the next section we will produce arguments

to justify this contention for that portion of the total composition space occupied by natural silicate liquids. We remark finally that as our interest in the thermodynamic properties of silicate liquids is motivated by petrological problems, we have confined our attention to experimental phase relations in multicomponent, natural silicate liquids with the aim of restricting the applicability of our thermodynamic modelling to magmas.

Basic thermodynamic expressions

The total Gibbs free energy, G , of a heterogeneous mixture of solid and liquid phases, say coexisting phenocrysts and silicate liquid, can be written:

$$G = G^{(\text{liquid})} + G^{(\text{solid})} \quad (1)$$

where $G^{(\text{liquid})}$ represents the Gibbs free energy of the liquid and $G^{(\text{solid})}$ that of the solid. Specifying n thermodynamic components indexed on i and symbolized by n_i to describe the composition of the liquid, we may write:

$$G^{(\text{liquid})} = \sum_{i=1}^n \mu_i^0 n_i + G^{\text{mix}} \quad (2)$$

where μ_i^0 is the standard state chemical potential of the i th component and G^{mix} is the Gibbs free energy of mixing in the liquid relative to the standard state. The standard state convention is chosen here to be unit activity for all pure substances at any temperature and pressure. As we have indicated in the introduction the crux of the problem is to find an expression for G^{mix} . G^{mix} can be written:

$$G^{\text{mix}} = G^{\text{ideal}} + G^{\text{excess}} \quad (3)$$

where from elementary solution theory we have

$$G^{\text{ideal}} = NRT \sum_{i=1}^n X_i \ln X_i. \quad (4)$$

Here N is the sum of all n_i , R is the universal gas constant, T the absolute temperature and X_i denotes component mole fractions ($X_i = n_i/N$). From Eqs. (3) and (4) we may write

$$\begin{aligned} V^{\text{mix}} &= \left(\frac{\partial G^{\text{mix}}}{\partial P} \right)_{T, \text{composition}} \\ &= \left(\frac{\partial G^{\text{excess}}}{\partial P} \right)_{T, \text{composition}} \end{aligned} \quad (5)$$

where V^{mix} is the volume of mixing in the liquid and

$$\begin{aligned} C_P^{\text{mix}} &= -T \left(\frac{\partial^2 G^{\text{mix}}}{\partial T^2} \right)_{P, \text{composition}} \\ &= -T \left(\frac{\partial^2 G^{\text{excess}}}{\partial T^2} \right)_{P, \text{composition}} \end{aligned} \quad (6)$$

where C_P^{mix} is the heat capacity of mixing in the liquid. As was discussed at some length in our previous paper (Ghiorso and Carmichael 1980) there exists no experimental data on anhydrous silicate liquids of the range

¹ SiO_2 , TiO_2 , Al_2O_3 , Fe_2O_3 , FeO , MnO , MgO , CaO , Na_2O , K_2O , P_2O_5

in composition found in nature which indicates, within an estimated average two percent experimental uncertainty, finite values for V^{mix} and C_P^{mix} .² As far as V^{mix} is concerned this statement can be extended to synthetic two- and three-component systems (Ghiorso and Carmichael, in press) and multicomponent liquids containing substantial ferric iron and aluminum (Mo et al. 1982) as well. Thus G^{excess} must be pressure independent and any excess entropy of mixing must be temperature and pressure independent [i.e. $-(\partial G^{\text{excess}}/\partial T)_{P, \text{composition}} = \text{constant}$]. The simplest form for G^{excess} consistent with these boundary conditions is to set it equal to zero, which is an attempt to describe silicate liquids as ideal solutions. Phenomena such as liquid immiscibility and non-zero heats of mixing (c.f. Weill et al. 1980) however, necessitate a compositional dependence of G^{excess} since these phenomena are generated by non-ideal undulations in the total free energy of mixing surface for the liquid. A simple mathematical form for G^{excess} which is consistent with the available experimental data (Ghiorso and Carmichael 1980) is that of a regular solution. We may define:

$$G^{\text{excess}} = N \frac{1}{2} \sum_{i=1}^n \sum_{j=1}^n W_{ij} X_i X_j \quad (7)$$

where the W_{ij} are temperature/pressure independent binary component interaction parameters which are symmetric ($W_{ij} = W_{ji}$) and describe attractive or repulsive forces between unlike molecules ($W_{ii} = 0$).³ The $\frac{1}{2}$ in Eq. (7) insures that the energy attributed to the interaction of each component pair is counted only once in the sum. Thus from Eqs. (2), (3), (4) and (7) we have

$$G^{(\text{liquid})} = \sum_{i=1}^n \mu_i^0 n_i + NRT \sum_{i=1}^n X_i \ln X_i + N/2 \sum_{i=1}^n \sum_{j=1}^n W_{ij} X_i X_j. \quad (8)$$

Since

$$\left(\frac{\partial G^{(\text{liquid})}}{\partial n_i} \right)_{T, P, n_j} = \mu_i = \mu_i^0 + RT \ln a_i \quad (9)$$

where a_i is the activity of the i th component in the liquid, from Eq. (8) we obtain

$$\left(\frac{\partial G^{(\text{liquid})}}{\partial n_i} \right)_{T, P, n_j} = \mu_i^0 + RT \ln X_i + \sum_{j=1}^n W_{ij} X_j - \frac{1}{2} \sum_{j=1}^n \sum_{k=1}^n W_{jk} X_j X_k$$

2 It should be emphasized that these measurements have been done at 1 bar. C_P^{mix} and V^{mix} may not be zero at elevated pressures

3 Equation (7) contains only binary interaction parameters. Ternary and higher order interactions may also be specified as long as all are independent of temperature and pressure (i.e. V^{mix} and C_P^{mix} are still zero). The number of unknowns (W 's) in the expression for G^{excess} rapidly increases as the higher order terms are added however (number = $n! / [(n - \text{terms})!]$), and in most practical applications, the data necessary to define them is lacking. We will show later that this is the case for silicate liquids

so that with $a_i \equiv X_i \gamma_i$,

$$RT \ln a_i = RT \ln X_i + RT \ln \gamma_i$$

and

$$RT \ln \gamma_i = \sum_{j=1}^n W_{ij} X_j - \frac{1}{2} \sum_{j=1}^n \sum_{k=1}^n W_{jk} X_j X_k. \quad (10)$$

γ_i is the activity coefficient of the i th component and $RT \ln \gamma_i$ is the partial molar excess free energy of the i th component. In addition we can state the following equations, obtained by taking appropriate derivatives of Eq. (8), for the partial molar entropy (\bar{s}_i), volume (\bar{v}_i), enthalpy (\bar{h}_i) and heat capacity ($\bar{c}_{P,i}$) all consistent with Eq. (7):

$$S^{(\text{liquid})} = - \left(\frac{\partial G^{(\text{liquid})}}{\partial T} \right)_{P, \text{composition}} = \sum_{i=1}^n \bar{s}_i n_i = \sum_{i=1}^n \bar{s}_i^0 n_i - NR \sum_{i=1}^n X_i \ln X_i, \quad (11)$$

$$V^{(\text{liquid})} = \left(\frac{\partial G^{(\text{liquid})}}{\partial P} \right)_{T, \text{composition}} = \sum_{i=1}^n \bar{v}_i n_i = \sum_{i=1}^n \bar{v}_i^0 n_i, \quad (12)$$

$$H^{(\text{liquid})} = G^{(\text{liquid})} + TS^{(\text{liquid})} = \sum_{i=1}^n \bar{h}_i n_i = \sum_{i=1}^n \bar{h}_i^0 n_i + N/2 \sum_{i=1}^n \sum_{j=1}^n W_{ij} X_i X_j, \quad (13)$$

and

$$C_P^{(\text{liquid})} = \left(\frac{\partial H^{(\text{liquid})}}{\partial T} \right)_{P, \text{composition}} = \sum_{i=1}^n \bar{c}_{P,i} n_i = \sum_{i=1}^n \bar{c}_{P,i}^0 n_i. \quad (14)$$

Having postulated a mathematical model for $G^{(\text{liquid})}$ we must now specify a means of calibrating it using available thermodynamic data and experimental measurements on the compositions of coexisting solid/liquid pairs. To see how this may be done let us consider a mineral, M , which coexists with a silicate liquid. M may be an end-member component of a solid solution series or a pure mineral. One can write the equilibrium reaction:



where C_i are the actual components which describe the liquid's composition and the v_i 's are the stoichiometric numbers of each of these components in the mineral formula. The mass action expression corresponding to Eq. (15) is given by

$$RT \ln K = \sum_{i=1}^n v_i RT \ln a_i^{(\text{liquid})} - RT \ln a_M^{(\text{solid})} \quad (16)$$

where K denotes an equilibrium constant and $a_j^{(\text{liquid}, \text{solid})}$ the activity of the j th component in the

liquid or the activity of M in the solid, respectively. Equation (16) can be rearranged and combined with Eq. (10) to yield:

$$RT \ln K + RT \ln a_M^{(\text{solid})} - \sum_{i=1}^n v_i RT \ln X_i = \sum_{i=1}^n v_i \sum_{j=1}^n W_{ij} X_j - \frac{1}{2} \sum_{i=1}^n v_i \sum_{j=1}^n \sum_{k=1}^n W_{jk} X_j X_k. \quad (17)$$

Equation (17) is only valid in so far as regular solution theory describes the excess free energy of the liquid. This has not been experimentally established for silicate melts containing water. In Appendix 3 we review the experimental data on water solubility in silicate melts and postulate an extended form of Eq. (17), Eqs. (A3-15) and (A3-16), applicable to hydrous liquids.

The quantities on the left hand side of Eq. (17) can be calculated from the compositions of coexisting solids and liquids equilibrated at a given temperature and pressure. It should be noted that each end-member component in each solid-solution phase that coexists with the liquid at a given T and P will give rise to one statement of Eq. (17). We shall refer to these measurements of solid/liquid equilibria as the experimental database. Its construction and scope will be discussed in some detail below. In addition, to calculate a specific $RT \ln K$ we must know the standard state chemical potential of M and those of the appropriate liquid components at the temperature and pressure of interest, since

$$RT \ln K = \mu_M^0 - \sum_{i=1}^n v_i \mu_i^0. \quad (18)$$

The construction of the thermodynamic database which allows the evaluation of Eq. (18) at appropriate P 's and T 's is discussed below and in Appendix 1. The evaluation of $RT \ln a_M^{(\text{solid})}$ requires knowledge of activity/composition relations within solid phases of experimental interest (plagioclases, olivines, pyroxenes, etc.). Such relations are mentioned below and discussed in some detail in Appendix 2. Finally, to specify the various X_i 's

some decision must be made concerning the choice of thermodynamic components. Given that the necessary data can be assembled the only unknowns which remain in Eq. (17) are the regular solution binary interaction parameters, the W_{jk} 's. Given a sufficiently large "experimental database" which is to say a sufficiently large number of statements of Eq. (17), the values of the W_{ij} become overdetermined and may be approximated by some numerical procedure such as least squares. The details of the calibration of the W_{ij} 's in Eq. (17) are discussed in Appendix 4. The important aspect to keep in mind is that they are defined from experimental data on coexisting solid/liquid pairs. Once calibrated, these interaction parameters describe, through Eqs. (3), (4) and (7) the free energy of mixing. This G^{mix} is a *local* approximation to the experimental database and is consistent with the available solid/liquid thermodynamic data. The calibration defines the shape of a multidimensional (multicomponent) hypersurface by specifying as many determinations of the derivatives (through Eq. 17) of this surface as possible. Once this hypersurface is defined its undulations can be used to predict liquid immiscibility and, when combined with thermodynamic data for the solids, mineral stabilities as a function of temperature and pressure. We proceed now to a more detailed discussion of the construction of the "experimental database" and other thermodynamic quantities necessary for the evaluation of Eq. (17).

Experimental database

The experimental database used to calibrate the interaction parameters (W_{ij}) through Eq. (17) is indicated in Tables 1 through 3. Table 1 consists entirely of references to data from the literature and substantially includes the original olivine-liquid, plagioclase-liquid anhydrous database of Ghiorso and Carmichael (1980). We have indicated in Table 1 the pressure and temperature range of the data as well as the number of cases or statements of mineral-solution equilibria (Eq. 17)

Table 1.

Anhydrous Data	Number in each category													
	Experiment	P (kbars)	T (K)	Cases	pl	ol	opx	cpx	sp	lc	rhm	mel	ksp	qtz
Bender et al. 1978 (MORB)	0.001	1,478–1,541	34	5	12									
	8–15	1,513–1,613	18	2	6	1								
Carmichael 1960 (Rhyolite)	2	1,223	1				1							
Carmichael 1962 (Pantellerite)	3	1,198	1			1	1							
Grove et al. 1982 (Basaltic Andesite)	0.001	1,332–1,619	197	45	38	8	1							
Leeman 1974 (Basalt)	0.001	1,344–1,623	42	8	13									
Roeder 1974 (Basalt)	0.001	1,427–1,579	32		16									
Stolper 1980 (Tholeiite)	10–20	1,523–1,723	38	1	8	5								
Takahashi 1980 (Alkali-Olivine Basalt)	14	1,543–1,548	16		2	3								
Thompson 1974, 1975 (Basalt)	8–12	1,398–1,498	14		7									
Walker et al. 1979 (MORB)	0.001	1,379–1,498	44	14	8									
Total (including Table 2)			1,168	123	215	21	84	61	42	8	2	1		

Table 2. Analyses of lavas used for solid-liquid experiments by Sack. The phases encountered (without temperature or composition

T K	Leucite basanite (Vesuvius)		Basanite (Colima)		Andesite (Colima)	Basanite (San Quintin)	High alumina basalt	Trachy-basalt	Leucite basanite (Korath Range)			Alkali olivine basalt		Ugandite			
	94-8	94-18	501	7E	Col-11	CSQ-3	HC-63	253	K-8	K-15	K-14	SSC-1	SSC-2	U-50	U-105	U-111	U-150
	1,433	1,389–1,418	1,365.5–1,574	1,337–1,603	1,418–1,476	1,365.5–1,543	1,410–1,508	1,406–1,508	1,365.5–1,507			1,365.5–1,507		1,394–1,507			
SiO ₂	47.84	48.16	49.48	48.20	56.55	46.58	48.46	47.41	43.52	48.50	45.51	45.81	45.70	40.52	36.71	43.48	39.43
TiO ₂	1.24	0.98	1.60	1.64	0.78	2.41	1.07	2.13	2.45	1.49	2.10	2.44	1.98	5.28	5.54	4.50	4.73
Al ₂ O ₃	17.90	15.20	13.51	11.62	16.63	15.08	17.39	15.78	15.76	18.86	16.93	15.01	13.59	8.17	9.30	9.75	8.07
Fe ₂ O ₃	1.88	3.03	2.84	4.22	1.46	2.09	1.76	2.18	2.82	2.78	2.30	2.13	2.68	6.33	9.44	8.64	10.09
FeO	6.21	4.56	5.36	3.27	5.23	8.60	7.97	7.87	7.14	5.74	6.43	8.83	7.29	6.29	4.24	3.78	2.04
MnO	0.17	0.14	0.15	0.11	0.11	0.19	0.18	0.18	0.16	0.22	0.19	0.10	0.18	0.21	0.26	0.16	0.22
MgO	3.87	6.34	9.80	11.81	5.94	9.42	8.64	8.04	9.57	3.28	7.06	8.33	11.45	11.57	6.34	8.83	9.52
CaO	8.68	11.37	9.07	8.32	7.75	8.86	11.10	8.75	12.28	8.26	10.72	11.75	12.42	12.55	14.08	11.81	13.97
Na ₂ O	2.78	2.23	2.97	3.28	4.03	3.42	2.80	3.73	3.02	5.85	4.09	3.01	2.74	2.50	2.40	2.86	1.16
K ₂ O	7.43	5.94	3.69	3.58	1.06	1.51	0.22	1.72	1.43	3.01	2.18	1.04	1.05	3.75	6.05	4.65	6.44
P ₂ O ₅	0.92	0.78	0.99	1.32	0.20	0.52	0.12	0.55	0.41	0.45	0.48	0.65	0.39	0.44	1.11	0.66	0.86
H ₂ O ⁺	0.43	0.45	0.45	1.59	0.15	0.35	0.07	0.58	0.83	0.81	1.13	0.41	0.37	1.31	1.82	0.23	1.11
H ₂ O ⁻	0.02	0.05	0.29	0.37	0.05	0.04	0.08	0.28	0.24	0.16	0.22	0.07	0.03	0.40	0.42	0.17	1.08
Rest	0.61	0.67				0.33		0.10	0.09	0.11	0.35			0.41	1.30	0.69	0.78
Total	99.98	100.00	100.20	99.33	99.94	99.40	99.86	100.30	99.72	99.52	99.69	99.58	99.87	99.73	99.60	100.21	99.49
(experiments/cases)	(2/7)	(5/37)	(14/35)	(9/37)	(5/18)	(10/42)	(4/10)	(6/26)		(13/92)		(7/40)			(20/131)		
Phases found with liquid (number)	Oliv (2)	Oliv (5)	Oliv (12)	Oliv (9)	Oliv (5)	Oliv (10)	Oliv (2)	Oliv (6)		Oliv (14)		Oliv (6)			Oliv (16)		
		Plag (5)	Plag (3)		Plag (2)	Plag (5)	Plag (1)	Plag (5)		Plag (10)		Plag (5)					
	Spin (1)	Spin (1)	Spin (1)	Spin (3)		Spin (2)	Spin (1)	Spin (1)		Spin (8)		Spin (4)			Spin (17)		
	Leuc (2)	Leuc (11)	Leuc (2)	Leuc (1)											Leuc (11)		
		Cpx (1)	Cpx (1)	Cpx (1)		Cpx (1)	Cpx (1)			Cpx (9)		Cpx (1)			Cpx (21)		
					Opx (1)												
						Ilm (2)		Ilm (1)									
					Kspar (1)												

they generated and how these were distributed amongst the mineral phases found in each experiment. A critical variable that dictated inclusion in the database was knowledge of the fugacity of oxygen, since all bulk liquid analyses were corrected to have the appropriate ferrous/ferric ratio at the temperature of interest using the equations of Sack et al. (1981). Thus the experimental work of Green et al. (1979) and Drake (1972)⁴ was excluded; in addition the absence of alkali determinations on some lunar liquids (Longhi et al. 1978) and the large uncertainty in Na₂O concentration (Mysen and Kushiro 1977) eliminated others. Liquids which

were doped with CoO and NiO (Takahashi 1978) were also excluded, as the high concentrations of Co₂SiO₄ and Ni₂SiO₄ in the associated olivines precluded the use of the activity/composition relations adopted for the Fe₂SiO₄ and Mg₂SiO₄ olivine components (see Appendix 2). To those data of Ghiorso and Carmichael remaining have been added the more recent work of Grove et al. (1982), Stolper (1980) and Takahashi (1980). We have also rejected all experimental results at oxygen fugacities substantially higher than the hematite-magnetite buffer.

What was characteristic of the Ghiorso and Carmichael (1980) database and is still true of the experiments indicated in Table 1, is that the liquids represented are essentially basaltic. In the need to expand

⁴ Drake's (1972) experiments in the Fe absent simple system Ab–An–Di were not considered

of solid-liquid) are also listed for each bulk composition

Leucite melilite (Congo)		Nephelinite (Congo)	Etindite (Cameroun, West Africa)	Melilite leucitite	Melilite leucitite (Rome)	Tholeiite (FAMOUS)	Tholeiite (Puerto Rico Trench)	Tholeiite (Whin sill)	Andesite		Totals
20424	20421	RG69010	X-973	96-6	90-05	FG	PRT	WS	766-70	X23	
1,337-1,474		1,389- 1,474	1,365.5- 1,422	1,394- 1,566	1,474- 1,603	1,410- 1,543	1,365.5- 1,476	1,365.5- 1,418	1,574	1,398	
35.32	46.91	39.31	38.76	42.80	54.47	48.45	52.48	51.73	65.67		
2.68	1.10	2.51	4.42	0.96	0.53	0.75	2.18	2.49	0.42		
12.31	20.91	17.46	13.96	15.36	20.73	15.30	15.92	13.82	17.52		
8.81	2.99	1.35	5.97	4.61	2.28	1.28	1.54	2.04	1.14		
2.78	3.26	9.37	6.34	3.97	1.46	9.00	8.55	10.49	2.05		
0.34	0.20	0.26	0.27	0.18	0.19	0.16	0.09	0.21	0.06		
5.13	1.28	3.55	5.88	4.34	0.74	10.25	6.85	5.67	1.96		
16.13	4.33	10.40	14.08	12.22	3.24	11.82	7.43	9.51	5.38		
4.65	6.90	6.75	4.42	2.84	4.37	2.24	4.25	2.65	4.52		
4.43	9.15	6.56	2.55	9.79	10.18	0.26	0.73	0.96	1.12		
1.63	0.41	1.18	1.22	0.48	0.13	0.16	0.24	0.32	0.11		
1.47	0.86	0.30	0.74	1.78	0.43				0.00		
0.33	0.30		0.16	0.17	0.35				0.03		
3.75	1.05	0.88	0.77	0.68	0.68	0.06	0.06	0.06			
99.76	99.65	99.88	99.54	100.17	99.78	99.73	100.33	99.97	99.98		
	(9/69)	(3/39)	(5/34)	(6/23)	(4/4)	(5/20)	(6/28)	(6/34)	(1/2)	(1/6)	(734)
						Oliv (5)	Oliv (6)	Oliv (6)		Oliv (1)	Oliv (105)
			Plag (1)			Plag (2)	Plag (4)	Plag (4)	Plag (1)		Plag (48)
	Spin (7)	Spin (6)	Spin (3)	Spin (3)			Spin (1)	Spin (2)			Spin (61)
	Leuc (5)	Leuc (1)		Leuc (5)	Leuc (4)						Leuc (42)
	Cpx (17)	Cpx (7)	Cpx (10)	Cpx (5)		Cpx (2)		Cpx (4)			Cpx (81)
										Opx (2)	Opx (3)
						Ilm (1)	Ilm (3)	Ilm (1)			Ilm (8)
	Melil (2)										Kspar (1)
											Melil (2)

the composition range to include other basic lavas and andesites one of us (Sack) has performed platinum-loop melting experiments at controlled oxygen fugacity (close to QFM) and 1 bar over a range of temperatures on the liquids whose bulk compositions are listed in Table 2 (see Sack in prep., 1982a, 1982b for details). In Table 2 we have also provided a summary of the experimental liquidus relations, including the number of solid/liquid equilibria for each mineral/rock type and the total number for each phase. It is important to realize that these experimental results were obtained under anhydrous conditions as were those taken from the literature (Table 1). Though comprising a large dataset, generating 1,168 statements of Eq.(17) involving the mineral phases plagioclase, olivine, orthopyroxene, cli-

nopyroxene, spinel, leucite, hematite-ilmenite (rhombohedral oxides), melilite and potassium feldspar, they suffer from this limitation. Thus we have compiled additional experimental results from the sources listed in Table 3 on the compositions of coexisting solids and liquids in hydrous silicate melts; as well as the solubility of water in natural basaltic, andesitic and granitic liquids. Some data from natural rhyolites is also indicated. The hydrous liquid data of Table 3 will serve to constrain derivatives (solubilities of water) of the hydrous free energy of mixing surface. These derivatives will be defined through equations like Eq.(17) that are developed in Appendix 3. Conspicuously missing from Table 3 is the experimental work of Helz (1973, 1976) which was excluded because of the uncertainties as-

Table 3.

Hydrous Data			Number in each category										
Experiment	<i>P</i> (kbars)	<i>T</i> (K)	Cases	pl	ol	opx	cpx	sp	lc	rhm	mel	ksp	qtz
Eggler 1972 (Andesite)	1	1,303	6		1	1							
Hildreth 1978 (Rhyolite)	1.5–2.5	998–1,070	56	6		4	4	6		6			6
Burnham and Jahns 1962 (Pegmatite)	1–5	943–1,173	6	} water solubility									
Khitarov et al. 1959 (Granite)	1–3	1,173–1,273	5										
Khitarov and Kadik 1973 (Granite)	2–5	1,473	3										
Oxtoby and Hamilton 1978 (Granite)	0.5–3	1,373	4										
Total			80	6	1	5	4	6		6			6

sociated with the concentrations of both H₂O and the alkalis in her experimental liquids.

Activity composition relations

Solids

The numerical evaluation of Eq. (17) requires the calculation of $RT \ln K$ and $RT \ln a_M^{(solid)}$ for a particular mineral species or solid-solution end member, *M*. This implies that adequate thermodynamic data exist for *M* and that activity composition relations for the solid phase have been defined. These quantities are discussed and tabulated in Appendices 1 and 2, where we have endeavored to treat as completely as possible all solid phases identified in the experimental work (Tables 1, 2 and 3).

In olivines the tephroite (Mn₂SiO₄) component was excluded since a value for its activity coefficient could not be stated that was consistent with the activity coefficient model for the solid solution Fe₂SiO₄–Mg₂SiO₄ (Wood and Kleppa 1981). The same argument applies to the trace element components (such as MnSiO₃) in orthopyroxene, trace element, Al and Ti bearing components in clinopyroxene, the NaAlSi₂O₆ component of leucite and all end-member components of nepheline. The Sr and Ba components of plagioclase, though acceptably modelled as ideal diluents in the solid, were not included as statements of Eq. (17) due to insufficient and imprecise compositional data on the coexisting liquids. For this reason we have also neglected equilibria involving trace element components of alkali-feldspar, the Cr⁺³ bearing components of the spinels and other Fe–Ti oxides not listed in Appendix 1. Mineral components involving Fe⁺³ were not treated (with the exception of the Fe₃O₄ component of spinel coexisting with the hydrous liquids) due to the high relative uncertainties associated with the calculated value of the ferric iron component in the liquids (see below). In addition, as the melillites encountered in this study were substantially akermanitic, equilibria involving the gehlenite component were not computed. Further criteria employed in generating statements of Eq. (17) for purposes of parameter calibration are discussed in Appendix 4.

Liquids

As we have already postulated a mathematical form for the solution properties of natural silicate liquids (Eq. 8)

our task here is to select a suitable way of expressing their composition in terms of thermodynamic components. The problems associated with choosing components for silicate liquids have already been discussed in some detail (see Nicholls 1976, Carmichael et al. 1977, Ghiorso and Carmichael 1980). They are three fold: 1) such components must span the composition space defined by natural liquids; preferably the quantity of each should be positive in this space, 2) adequate thermodynamic data must exist to describe the chemical potential of each pure liquid component over the *T, P* range of interest, and 3) they must preserve, by a suitable linear transformation, the ideal mixing behavior discussed above and identified by Eqs. (5) (volume) and (6) (heat capacity). In addition, it would be most desirable if components could be chosen that successfully described the configurational entropy of the liquid. This would, of course, necessitate knowing the stoichiometry of the actual molecules and polymeric units which form in these liquids as a function of *T, P* and composition. The desirability of properly modelling the configurational entropy arises from our need to approximate the local shape of G^{mix} in the compositional range of natural liquids. If the configurational free energy is improperly modelled, the excess free energy (i.e. the *W*'s of Eq. 7), will adjust itself to reflect the experimentally inferred G^{mix} . Thus, if the interaction parameters are to have physical meaning, accounting solely for real excess enthalpy terms, then the molecular species which actually interact should be chosen as components.

This discussion can be illustrated with the following calculation. Let us consider equilibria in the system NaAlSi₃O₈–CaAl₂Si₂O₈–CaMgSi₂O₆. Weill et al. (1980) have developed an expression for the free energy of mixing in this system that accurately reproduces the phase diagram and the measured thermodynamic properties of the liquid. Their expression involves a two-lattice model to approximate the configurational entropy. Suppose we limit our discussion to the crystallization of haplobasaltic liquids in this ternary and consider the values of the configurational entropy along the cotectic between Di_{47.5} and Di₂₃. If we abandon Weill et al.'s (1980) configurational term and model the entropy as the ideal mixing of the components CaMgSi₂O₆–NaAlSi₃O₈–CaAl₂Si₂O₈ in the liquid, the difference between $G^{configurational}$ and G^{ideal} can be fitted to an equation for G^{excess} of the correct form for a

regular solution⁵ with a standard error of ± 23 cal. Now if Weill et al.'s (1980) configurational entropy for Diopside-Anorthite-Albite is correct, the interaction parameters of G^{excess} that we obtained are little more than fit parameters – they do not really describe the microscopic energetics of the liquid nor are they applicable to calculations in the binaries. On the other hand, these parameters do reproduce G^{mix} along the haplobasaltic cotectic. It could be argued that if one's interests are confined to just this portion of the phase diagram (the region of petrologic interest) either approach to modeling G^{mix} is valid.

In selecting components to describe the compositions of naturally occurring silicate liquids we are faced with the task of merging the available data on the structures of these liquids with the macroscopic thermodynamic observations that led to our choice of regular solution theory to model the G^{excess} . Researchers interested in modelling phase diagrams (Hon et al. 1981) or applying polymer theory to silicate melts (Toop and Samis 1962; Masson 1968; Hess 1971, 1980) have often described silicate liquids in terms of lattice models where mixing occurs on framework and interstitial sites or in terms of mixing of various polymeric units of different molecular weight. Nesbitt and Fleet (1981) have shown that for the system $\text{PbO} - \text{SiO}_2$ the molecular units PbO , SiO_2 and Pb_2SiO_4 mix ideally, a result which they argue is consistent with predictions made by the model of Toop and Samis (1962). Using these three species alone Nesbitt and Fleet (1981) are able to reproduce the available thermochemical, conductivity and density data for the binary. The formation of the Pb_2SiO_4 complex in this system is consistent with Masson's (1968) contention that "the ion SiO_4^{4-} is the most abundant single species of discrete silicate ion at all silica contents". Other "common" silicate melt species have been suggested by Mysen et al. (1982) in a recent summary of the structures of silicate glasses. They conclude "that the anionic network in natural magma can generally be described in terms of chain, sheet, and three dimensional network structures", consisting of molecular units containing SiO_3^- , Si_2O_5^- , and SiO_2 or their aluminum bearing equivalents. The Knudsen cell activity measurements of Rammensee and Fraser (1982) substantiate Mysen et al.'s claim in that these authors find network like structures ($\text{NaAlSi}_3\text{O}_8$, KAlSi_3O_8 , KAlSi_2O_6 and SiO_2) in the molten system $\text{NaAlSi}_3\text{O}_8 - \text{KAlSi}_3\text{O}_8$. With regard to these network species, it has long been Burnham's contention that feldspar like molecules exhibit ideal mixing in the system Albite-Anorthite-Potassium feldspar- H_2O (Burnham 1974, 1975a, 1975b, 1979). In a summary of the properties of multicomponent aluminosilicate melts involving the feldspar liquids, water and silica, Burnham (1981) expands the list of melt species to 19, each having a stoichiometry related to some solid phase which precipitates from the system. These include network, sheet and chain units.

⁵ $G^{\text{excess}} = -522 X_{\text{An}} X_{\text{Di}} - 6,615 X_{\text{Di}} X_{\text{Ab}} + 1,966 X_{\text{An}} X_{\text{Ab}}$. Barron (1972) has shown that the entire phase diagram $\text{Di} - \text{An} - \text{Ab}$ as well as Quartz-Fayalite-Leucite and the granite system can essentially be approximated using an ideal entropy and regular solution theory for the excess free energy

In the system Albite-Anorthite-Forsterite- H_2O , Burnham (1981) postulates the presence of network, chain and orthosilicate units.

A fairly safe conclusion to draw from most of the above mentioned structural studies of both simple and complex silicate liquids (and their quenched glasses) is that the molecular species present are probably fairly simple. With this in mind we have chosen the molecular units listed in Table 4 as components to describe the compositions of natural silicate liquids. This set is an expanded version of the "stoichiometric mineral" components used by Ghiorso and Carmichael (1980) and is meant to be applied to all natural silicate liquids, not just to those that are met-aluminous. The reader will notice that this set consists mostly of stoichiometric units related to network, orthosilicate and chain type structures. We have placed the anhydrous molecules on an 8-oxygen basis because it was found that the melt species so defined were most compatible with the regular solution form of G^{excess} (Eq. 7), generating the smallest residuals of Eq. (17) following regression of the experimental database. These components are used to compute the ideal free energy of mixing and approximate the configurational free energy of the liquid. It should be borne in mind that the selection of these components was also dictated by the availability of adequate thermodynamic data for the pure liquids (Appendix 2) such that a minimum of estimation and uncertainty is associated with the given thermodynamic constants.

Calibration of the interaction parameters

The numerical procedures used to calibrate the regular solution interaction parameters of Eq. (7) to the combined experimental and thermodynamic (Appendix 2) database are discussed in some detail in Appendix 4. These techniques are mainly based upon generalized matrix inverse theory and have been developed to take into account estimated uncertainties in the data. Values of the interaction parameters so calibrated may be found in Table A4-3. Though there are 45 anhydrous interaction parameters listed, these constitute linear combinations of only 26 independent coefficients determined by least squares analysis. Thus the "real" number of variables required to fit the anhydrous database is 26. The reader interested in the mechanics of these manipulations should refer to Appendix 4 for more details. The standard error in the model after calibration is 587 cal for the anhydrous database and 788 cal for the hydrous database. Both of these values are at the level of estimated uncertainty in the contributing thermodynamic data (Appendix 2) and we conclude that our model equations for $RT \ln \gamma_i$ fit the experimental/thermodynamic database to within the accuracy of measurement.

Statistical results: implied uncertainties in experimental quantities

Using the parameters of Table A4-3, estimates of the right hand side of Eq. (17) (or for hydrous liquids Eqs. A3-15 or A3-16) can be calculated for a given experimental liquid composition and compared to the

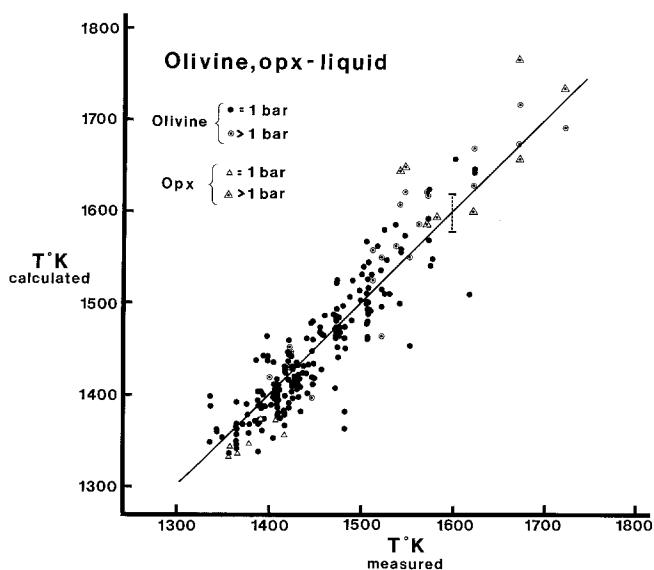


Fig. 1. Calculated temperature plotted against experimental temperature for olivine- and orthopyroxene-liquid assemblages at pressures of 1 bar and greater. Error bar is two standard deviations ($\pm 32^\circ$)

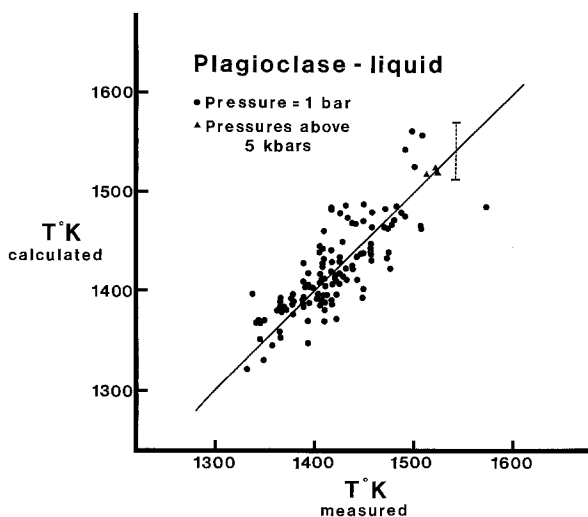


Fig. 2. Calculated temperature plotted against experimental temperature for plagioclase-liquid assemblages. Error bar is two standard deviations ($\pm 30^\circ$)

actual quantities. The differences between the two numbers are residuals, and the average of these is tabulated for each of the component/liquid equilibria used in calibrating the model in Tables 5 and 6. The standard deviations of these averages are also provided. The values are given in calories. In addition, for each mineral phase, averages and standard deviations of residuals are also given, as well as the correlation coefficient (or correlation matrix) that describes component-component effects in the solid. Thus, the fit for olivine is better than the individual fits for the olivine components forsterite and fayalite separately.

If temperature is treated as a variable in the terms on the left hand side of Eq. (17) then the calculated estimates of the right hand side can be used to predict

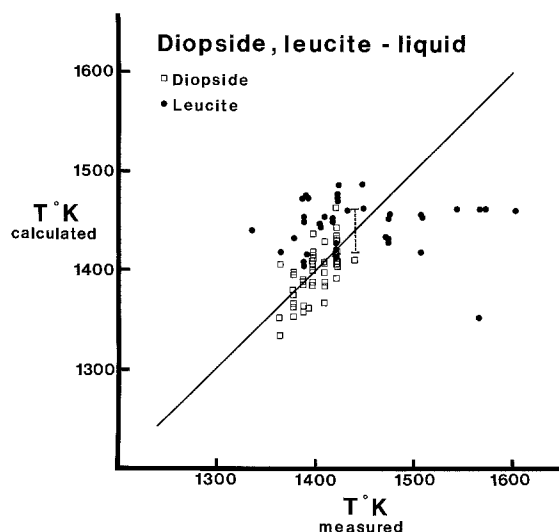


Fig. 3. Calculated temperature plotted against experimental temperature for augite (diopside, hedenbergite)- and leucite-liquid assemblages. Error bar is two standard deviations ($\pm 24^\circ$) for the pyroxene equilibria. The wide scatter in the leucite data is attributable to the fact that leucite of essentially the same composition crystallizes from liquids of widely different composition. Therefore its use as a solid/liquid geothermometer is substantially poorer than for the other solid phases

values of the equilibrium temperature.⁶ This is identical to the geothermometer approach of Ghiorso and Carmichael (1980) here expanded to include many more phases of igneous interest. Predicted versus experimental temperatures for the solid/liquid anhydrous equilibria are plotted in Figs. 1 through 4. These data are also summarized as average residuals and standard deviations of these residuals in Table 5 and for the hydrous liquids in Table 6. As with the caloric quantities, average deviations, standard deviations and correlation coefficients for each mineral phase are given. The utility of the solution model as a geothermometer may be judged from Tables 5 and 6. The great diversity of liquid compositions which comprise the database should be kept in mind when assessing these results.

If the sole purpose of generating a solution model for silicate liquids were to improve the current state of geothermometry, then the results in Tables 5 and 6 would be disappointing. The empirical equations of Smith (1983) provide a better feldspar-liquid geothermometer for example but, of course, have no constraints consistent with any other solid liquid/equilibria. As was discussed in the introduction the utility of adopting a thermodynamic form for our model is in predicting liquid phenomena beyond the database. We hope to demonstrate these advantages in subsequent sections.

A Monte Carlo error simulation has been performed in an effort to determine how much of the residual standard deviation seen in Table 5 is due to the precision of liquid/solid compositions determined by elec-

⁶ Equation (17) defines a non-linear equation in temperature which we solve iteratively using Newton's method. The computer program mentioned later performs these rather laborious geothermometric calculations

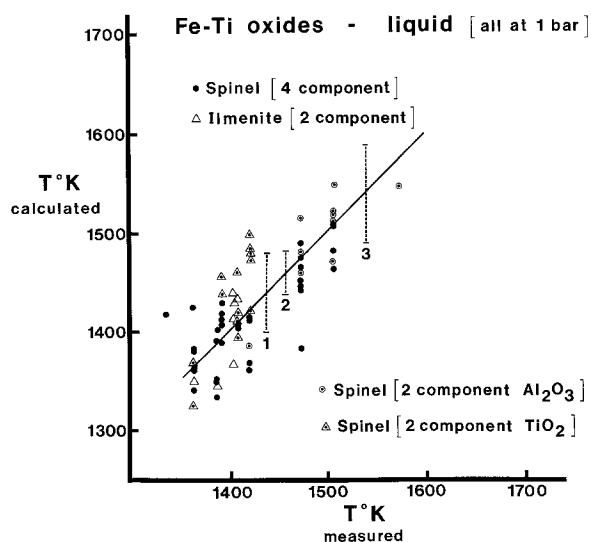


Fig. 4. Calculated temperature plotted against experimental temperature for Fe–Ti oxide assemblages with liquid. Error bars are two standard deviations and refer to (1) spinels; just considering the components Fe_2TiO_4 and Mg_2TiO_4 ($\pm 73^\circ$), (2) spinels; with just FeAl_2O_4 and MgAl_2O_4 components ($\pm 20^\circ$), and (3) spinels; with both Ti and Al components ($\pm 42^\circ$)

tron microprobe. For a typical experimental run (Sack 1983a, Korath #8–15, see Table 2) which consisted of liquid coexisting with olivine, plagioclase, clinopyroxene and spinel, we assumed analytical uncertainties (standard deviations) in the wt. % abundances of each oxide to be the maximum of 3 % of the amount present or 0.05. This is obviously an upper estimate for some elements and a low one for others. From these estimates, by generating multinormal random deviates, a set of 100 “experimental runs” were calculated, all compositionally distributed about the original result. These “data” were processed through Eq. (17) and equilibration temperatures for each component-phase predicted. The results are given in Table 7. As in the two previous Tables we have listed average temperatures and standard deviations for each mineral phase as well as component correlation coefficients in addition to standard deviations in the calculated mole fractions of forsterite and fayalite in olivine and albite and anorthite in plagioclase. The results reveal the minimum uncertainty in predicted temperature due to analytical technique (overall $\pm 14^\circ\text{C}$ and up to 42°C at the 95 % confidence level). This is a minimum in that the test does not involve true replicates nor does it assess variation between electron microprobe laboratories. We have not been able to model uncertainties attributed to the latter but believe that some portion of the differences between the residual standard deviations of Table 5 and the simulation of Table 7 is due to this cause.

We have used Eq. (10) and the parameters of Table A4-3 to calculate an estimate of the activity of silica in experimental liquids that coexist at T and P with both olivine and orthopyroxene. These estimates are provided in Table 8 and are compared to liquid silica activities defined by the coexistence of the solid phases olivine and orthopyroxene:

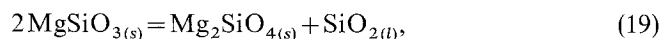


Table 4. Adopted Components

* Si_4O_8	0.25	$(\text{SiO}_2 - 0.5(\text{FeO} + \text{MnO} + \text{MgO} + \text{NiO} + \text{CoO} + \text{CaO}) - \text{Na}_2\text{O} - \text{K}_2\text{O})$
* Ti_4O_8	0.25	TiO_2
* $\text{Al}_{16/3}\text{O}_8$	0.375	Al_2O_3
* $\text{Fe}_{16/3}\text{O}_8$	0.375	Fe_2O_3
* $\text{Cr}_{16/3}\text{O}_8$	0.375	Cr_2O_3
* $\text{Fe}_4\text{Si}_2\text{O}_8$	0.25	FeO
* $\text{Mn}_4\text{Si}_2\text{O}_8$	0.25	MnO
* $\text{Mg}_4\text{Si}_2\text{O}_8$	0.25	MgO
* $\text{Ni}_4\text{Si}_2\text{O}_8$	0.25	NiO
* $\text{Co}_4\text{Si}_2\text{O}_8$	0.25	CoO
* $\text{Ca}_4\text{Si}_2\text{O}_8$	0.25	CaO
* $\text{Na}_{16/3}\text{Si}_{8/3}\text{O}_8$	0.375	Na_2O
* $\text{K}_{16/3}\text{Si}_{8/3}\text{O}_8$	0.375	K_2O
* $\text{P}_{16/5}\text{O}_8$	0.625	P_2O_5
* Sr_8O_8	0.125	SrO
* H_2O		H_2O

If moles of the simple oxides are first computed, they can be transformed into moles of the new components in the manner indicated in the right hand column

and



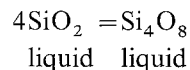
For which

$$RT \ln a_{\text{SiO}_2}^{\text{liquid}} = RT \ln K_{19} - RT \ln (a_{\text{Mg}_2\text{SiO}_4}^{\text{olivine}} / (a_{\text{MgSiO}_3}^{\text{opx}})^2)$$

and

$$RT \ln a_{\text{SiO}_2}^{\text{liquid}} = RT \ln K_{20} - RT \ln (a_{\text{Fe}_2\text{SiO}_4}^{\text{olivine}} / (a_{\text{FeSiO}_3}^{\text{opx}})^2).$$

All these calculations of the activity of silica are given in calories in Table 8. The average standard deviation of residuals (453 calories) compares quite favorably with estimated uncertainties in the thermodynamic parameters and with the residuals for the overall fit of the model (Table A4-4). At this point it should be emphasized that to develop the regular solution model, the simple oxide components were recalculated onto an 8-oxygen basis, so that $1/4 \mu_{\text{Si}_4\text{O}_8}$ equals μ_{SiO_2} or equivalently $1/4 RT \ln a_{\text{Si}_4\text{O}_8}$ equals $RT \ln a_{\text{SiO}_2}$. In other words the free energy change for the reaction:



is zero. This clearly must be the case at equilibrium.

The residuals of Table 8 ($\Delta(\text{Fo}-\text{En})$ and $\Delta(\text{Fa}-\text{Fs})$) exhibit a slight inverse pressure dependence (coefficient of variation, r^2 , of 0.49 and 0.35, respectively). We suspect this pressure dependence is a consequence of inappropriate volume or compressibility data for pure silica liquid, though potentially it could be pointing to excess volume of mixing terms for silica.

The shape of the free energy of mixing surface

To understand more intuitively the free energy surface described by the parameters of Table A4-3, we must acquire some idea of its topology. It is extremely important to locate, in our 16 dimensional component space, all minima and maxima, and their magnitudes, in order to determine this topology. If some general-

Table 5. Statistical results from back calculation using the model data – anhydrous liquids

Number	Component or phase	Average error in predicting T (K)	Standard deviation	Correlation	Average distance from free energy surface (cals)	Standard deviation	Correlation
215	Forsterite	0.05	36.68		-8.63	482.06	
215	Fayalite	0.66	56.19		12.34	635.05	
215	Olivine	0.71	31.92	-0.1039	3.70	378.99	-0.0999
2	Akermanite	-6.16	0.09		92.34	1.30	
19	Enstatite	14.95	67.30		-163.11	566.22	
19	Ferrosilite	-0.50	77.43		25.62	378.96	
	Opx	7.22	57.12	0.2424	-68.74	383.21	0.2870
85	Diopside	-0.63	22.62		9.26	328.30	
86	Hedenbergite	0.94	41.08		-7.15	502.11	
	Cpx	0.16	23.62	0.0175	1.06	301.33	0.0100
1	Sanidine	2.02			-28.00		
1	Albite	68.64			-606.28		
	Kspar	35.33		-	-317.14		
123	Albite	-1.55	52.72		21.88	446.40	
124	Anorthite	3.24	36.63		-55.92	659.00	
123	Plagioclase	1.72	30.03	-0.1352	-34.50	372.85	-0.1378
42	Leucite	-0.32	66.94	-	14.90	775.31	
8	Ilmenite	0.75	21.76		-7.61	270.85	
8	Geikielite	1.09	43.55		-15.07	374.71	
	Rhombohedral Oxide	0.92	29.34	0.5663	-11.34	286.51	0.5645
44	Spinel	-3.19	20.27		62.73	399.66	
44	Hercynite	-2.05	28.60		65.20	552.41	
48	Ulvospinel	-0.25	37.36		7.42	525.88	
48	Mg-titanate	0.44	136.23		-10.91	846.95	
	sp + hc	-2.62	20.16	0.3425	63.97	386.22	0.2985
	uv + mt	0.10	73.43	0.1588	-1.75	537.55	0.1818
	all four	-2.27	42.09	*	26.00	335.95	*
1,160	Summary	0.32	51.40		2.20	555.78	

* Correlation coefficient matrices

cals	hc	uv	mt	T	hc	uv	mt
sp	$\begin{bmatrix} 0.2193 & 0.0428 & 0.5340 \\ & 0.4679 & -0.5135 \\ & & -0.0011 \end{bmatrix}$			sp	$\begin{bmatrix} 0.2730 & 0.0630 & 0.5718 \\ & 0.4761 & -0.4698 \\ & & 0.0228 \end{bmatrix}$		
hc				hc			
uv				uv			

izations can be made concerning the shape of this surface the chemistry of the liquids might be more readily understood. Fortunately, some progress can be made along these lines.

The molar excess free energy of mixing, \hat{G}^{excess} , is from Eq. (7):

$$\hat{G}^{\text{excess}} = \frac{1}{2} \sum_{i=1}^n \sum_{j=1}^n W_{ij} X_i X_j \quad (21)$$

which can be written in the vector notation introduced in Appendix 4 as:

$$\hat{G}^{\text{excess}} = \frac{1}{2} X^T W X. \quad (22)$$

Inspection of Table A4-3 will reveal that there are twelve binary subsystems which possess positive interaction parameters and therefore show immiscible phe-

nomena at finite temperature. A maximum excess free energy of mixing is attained at the midpoint of the $\text{Ti}_4\text{O}_8 - \text{Mg}_4\text{Si}_2\text{O}_8$ join (3,168.4 cal/mol). It is easy to verify that there are only two ternary subsystems where all three regular solution parameters are positive ($\text{Si}_4\text{O}_8 - \text{Fe}_{16/3}\text{O}_8 - \text{Mn}_4\text{Si}_2\text{O}_8$ and $\text{Fe}_{16/3}\text{O}_8 - \text{Ca}_4\text{Si}_2\text{O}_8 - \text{Mn}_4\text{Si}_2\text{O}_8$) and that in no higher m -order systems do m positive interaction parameters occur. Furthermore in these two strictly positive ternaries the relative magnitudes of the W_{ij} 's are such that no internal maxima in the \hat{G}^{excess} surface occur (ternary system category IVA of Meijering 1950, 1951). Thus all excess free energy values in the 16-component space are lower than 3,168.4 cal/mol. Whether any internal minima exist can be evaluated by extracting the critical or stationary points of \hat{G}^{excess} (Eq. 22). For a regular solution \hat{G}^{excess} possesses the mathematical properties of a quadratic form; in particular, if the function is dis-

Table 6. Statistical results from back calculation using the model data – hydrous liquids

Number	Component or phase	Average error in predicting T (K)	Standard deviation	Correlation	Average distance from free energy surface (cals)	Standard deviation	Correlation
1	Forsterite	-58.56			693.66		
1	Fayalite	218.89			-2,991.63		
	Olivine	80.17			-1,148.99		
5	Enstatite	50.94	89.96		-286.70	571.25	
5	Ferrosilite	-33.06	138.82		272.98	953.97	
	Opx	8.94	42.00	-0.8320	-6.86	287.05	-0.8131
4	Diopside	10.53	33.21		-133.08	394.72	
4	Hedenbergite	-13.25	38.89		174.37	504.93	
	Cpx	-1.36	23.19	-0.1800	20.65	289.41	-0.1900
6	Albite	9.53	8.86		-81.25	75.20	
6	Anorthite	2.94	38.87		-38.64	625.33	
	Plagioclase	6.24	20.74	0.1900	-59.95	321.05	0.1700
	β -quartz	892.42	1,556.83		2.42	28.87	
6	Ilmenite	68.10	37.53		-890.14	480.47	
6	Magnetite	0.57	53.33		6.37	826.94	
6	Ulvospinel	-54.01	54.84		915.33	937.23	
	mg + uv	-26.72	49.86	0.7000	460.86	818.27	0.7200
22	water				0.00	752.44	
80	Summary	71.95	460.62		-44.70	791.32	

Table 7. Statistical results from the Monte Carlo error simulation (Sack, K-8-15). Olivine, plagioclase, clinopyroxene, spinel-liquid assemblage

Component or phase	Average T (K)	Standard deviation	Correlation	Average Mole fraction ^a	Standard deviation
Forsterite	1,412.12	9.86		0.7112	0.0149
Fayalite	1,364.82	7.16		0.3176	0.0038
Olivine	1,388.47	3.62	-0.6798		
Albite	1,408.06	12.58		0.1835	0.0052
Anorthite	1,426.09	7.38		0.8193	0.0217
Plagioclase	1,417.08	6.90	-0.1200		
Diopside	1,396.42	5.36			
Hedenbergite	1,394.14	9.31			
Cpx	1,395.28	5.46	0.0365		
Spinel	1,408.36	7.27			
Hercynite	1,417.95	6.10			
Ulvospinel	1,545.55	4.52			
Mg-Titanate	1,546.09	20.48			
sp + hc	1,413.15	6.05			
uv + mt	1,545.82	10.18			
Total	1,479.49	6.79			

Correlation coefficient matrix

	hc	uv	mt
sp	0.6376	0.0224	0.6393
hc		0.3993	-0.1499
uv			-0.1385

^a For olivine these numbers are the square root of the activity and represent an approximation

The analysed phases correspond to activities of Fo=0.5276, Fa=0.1299, Ab=0.1911 and An=0.7948

Table 8. Partial Molar Free Energies of SiO₂ in Calories/Mole

	<i>P</i> (kbars)	<i>RT</i> ln <i>a</i> _{SiO₂} ^{liq}			Solution model - ^{1/4} (μ _{Si₄O₈} ⁰ - μ _{Si₄O₈} ⁰)	<i>RT</i> ln <i>a</i> _{SiO₂} ^{liq} - ^{1/4} (μ _{Si₄O₈} ⁰ - μ _{Si₄O₈} ⁰)	
		<i>T</i> (K)	Fo-En	Fa-Fs		Δ(Fo-En)	Δ(Fa-Fs)
Stolper (1981)							
519-12	10.0	1,623	-2,738	-3,136	-3,360	622	224
519-10	10.0	1,573	-2,865	-3,160	-3,450	585	290
519-52	15.0	1,673	-3,516	-3,399	-3,560	44	161
519-16	20.0	1,723	-4,275	-4,357	-3,773	-502	-584
519-14	20.0	1,673	-4,334	-3,970	-3,495	-839	-475
Takahashi (1980)							
	14.0	1,543	-3,737	-3,593	-3,096	-641	-497
	14.0	1,548	-4,013	-3,340	-3,169	-844	-171
Grove et al. (1982)							
187.3	0.001	1,408	-1,717	-1,508	-2,046	329	538
187.4	0.001	1,392	-1,754	-1,838	-1,998	244	160
79-38B5	0.001	1,410	-1,384	-1,476	-2,012	628	536
79-9C11	0.001	1,366	-1,383	-1,553	-1,495	112	-58
79-9C7	0.001	1,358	-1,182	-1,804	-1,473	291	-331
standard deviation (both components) (correlation coefficient)						562 (453) (0.79)	395

cussed (with no loss of generality) on the unit sphere, where $X^T X = 1$, then its stationary points are specified by the eigenvectors of W (Parlett 1980). Thus the solutions \hat{X} , to

$$WX = \lambda X \quad (23)$$

define the compositions of all minima, maxima or saddle points on the surface. These compositions can be uniquely translated from the unit sphere ($X^T X = 1$) to the unit plane ($X^T 1 = 1$) as can the topological meaning we will attach to these unit sphere eigenvectors in the discussion that follows. For each \hat{X} there exists an eigenvalue, λ , which has physical meaning:

$$\begin{aligned} \hat{G}^{\text{excess, critical}} &= \frac{1}{2} \hat{X}^T W \hat{X} \\ &= \frac{1}{2} \hat{X}^T \lambda \hat{X} \end{aligned}$$

which since λ is a scalar

$$\hat{G}^{\text{excess, critical}} = \frac{1}{2} \lambda \hat{X}^T \hat{X}$$

but we have restricted our attention to $X^T X = 1$, therefore:

$$\lambda = 2 \hat{G}^{\text{excess, critical}}$$

The eigenvalues of W are just twice the values of the excess free energy of mixing at the critical points. There are 16 eigenvectors and eigenvalues of the matrix W . In the present case (W defined by Table A4-3), only one eigenvector lies within the compositional subspace spanned by positive mole fractions. Five others correspond to the pure ideal diluents (Cr_{16/3}O₈, etc. ...). Liquid compositions corresponding to two permissible multicomponent eigenvectors have been extracted for both the anhydrous and hydrous parameters. These are provided along with their excess free energies of mixing

in Table 9. Since \hat{G}^{excess} obviously assumes both negative and positive values as a function of X , the matrix W is indefinite and all the eigenvectors represent the compositions of saddle points on the surface (Flanigan and Kazdan 1971). There are no internal minima or maxima and thus inspection of Table A4-3 will reveal that the lowest value that the excess free energy of mixing can assume is at the midpoint of the Na_{16/3}Si_{8/3}O₈ - Al_{16/3}O₈ join: -33,904 cal/mole. This analysis shows that the \hat{G}^{excess} defined by our multicomponent database is a sloping surface and is negative over the geologically relevant portions. It contains a single point, quite asymmetrically placed, where the determinant of the matrix of the compositional second derivatives goes to zero.⁷ In the language of phase diagrams this point is a spinodal locus (Barron 1978). The key to understanding the physical phenomena this surface implies is embedded in its asymmetry. The total free energy of mixing is the sum of the excess and ideal terms, and the ideal free energy of mixing is a monotonic function of temperature which is symmetric about the compositional midpoint of the system. The wt. % composition corresponding to this midpoint for anhydrous liquids ($X_i = 1/15$) is also given in Table 9 along with its excess free energy of mixing. Note how much more positive this value is than that of the anhydrous "saddle point" eigenvector, or that of the typical tholeiite given in the last column. Along with each composition in Table 9 we have provided the value of the ideal entropy of mixing, \hat{S}^{ideal} from which \hat{G}^{ideal} can be calculated as a function of temperature:

$$\hat{G}^{\text{ideal}} = -T \hat{S}^{\text{ideal}}$$

⁷ The second derivative matrix of Eq. (22) restricted to the unit sphere and evaluated at the eigenpoint is $W - \lambda I_n$. Its determinant is zero since $\det(W - \lambda I_n) = 0$ defines the eigenvalues

Table 9. Shape of the free energy of mixing surface

	Eigenvectors of the W matrix (wt%)		Anhydrous maximum entropy composition	Typical tholeiite (Philpotts)
	hydrous	anhydrous		
SiO ₂	33.45	34.31	27.84	22.36
TiO ₂	9.87	10.26	7.72	5.58
Al ₂ O ₃	15.02	15.00	9.44	4.74
Fe ₂ O ₃	1.88	0.05	4.05	7.43
Cr ₂ O ₃	0.00	0.00	3.83	7.07
FeO	7.73	8.19	6.47	5.01
MnO	0.01	0.02	2.69	4.95
MgO	4.86	4.95	3.79	2.81
NiO	0.00	0.00	2.82	5.21
CoO	0.00	0.00	2.83	5.23
CaO	9.09	9.20	6.34	3.91
Na ₂ O	7.30	7.32	4.92	2.88
K ₂ O	10.43	10.70	7.28	4.38
P ₂ O ₅	0.00	0.00	2.15	3.96
SrO	0.00	0.00	7.83	14.46
H ₂ O	0.36			
\hat{G}_{excess}	-27,917	-30,296	-17,261	-7,822.8
\hat{S}_{ideal}	4.3756	4.0970	5.1361	5.3816

(*) Compositional midpoint between anhydrous eigenvector and anhydrous maximum entropy composition

At any finite T , it can be seen that the ideal contribution to \hat{G}^{mix} will be most strongly pronounced at the midpoint composition, and less so everywhere else. As T increases above absolute zero a minimum will begin to form in the \hat{G}^{mix} surface at this midpoint due to \hat{G}^{ideal} . This minimum will become stronger as T increases, until it completely dominates the shape and magnitude of the surface at elevated temperature. Now a multidimensional saddle point behaves very much like a “partial” minima; that is, at this point the gradient of \hat{G}^{excess} is zero but its second derivatives do not indicate that the function is everywhere convex. At a given temperature a liquid of a particular bulk composition might lower its free energy by separating into two, the compositions of each being expressions of their geometrical placement on the slopes of the “minima” of the ideal and nonideal free energy terms. We have then a plausible argument for the existence of liquid immiscibility based upon the shape of a free energy of mixing surface whose excess terms are strongly negative! It remains now to demonstrate the existence and calculate the compositions of these binodal liquids, and determine whether some or all natural silicate liquids fall into the compositional volume that exhibits immiscibility. We take up these matters below.

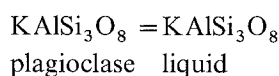
Extensions to the regular solution model for met-aluminous silicate liquids

Applications of a regular solution model as a solid/liquid geothermometer or as a means of calculating activities of petrologically interesting liquid components has been discussed before (Ghiorso and Carmichael 1980). Our present model offers little more than an expanded compositional basis for these calculations and we shall not discuss them further.

However there are some revisions resulting from the expanded database and the more stable regression techniques that should be briefly noted.

Activity coefficients of minor components in olivine and plagioclase

In our previous work (Ghiorso and Carmichael) we made estimates of the Henry's law activity coefficient for the KAlSi_3O_8 component in plagioclase by averaging a value for $\gamma_{\text{KAlSi}_3\text{O}_8}^{\text{plagioclase}}$ assuming the equilibria



held for each plagioclase/liquid experimental datum. Our new model and data generates a revised estimate for this quantity: 4.870 ± 1.279 . The value shows no T or P dependence, is consistent with ideal solution in the plagioclases, is based upon 27 experimental results over the temperature range 1,337 K to 1,418 K, and falls within two standard deviations of our previous estimate. From similar considerations an estimate of the average excess free energy of the Mn_2SiO_4 component in olivines can be made ($RT \ln \gamma_{\text{Mn}_2\text{SiO}_4}^{\text{olivine}}$). Our value of 33,972 cal/mol may be quite inaccurate owing to the absence of other Mn minerals in calibrating the model parameters. Similar calculations can be performed for a number of trace constituents in the solids, as long as suitable thermodynamic data are available. Thus a whole collection of trace element “distribution coefficients” could easily be calculated for a wide range of liquid compositions from a minimal amount of experimental data. These coefficients would perforce be compositionally dependent. We will not make such calculations here, but only wish to suggest how the solution model can help quantify their compositional dependencies and facilitate their calculation.

Activity of silica and a petrogenetic grid for basic lavas

If there is any parallel between aqueous solutions and silicate liquids, then the role of pH in the former has as its equivalent the activity of silica in the latter. As the relationship between so many igneous minerals can be expressed in terms of silication reactions [for example Mg_2SiO_4 (forsterite) + SiO_2 (liquid) = 2MgSiO_3 (enstatite)], the silica activity of any natural liquid will have a dominant influence on the mineral species that eventually precipitate as the liquid cools at equilibrium.

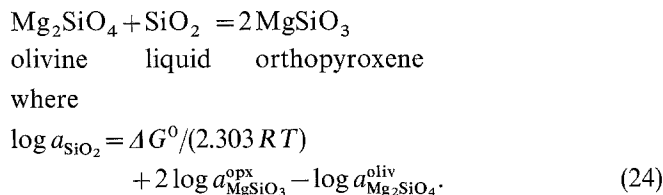
One of the properties of regular solutions is that for any component such as Si_4O_8 :

$$(\partial \ln a_{\text{Si}_4\text{O}_8} / \partial P)_{T, n_j} = (\bar{v}_{\text{Si}_4\text{O}_8}^{\text{liq}} - v_{\text{Si}_4\text{O}_8}^{\text{liq}, 0}) / RT = 0$$

where $\bar{v}_{\text{Si}_4\text{O}_8}^{\text{liq}}$ and $v_{\text{Si}_4\text{O}_8}^{\text{liq}, 0}$ represent the partial molar volume of Si_4O_8 in a multicomponent liquid and the molar volume of pure liquid Si_4O_8 respectively. Clearly, since the difference between these two quantities is zero, the activity of silica will not be a function of pressure, and it will only change in an ascending magma in response to a change in temperature or composition.

Based on this simple relationship, a petrogenetic grid can be constructed which depicts the conditions of equilibration of various magma types with an idealized mantle or source assemblage. To simplify our discussion we shall assume that during their ascent to the surface, magmas have their $\text{Fe}_2\text{O}_3/\text{FeO}$ ratios stipulated by an oxygen fugacity which follows the QFM buffer. Otherwise the basic magmas that arrive at the earth's surface as lavas are taken to represent liquid compositions generated at depth, so that effects such as mass transfer or crystal fractionation, which could modify the magma's composition en route to the surface, are ignored.

If it is granted that olivine and orthopyroxene could coexist in equilibrium in the source regions of all basic magmas, then the activity of silica will be given by the buffer reaction



It can be assumed that the log terms on the right hand side of Eq. (24) cancel. This is true if both solid phases are pure (the standard state) and approximately so under mantle conditions where both solids are diluted with iron components at pressures where the concentration of Al in the M1 site of the pyroxene is small. This follows since an olivine of Fo_{90} composition, whose activity is approximately $X_{\text{Mg}_2\text{SiO}_4}^2$, is typically in equilibrium in the mantle with En_{90} , which has the stoichiometric coefficient 2 preceding the log of its activity (≈ 0.90). Given this assumption, the calculated isobaric curves of silica activity corresponding to Eq. (24) are shown in Fig. 5. Also shown in Fig. 5 is the variation of the calculated $\log a_{\text{SiO}_2}$ for six lava types whose analyses are provided in Table 10, and which may have been in equilibrium with an olivine-orthopyroxene assemblage in their respective source regions. The slope of these curves of $\log a_{\text{SiO}_2}$ vs $1/T$ is opposite in sense to those calculated by Ghiorso and Carmichael (1980). This is solely a response to the value of the activity coefficient of silica being different, and hopefully more likely correct, in the present study.

The conditions of anhydrous equilibration, at oxygen fugacities equal to QFM, are represented by the intersection of the curves which describe $\log a_{\text{SiO}_2}$ as a function of T for the lavas with the isobaric mantle source assemblage curves. The effect of small amounts of water dissolved in the liquids is to reduce the activity of silica⁸, and thus either increase the equilibration pressure at a given T , or reduce the temperature at a constant pressure.

Aside from the komatiite, all the liquidus temperatures are taken to be 1,100°C, and at any given temperature such as 1,350°C, the progressive increase in the

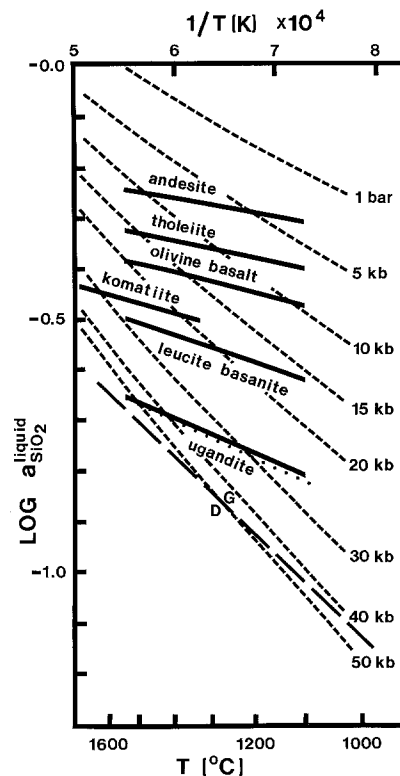
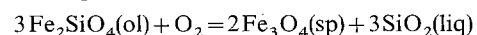


Fig. 5. Predicted temperature variations of $\log a_{\text{SiO}_2}^{\text{liq}}$ in typical lavas of various compositions (Table 12) compared to that obtained from olivine-orthopyroxene mineral buffers as a function of temperature and pressure

activity of silica in these lava types necessitates equilibration with an olivine-orthopyroxene assemblage at progressively lower pressures, or shallower depths. Indeed, in the case of the andesitic lava, so shallow is the depth, that it is geologically unreasonable that anhydrous equilibration occurred. The very high liquidus temperature of komatiite lavas ($\approx 1,500^\circ\text{C}$) requires that their source regions be very deep if the source region has its silica activity defined by olivine-orthopyroxene.⁹

The silica-poor potash-ankaratrite from Uganda (Table 10) has about the lowest activity of silica of any terrestrial silicate magma, and in character with alkali-rich lavas, has a relatively high $\text{Fe}_2\text{O}_3/\text{FeO}$ ratio (Sack et al. 1981). If this rock ratio is used to calculate silica activity as a function of temperature, rather than the variable $\text{Fe}_2\text{O}_3/\text{FeO}$ ratio calculated from the oxygen fugacity of the QFM buffer, there is a slight decrease in

9 There is nothing in the thermodynamic approach which requires olivine and orthopyroxene to be physically present in the source region, only that the activity of silica be constrained to that defined by an olivine-orthopyroxene assemblage. Presumably, this could also be achieved by olivine alone, for as an Fe-Mg phase it is subject to the oxidation equilibrium:



and it may be able to limit the activity of silica within the olivine-orthopyroxene range. The calculation procedure depends on equating activities or chemical potentials, regardless of how these are defined

8 The effect of water reducing the activity of silica is seen for example in the experiments of Egger (1972) on a Paricutin andesite where liquidus orthopyroxene is replaced by olivine with addition of water (Egger, Fig. 4).

Table 10. Analyses of lavas used in Fig. 5

	Ande- site	Tho- leiite	Olivine- basalt	Kom- atiite	Leucite- basanite	Potash- ankara- triite
SiO ₂	61.61	52.29	50.20	47.96	44.54	36.71
TiO ₂	0.60	1.17	2.43	0.36	2.16	5.54
Al ₂ O ₃	17.82	14.75	16.65	7.44	15.50	9.30
FeO _T	4.85	12.25	10.28	11.39	9.15	12.73
MnO	0.10	0.22	0.24	0.20	0.19	0.26
MgO	2.54	5.30	3.62	24.35	9.12	6.34
CaO	5.70	9.89	7.53	7.46	11.14	14.08
Na ₂ O	4.77	2.60	5.27	0.64	4.08	2.40
K ₂ O	1.43	0.33	2.16	0.06	1.82	6.05
P ₂ O ₅	0.20	0.16	0.82	0.03	0.61	1.11

From left to right analyses taken from: Luhr and Carmichael (1980), Philpotts (1979), Brown and Carmichael (1971) Nisbet et al. (1977), Brown and Carmichael (1969) and Brown (1971)

silica activity with decreasing pressure, as shown by the dotted line in Fig. 5.

Also shown in Fig. 5 is the diamond-graphite equilibrium curve (Clark 1966) drawn on the assumption that as olivine and orthopyroxene are found as inclusions in diamond (Meyer and Boyd 1972) the $P-T$ region of diamond stability in the mantle must coincide with silica activities defined by the assemblage olivine-orthopyroxene under the same $P-T$ conditions. Only silicate liquids with very low activities of silica are likely to be generated in the diamond field (with olivine and orthopyroxene) and in so far as the rock-type kimberlite may have a volcanic equivalent, it may be broadly similar to these potash-ankaratrites from Uganda.

The general conclusion of the relations displayed in Fig. 5 is that the more silica-rich lavas such as tholeiites would have a more shallow source than the more silica-poor, alkali-rich lavas. This is in accord with current petrological belief, although with the solution model proposed here it is possible to calculate the equili-

bration conditions of any magma with any specified Fe₂O₃/FeO ratio and any source assemblage using as large a number of component activities as can be defined (e.g. Fe₄Si₂O₈, Mg₄Si₂O₈, etc.).

It may be noted in passing that basic lavas with high activities of silica are most voluminous in the earth's volcanic economy, whereas the most silica-poor lavas tend to be erupted in small volume forming an insignificant fraction of the volcanic record, and yet are represented by an undue proliferation of rock names. These silica-poor, low silica-activity lavas tend to be rich in P₂O₅, and accordingly in all those other elements, such as Ta, Th, U, Hf, Zr and the REE, which are highly correlated with P₂O₅ (Beswick and Carmichael 1978).

Prediction of enthalpies of fusion

Measurements of the enthalpies of fusion of minerals of geologic interest are for the most part scarce and subject to considerable uncertainty. More often than not literature values are based upon estimates of entropies of fusion, and the attendant uncertainties in the enthalpy can be as large as ± 10 kcal/mol. It would be convenient if fusion enthalpies could be estimated more securely as their use in interpreting phase diagrams and in other aspects of petrological modelling (c.f. Bottinga and Richet 1978) is extensive. We have estimated fusion enthalpies for a number of igneous minerals and report them in Table 11. All estimates were made on minerals for which some external comparison could be made, and all values of ΔH_{fusion} are excluded from Table 11 that form part of the solution model thermodynamic database. The calculations were performed by determining for the solid its apparent enthalpy of formation at the temperature of melting, using the data of Appendix 2. The same quantity is computed for the liquid using Appendix 2, the constants of Table A4-3 and Eq. (13). The liquid mole fractions are determined directly from the mineral formula. The difference between these two calculated quantities

Table 11. Calculated enthalpies of fusion of stoichiometric simple compounds

Phase	Composition	Calculated ΔH_f (kcal)	Measured ^a ΔH_f (kcal)	Reference
Anorthite	CaAl ₂ Si ₂ O ₈	29.297	32.4 \pm 2.1	Weill et al., 1980 b
Albite	NaAlSi ₃ O ₈	13.005	15.5	Stebbins et al., 1980
Sanidine	KAlSi ₃ O ₈	19.505	13.11	Stebbins and Carmichael, 1981 a
Sphene	CaTiSiO ₅	25.750	29.59	King et al., 1954
Fayalite	Fe ₂ SiO ₄ ^b	18.930	22.5	Stebbins and Carmichael, 1981 b
Pseudowollastonite	CaSiO ₃	13.601	13.7 \pm 0.7	Adamkovicova et al., 1980
Enstatite	MgSiO ₃	18.284	14.7 {E} 18.0 {E} 19.576 {E}	Robie et al., 1978 Stull and Prophet, 1971 Ghiorso and Carmichael, 1980
Diopside	CaMgSi ₂ O ₆	27.510	32.48 34.435 {E}	Stebbins and Carmichael, 1981 a Ghiorso and Carmichael, 1980

^a Or estimated from the fusion curve. {E}

^b At FMQ: $X_{\text{Fe}_{1.63}\text{O}_8}/X_{\text{Fe}_4\text{Si}_2\text{O}_8} = 0.04411$ (Sack et al. 1981)

ΔH_f for Fayalite (Fe₂SiO₄), Tephroite (Mn₂SiO₄), Forsterite (Mg₂SiO₄) and Larnite (Ca₂SiO₄) were used in constructing the model, and are by default satisfied exactly

is our estimate of the enthalpy of fusion. A perusal of Table 11 will demonstrate that these estimates agree quite well with the corresponding measurements and fusion curve values reported. This is particularly intriguing when one considers that the calculation of liquid properties for compositions corresponding to these mineral formulae is a considerable extrapolation from the compositional subspace within which the model was calibrated. Fusion enthalpies were not calculated for phases which possess negative mole fractions in our component space, though this is thermodynamically feasible (Ghiorso and Carmichael 1980). However, the success of the present calculations should provide a means of estimating the liquid properties (H , C_p , G) of a number of geological materials as a function of T , P and f_{O_2} .

Prediction of multiphase equilibria

Liquid immiscibility

We have already discussed the geometrical arguments for the existence of liquid immiscibility in the proposed solution model. We now turn to methods of calculating coexisting binodal compositions and the extent of the inferred liquid immiscibility in natural liquids. Consider a liquid whose bulk composition is defined by the mole fraction vector X . The total free energy of mixing at X is (again using the vector notation of Appendix 4):

$$G^{\text{mix}} = n_x RT X^T \ln X + \frac{1}{2} n_x X^T W X \quad (25)$$

where it is understood that the logarithm operator is applied to the components of the vector X . Now consider two arbitrary compositional vectors Y and Z . If we require:

$$\begin{aligned} Y &\geq 0 \\ Z &\geq 0 \end{aligned} \quad (26)$$

and

$$n_x X = n_y Y + n_z Z$$

where n_y , n_z , n_x are the number of moles in the phases defined by Y , Z and bulk composition X , then the condition for two-phase immiscibility is:

$$G_{\text{at } Y}^{\text{mix}} + G_{\text{at } Z}^{\text{mix}} < G_{\text{at } X}^{\text{mix}} \quad (27)$$

for some set of finite Y , Z , n_y and n_z . Note that this condition is independent of the relative magnitudes of the standard state chemical potentials of the liquid components. The optimum values of Y , Z , n_y , and n_z – the ones that define a binodal tie line – are those which minimize the left hand side of Eq. (27). Thus to calculate whether a given bulk composition generates coexisting immiscible liquids we solve the problem:

$$\text{minimize } (G_{\text{at } Y}^{\text{mix}} + G_{\text{at } Z}^{\text{mix}})$$

subject to:

$$n_x X = n_y Y + n_z Z,$$

$$n_y Y \geq 0$$

and

$$n_z Z \geq 0 \quad (28)$$

and then check to make sure n_y and n_z are strictly greater than zero, Y does not equal Z , and that Eq. (27) is satisfied. The ratios n_y/n_x and n_z/n_x define the proportions of each of the coexisting immiscible phases. There is no reason why more than two immiscible liquids cannot coexist in an n component system (the number can never exceed n) and their compositions can be calculated or their existence verified using obvious extensions of the equations presented here.

With G^{mix} defined by Eq. (25), Eq. (28) becomes a problem in non-linear optimization in $2n$ unknowns. Two of us (Rivers and Ghiorso 1980) have described numerical methods useful to the solution of problem (28) that utilize the fact that at the minima, which is a stationary or critical point of $G_{\text{at } Y}^{\text{mix}} + G_{\text{at } Z}^{\text{mix}}$ (the point where the gradient – the vector of compositional first derivatives – is zero), the second derivative matrix (referred to as the Hessian) defines a surface which is everywhere convex upward. In mathematical terms the Hessian is strictly positive definite. We state the regular solution forms of these derivatives here for the convenience of the reader. They may be found in a slightly different form elsewhere (Ghiorso and Carmichael 1980). From

$$\left(\frac{\partial G^{\text{mix}}}{\partial n_i} \right)_{T, P, n_{i+1}} = RT \ln a_i$$

and Eq. (10) it follows that:

$$\begin{aligned} \left(\frac{\partial G^{\text{mix}}}{\partial n_i} \right)_{T, P, n_{i+1}} &= RT \ln X_i + NRT \ln \gamma_i \\ &= RT \ln X_i + \sum_{j=1}^n W_{ij} X_j \\ &\quad - \frac{1}{2} \sum_{j=1}^n \sum_{k=1}^n W_{jk} X_j X_k \end{aligned} \quad (29)$$

and thus

$$\left(\frac{\partial^2 G^{\text{mix}}}{\partial n_i^2} \right)_{T, P, n_{i+1}} = \frac{1}{N} \left[\frac{RT(1-X_i)}{X_i} - 2RT \ln \gamma_i \right] \quad (30)$$

and

$$\begin{aligned} \left(\frac{\partial \left(\frac{\partial G^{\text{mix}}}{\partial n_i} \right)_{T, P, n_{i+1}}}{\partial n_j} \right)_{T, P, n_{i+j}} &= \left(\frac{\partial \left(\frac{\partial G^{\text{mix}}}{\partial n_j} \right)_{T, P, n_{i+j}}}{\partial n_i} \right)_{T, P, n_{i+i}} \\ &= \frac{1}{N} (W_{ij} - RT - RT \ln \gamma_i - RT \ln \gamma_j). \end{aligned} \quad (31)$$

Equation (31) is required since the free energy is a path independent function. Equations (29), (30) and (32) may be used to construct numerical values for the gradient vector and the Hessian matrix¹⁰ for a given Y , Z , n_y and n_z .

¹⁰ In hydrous liquids, for all derivatives not involving the component H_2O add the term $RTX_{H_2O}/N(1-X_{H_2O})$ to the anhydrous quantity. For all other matrix entries subtract RT/N from the anhydrous term except for the diagonal element that corresponds to H_2O for which the term

$$RT/(1-X_{H_2O})/(NX_{H_2O})$$

should be added. Appropriate modification to the entries of the gradient vector are given by Eqs. (A3-15) and (A3-16)

We have developed a computer code (part of a software package available from the first author) which implements a modified Newton-projected gradient type algorithm developed by Gill and Murray (1974, for a review) to solve the problem posed by Eq. (28). As an example let us consider the tholeiite whose composition is provided in Table 9. This is a sample of Rattlesnake Hill basalt which exhibits liquid immiscibility and formed the subject of the experimental study of Philpotts (1979). Philpotts derives a composition for the mesostasis of this basalt which is related to the bulk composition by crystallization of phenocrysts of clinopyroxene and plagioclase. Unfortunately, this mesostasis composition can vary considerably depending on the extent of crystallization. Philpott's experimental work indicates that the mesostasis unmixes to two liquids at about 1,313°C, one of which is enriched in TiO₂, FeO_T, MnO, MgO, CaO and P₂O₅ the other in SiO₂ and less so in Na₂O, K₂O and Al₂O₃. Similar trends have been found in the lunar lavas and other tholeiites (Roedder 1979; Philpotts 1982). In addition Philpotts (1979) argues that the mesostasis composition intersects the immiscible dome in *T*-*X* space as it becomes depleted in the alkalis and alumina. If the bulk liquid composition could be made to cool while *preventing* the crystallization of solid phases it should intersect this immiscible dome at a lower temperature than the mesostasis. A rough approximation using Philpott's Fig. 11 (1979, p 116) is about 900°C. We have performed the calculation just described and predict unmixing into two liquids beginning at about 950°C, along the QFM buffer at 1 bar. The reported compositions in Table 12 are those solutions to problem (28) at 1,200 K. As the final compositions of coexisting immiscible globules found in the rocks represent the lowest temperature binodal achieved during the crystallization history of a greatly silica enriched residuum (Philpotts 1982), it is difficult to compare compositions derived from field, laboratory or theoretical considerations in any but a qualitative sense. That is, there is no guarantee that the three methods of investigation are comparing similar events in the crystallization history. In any case, the compositional *trends* reported in Table 12 should reflect those seen in experiment and those found in nature. The silica-rich phase in Table 12 is enriched in TiO₂, Al₂O₃, Na₂O and K₂O, while the silica poor phase is enriched in total FeO, MnO, MgO and P₂O₅. CaO is concentrated slightly into the more siliceous phase, contradicting available experimental and field evidence as does the distribution of TiO₂ into the SiO₂ rich fraction. It is not clear why the predicted elemental trends deviate from reality on these two points. It is probably a consequence of an inappropriate interaction parameter or group of interaction parameters in the model which create an antipathy, for certain bulk compositions, between MgO or FeO and TiO₂ and CaO and FeO. Methods to correct this problem are currently under investigation. Immiscible liquid calculations on tholeiites of composition quite different from the Rattlesnake Hill basalt exhibit the "correct" distribution (between phases) of TiO₂ and CaO. We can only conclude that there is a strong compositional and possibly temperature dependence to the behavior of TiO₂ and CaO during two-phase separation and our

Table 12. Calculated coexisting immiscible liquid compositions for the tholeiite of Table 9 (wt%)

	Liquid 1	Liquid 2
SiO ₂	45.87	53.21
TiO ₂	0.00	1.26
Al ₂ O ₃	9.06	15.28
Fe ₂ O ₃	6.98	1.58
FeO	18.95	10.05
MnO	0.95	0.17
MgO	7.98	5.16
CaO	8.99	10.04
Na ₂ O	0.59	2.76
K ₂ O	0.00	0.36
P ₂ O ₅	0.65	0.13

model does not allow generalizations to be made along these lines for tholeiites as a whole.

In performing immiscible liquid calculations for a wide range of igneous rock types, we have found that most liquids of tholeiitic composition should undergo some form of two phase separation close to (within 100°C) their liquidus temperature. More basic lavas should be substantially crystallized before their *bulk* compositions intersect the *T*-*X* immiscible dome and more acid lavas were never found to undergo two-phase separation, even when the metastable liquid was "cooled" to 500°C.¹¹ It should be noted, particularly for the latter, that these calculations were performed on anhydrous compositions. No three- or higher phase immiscibility has been calculated for any natural silicate liquid using the current model. Accordingly, natural silicate liquids at temperatures close to their liquidus, appear to intersect a two-phase immiscible liquid field that encompasses the composition tholeiite. A detailed description of the binodal surfaces in this region must await the computational ability to model crystallization phenomena in these liquids. Work along such lines is currently in progress.

Olivine-liquid equilibria

Ghiorso and Carmichael (1980) have discussed the hazards involved with interpreting regular solution interaction parameters, obtained in the manner described above - from solubility data, in an extra-thermodynamic sense. The inference of structural details in the liquid or the extrapolation of these multicomponent interaction parameters to infer solid/liquid relationships in simplified two or three component phase diagrams may be misleading. On the other hand, some insight on the utility of binary and ternary phase diagrams in representing multicomponent solid/liquid equilibria can be gained by seeing how these simple systems are projected out of this multicomponent solution model. That is, what do the simple phase diagrams look like when calculated with an appropriate subset of the thermodynamic data and regular solution interaction pa-

¹¹ Calculations have been performed on the silica enriched mesostasis compositions of the basic lavas tabulated in Philpotts (1982). For these compositions liquid immiscibility into a silica rich and silica poor phase is predicted. The elemental partitioning results are similar to those we have found for the bulk composition tholeiite (Table 12)

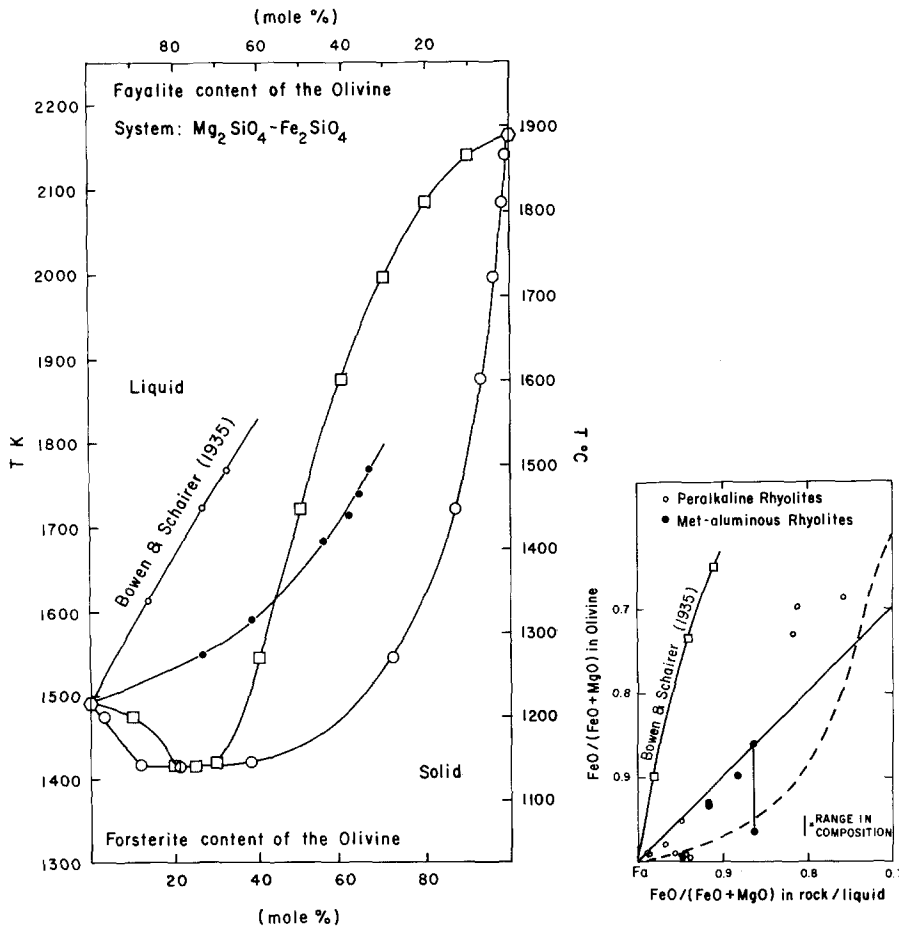


Fig. 6. Left: Calculated phase diagram for the system $Mg_2SiO_4 - Fe_2SiO_4$. Open squares define the liquidus, large open circles the solidus. Compare with the experimentally determined pseudobinary of Bowen and Schairer (1935). Right: Calculated and measured distribution coefficient for $FeO / (MgO + FeO)$ between olivine and liquid. Dashed line corresponds to that from the predicted phase diagram in the left hand figure. The solid line has unit slope. The data points are discussed in the text

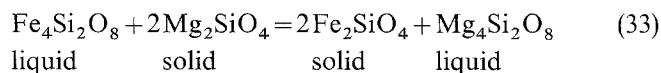
rameters? As an example of this approach we will consider the Mg-Fe olivine system. Ghiorso and Carmichael (1980) extracted a liquid interaction parameter for the Mg-Fe-olivine system of -24.1 kcal. The size of the W was ascribed to the necessity of considering all Fe as FeO in the experimental liquids (op. cit., p. 330). In this study, despite our provision for calculating the correct Fe_2O_3/FeO ratio in the liquid, using an entirely different set of components and a much expanded array of experimental liquids, we obtain -29.0 kcal (one-half of $W_{Fe_4Si_2O_8, Mg_4Si_2O_8}$). This is good agreement but is apparently in conflict with experimental data on the olivine system (Bowen and Schairer 1935). If this interaction parameter is used together with the activity/composition relations for Mg_2SiO_4 and Fe_2SiO_4 in olivines (Appendix 1), then liquid/solid equilibria can be calculated in the system $Mg_2SiO_4 - Fe_2SiO_4$, at oxygen fugacities low enough for most of the Fe to be present as FeO. The results of these calculations are portrayed in Fig. 6, together with the experimental results of Bowen and Schairer (1935) on the corresponding pseudobinary system; pseudobinary because iron-rich olivine melts incongruently to metallic iron plus a liquid with small amounts of Fe_2O_3 (ca. 2.5 wt. %). The calculated system shows a definite minimum, at an Fe_2SiO_4 mole fraction close to that found experimentally in the system $Ca_2SiO_4 - Fe_2SiO_4$ (Bowen et al. 1933). We did not expect our calculated phase diagram to coincide with the experimentally determined one as the value of $W_{Mg_4Si_2O_8, Fe_4Si_2O_8}$ is not

independent of the other interaction parameters and should not extrapolate to produce the binary system. In addition this interaction parameter has been calibrated from olivine-liquid relations where the whole database involves olivines which are more magnesian than iron-rich.

The calculated liquidus-solidus relationships shown in Fig. 6 suggest that between pure Fe_2SiO_4 and the composition of the minimum, liquids are more magnesian than the co-existing solid; in other words, the $FeO / (MgO + FeO)$ ratio of the solid is greater than that of the liquid in this composition span. Curiously enough, this relationship had been noted in the fayalitic phenocrysts of silicic volcanics (Carmichael 1967a), from which the development of a minimum, in projection, between liquid and solid was postulated. The data which led to this observation are also plotted in Fig. 6 together with more recent unpublished data and some from Mahood (1981) on mildly peralkaline rhyolites. In each case the microprobe analysis of the olivine was used in conjunction with the analysis of the whole rock. The latter is assumed to be the liquid composition, which is justified since, as the mass of phenocrysts is usually quite small, the composition of the residual glass enclosing the phenocrysts will be essentially the same as the rock itself. The concentration of FeO in the liquid was calculated (Sack et al. 1981) at the quench temperature and oxygen fugacities given by the iron-titanium oxides, and from this the $FeO / (FeO + MgO)$ ratio for each rock was derived (Fig. 6). Clear-

ly, there is an indication that in nature this reversal of Fe/Mg between olivine and liquid occurs, although a systematic analytical error in the over estimation of small amounts of MgO in the rocks could cause this. Perhaps the more extensive difference for the peralkaline rhyolites is an example of analytical error.

As the phenocryst assemblage in rhyolites did not equilibrate at 1 bar, the effect of pressure on the distribution of Mg and Fe between liquid and solid can be demonstrated by the reaction



for which ΔV can be evaluated at 1,200 K, the typical temperature of these rhyolites, by using the volume data given in Appendix 2. ΔV is positive at 1 bar and becomes increasingly so with pressure, so that as pressure is increased, the left-hand side of Eq. (33) is increasingly favored and a more iron rich liquid coexists in equilibrium with more magnesian crystals. The contrast between the FeO/(FeO+MgO) relation of the rhyolitic phenocrysts and their rocks and the experimental pseudobinary olivine system (Bowen and Schairer 1935) cannot therefore be ascribed to pressure.

The experimental results in the olivine system have been a cornerstone of the chemical tradition of phase equilibria applied to petrology, and yet one of the most salient features of the system, the enrichment of the Fe/Mg ratio of the liquid compared to that of the olivine has hardly been examined over the whole range of basaltic to rhyolitic liquids that precipitate olivine. That this reversal in rhyolites, documented in Fig. 6, can be predicted from olivine-basaltic liquid equilibria is an intriguing consequence of the regular solution model.

Calculation of early crystallizing phases

The experimental data used for the development of the multicomponent regular solution model is an assemblage of solid phases and liquids all of known composition, equilibrated at fixed temperatures. Now we wish to reverse the procedure and from the composition of the liquid calculate the composition and temperature at which the solid phase first appears when the liquid is cooled. It is conceptually simple to calculate the composition and amount of a particular solid phase precipitating at a particular temperature and then recalculate the composition of the liquid to account for the amount of solid, iterating the procedure until the liquid is completely crystalline. The computational details, however, are rather complex and computer software for this purpose is currently being developed.

As an example of the potential of a thermodynamic solution model to perform this procedure, we have calculated the precipitation temperatures and compositions of olivine and plagioclase in four mid-ocean ridge basalts experimentally investigated by Grove and Bryan (1983). Their determinations of olivine-, plagioclase-, clinopyroxene-, orthopyroxene- and spinel-liquid

equilibria in these MORBS did not form part of the experimental database.

The temperature at which any silicate liquid becomes saturated with a solid-solution like olivine or plagioclase can be demonstrated by plotting the parameter Σ_ϕ against temperature. This dimensionless quantity is a function of the thermodynamic affinity of the reaction describing the precipitation of the solid-solution from the liquid. It is unity at saturation, and less than unity when the liquid is undersaturated with the particular solid. The determination of Σ_ϕ has been discussed in some detail by Reed (1982) where it is defined as the sum of the *calculated* mole fractions of all the end-member components which comprise the solid-solution. In silicate liquids these mole fractions can be obtained from the composition of the liquid at a given T and P using Eq. (16), the parameters of Table A4-3 and the thermodynamic data and solid activity/composition relations in Appendices 1 and 2.

In Fig. 7 we have plotted the calculated values of Σ_ϕ for plagioclase and olivine as a function of temperature in the basaltic liquids studied by Grove and Bryan (1983). As can be seen the calculated saturation temperatures are within an average of 8°C of the experimental bracketing temperatures (7°, 2°, 3° and 20° for each of the four initial bulk compositions). At temperatures below the first appearance of olivine from bulk composition AII-96-42-2, the calculated values of Σ_ϕ for olivine in these olivine saturated liquids scatter within 5% of unity. Though not shown in Fig. 7 this is also the case for plagioclase in the plagioclase saturated liquids derived from the other three bulk compositions.

The calculated mole fractions of forsterite (Fo) and anorthite (An) in olivine and plagioclase are plotted in Fig. 7 against the experimentally determined compositions of the precipitated solids. The olivine and plagioclase compositions essentially fall within the limits of analytical error predicted by the Monte Carlo simulation of microprobe uncertainty (Table 7, i.e. 1.5% Fo and 2.2% An respectively). These error limits are shown as dotted lines in Fig. 7. Additionally, the predicted equilibration temperatures of all the solids with their coexisting liquids (not shown in Fig. 7) are within the limits given in Table 5.

Fortified by the close agreement between predicted and observed liquidus relations in these basaltic liquids, we have attempted similar calculations with the Thingmuli succession of lavas. These are believed to be related by crystal fractionation to a single liquid line of descent (Carmichael 1964, 1967b). This example using the Thingmuli lavas is rather simplified in that in performing the calculations we have not considered the precipitation of the spinel phase, which is invariably the earliest phase to crystallize in almost all basic liquids, and accordingly we have not altered the liquid composition to account for its precipitation. Our neglect of the spinels is preliminary, and is due in part to the complexity of the activity/composition model for this phase (Appendix 1).

In nature the Thingmuli lava series range from olivine tholeiites, through tholeiites, basaltic-andesites to icelandites and eventually to the silicic end-member, rhyodacite (Fig. 8). They form a distinctive iron-rich

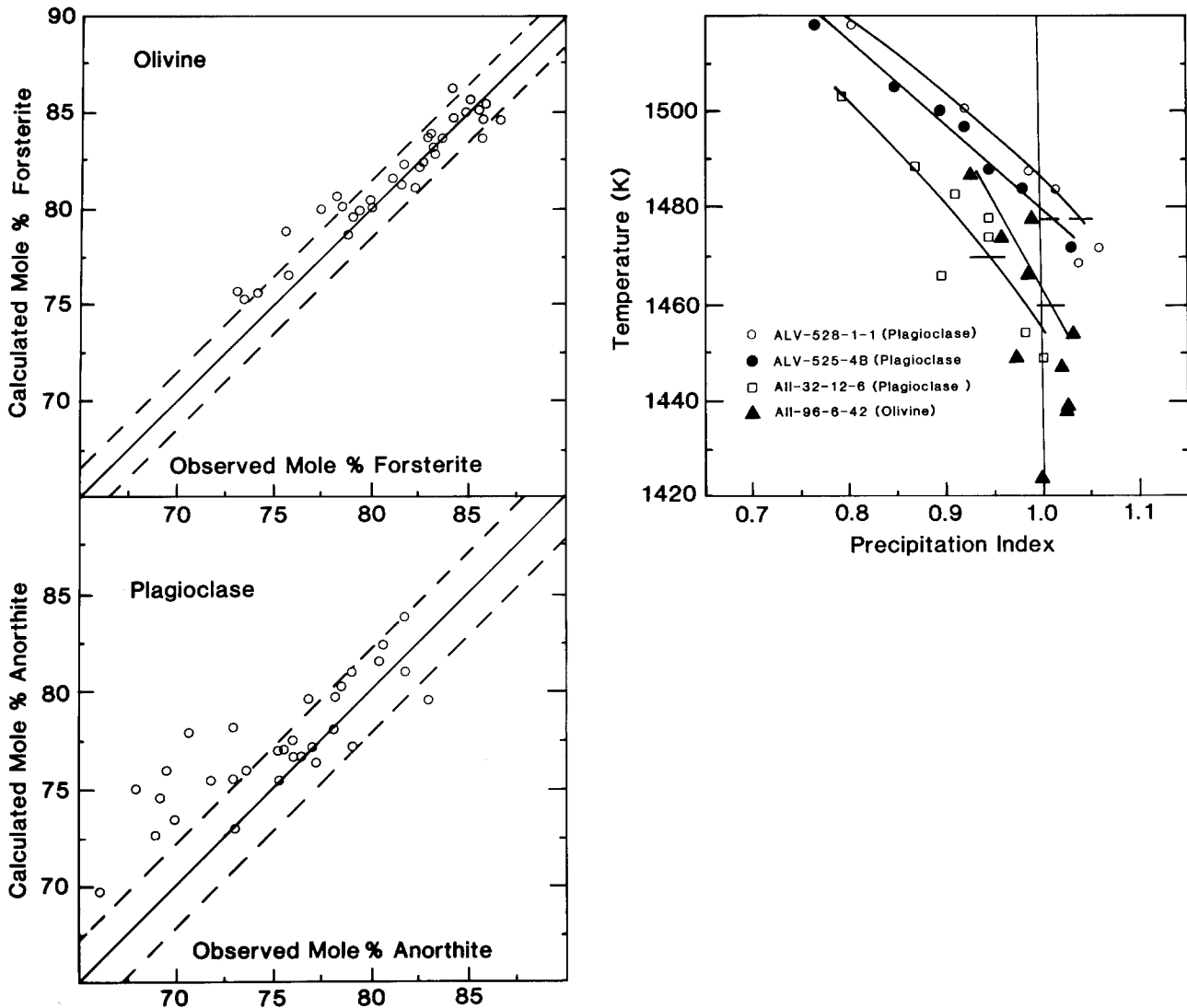


Fig. 7. Left: Calculated olivine (top) and plagioclase (bottom) compositions plotted against the observed compositions of these phases found in the solid-liquid experiments of Grove and Bryan (1983). The solid lines of unit slope indicate perfect agreement. The dotted lines refer to \pm one standard deviation in the composition of the solid that is attributable to analytical uncertainty (1.5% Fo, 2.2% An, see text). Right: The precipitation index (Σ_ϕ) for liquids saturated and undersaturated with plagioclase and olivine plotted against experimental temperature. Values of Σ_ϕ less than unity indicate undersaturation, greater than unity, supersaturation. Horizontal lines indicate the approximate experimentally determined saturation temperature. Compare these to the temperatures indicated by the intersection of the solid lines with the vertical line where Σ_ϕ equals unity (the predicted saturation surface)

series which have iron-titanium oxides among the early crystallizing phenocryst assemblage of olivine and plagioclase, contained in a groundmass of augite, pigeonite, plagioclase, Fe-Ti oxides and glass. The quench temperature deduced from the composition of the iron-titanium oxide micro phenocrysts (Buddington and Lindsley 1964) for the olivine tholeiites and tholeiites (open triangles in Fig. 8) refer to temperatures above which only plagioclase, olivine and occasional augite occur as early crystallizing phases. We have not predicted liquidus compositions for either augite or pigeonite, since for both minerals there is no detailed activity/composition model relating the minor constituents such as Al, Ti and Fe^{+3} (e.g. Sack and Carmichael 1983) with the major cations Ca, Mg and Fe^{+2} . In general, the monoclinic pyroxenes display such a subtle diversity of composition that we are unable yet to recalculate from the liquid/solid experiments

the complete composition of an augite, given just the composition of its coexisting liquid and the temperature.

The results of the calculations, at oxygen fugacities given by the QFM buffer, and at 1 bar are shown in Table 13 and in Fig. 8. In the olivine-tholeiites (nos 1 and 2) olivine appears before plagioclase, whose calculated composition falls within the observed range of the plagioclase phenocrysts, whereas in the tholeiites (nos. 3 to 10), plagioclase precipitates before olivine. The calculated temperature for orthopyroxene crystallization (the orthopyroxene being always more Mg-rich than the olivine) is well below the Fe-Ti oxide quench temperatures, and thus if the orthopyroxene is considered as a proxy for pigeonite, is correctly predicted to be restricted to the groundmass. By and large the calculated composition of both plagioclase and olivine falls within the range found in nature. Both would undoubt-

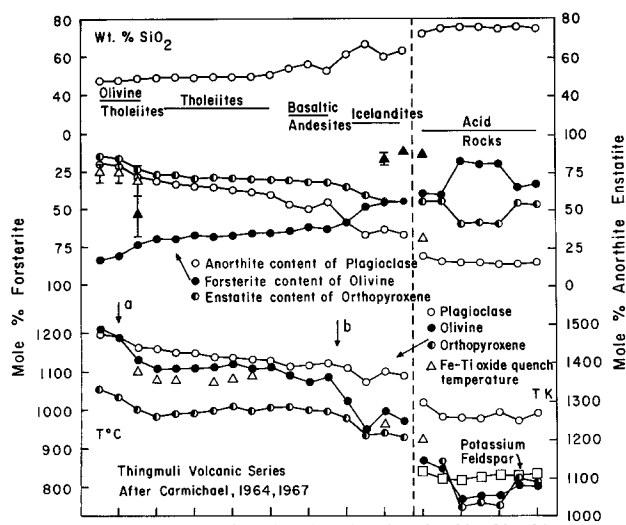


Fig. 8. Calculated first liquidus temperatures and mineral compositions for the Thingmuli volcanic series. Error bars on measured phenocryst compositions represent two standard deviations. Only the phases olivine, plagioclase and orthopyroxene were considered in the calculations

edly change composition slightly as a result of including spinel in the calculations. Olivine has not been found in several tholeiites, presumably because of a reaction relationship between olivine and liquid to stabilize Ca-poor pyroxene. This reaction has yet to be substantiated in the calculations.

In the more evolved basaltic-andesites (nos. 11, 12, 13), icelandites (nos. 14–17) and rhyodacite (no. 18), plagioclase is still the earlier silicate phase and in the more silica rich lavas (nos. 15, 16, 17) its calculated liquidus temperature is almost a hundred degrees above

that of olivine. This is an unlikely event for lavas with only sparse phenocrysts, and suggests that calculations at 1 bar may be inappropriate. The calculated olivine compositions tend to diverge from the observed more than is acceptable, presumably because the precipitation of augite and the Fe–Ti oxides, which we have neglected, has substantially altered the bulk liquid composition prior to their crystallization. The predicted liquidus temperatures of the observed phenocrysts of augite (Table 13) are consistent with the petrographic observation that spinel, plagioclase and augite crystallize prior to eruption and quenching of the groundmass Fe–Ti oxides. The agreement between observed and calculated plagioclase compositions in these siliceous lavas is poor, but unlikely to be close unless water and its effects were to be included in the calculations. We chose not to estimate these water contents for this calculation. The rhyodacite, no. 18, saturates with sanidine about 100° below the quench temperature, which is in accord with its absence as a phenocryst.

Overall, the calculated liquidus compositions and temperatures of the lavas shown in Table 13 and Fig. 8 represent a preliminary effort to determine the cooling history of a whole range of lavas. The agreement is good for the olivine tholeiites and tholeiites and worsens toward the more silica rich lavas. The experimental database upon which the solution model is calibrated contains so few experiments on liquids with greater than 65 wt. % SiO₂ and known amounts of dissolved water, that the calculations for phenocryst assemblages in silicic liquids are unlikely to be closely predicted even if appropriate estimates of the water contents of these magmas could be made. Perhaps the preliminary nature of these calculations highlights the need for experiments equilibrating solid assemblages of

Table 13. Calculated compositions and temperatures of early crystallizing phases, excluding oxides, of the Thingmuli, Iceland volcanic series, compared to compositions of observed phenocrysts (in parentheses) and Fe–Ti oxide quench temperatures. Data taken from Carmichael 1964, 1967b.

Anal. no.	Olivine			Plagioclase			<i>T</i> quench <i>K</i> ^a (Fe–Ti oxides)	Orthopyroxene			Clinopyroxene ^b
	<i>T</i> (K)	Mol%	(Obs. phen.)	<i>T</i> (K)	Mol%	(Obs. phen.)		<i>T</i> (K)	Mol%	(Obs. phen.)	
1	1,488	FO ₈₃	(FO ₈₃₋₇₄)	1,471	An ₈₁	(An ₈₁₋₆₈)	–	1,328	En ₈₆		
2	1,465	FO ₈₁	present	1,464	An ₇₉	(An ₈₁₋₆₈)	–	1,309	En ₈₃		
3	1,407	FO ₇₃	(FO ₇₅₋₅₅)	1,439	An ₇₂	(An ₈₀₋₆₀)	1,373	1,277	En ₇₇		
4	1,384	FO ₆₉	gdms.	1,436	An ₆₉		1,353	1,258	En ₇₃		
5	1,385	FO ₆₉	gdms.	1,426	An ₆₇		1,353	1,265	En ₇₃		
6	1,386	FO ₆₇		1,423	An ₆₆		–	1,267	En ₇₁		
7	1,389	FO ₆₈	gdms.	1,413	An ₆₅		1,348	1,273	En ₇₂		
8	1,397	FO ₆₇	gdms.	1,411	An ₆₃		1,358	1,284	En ₇₁		
9	1,383	FO ₆₆	–	1,407	An ₆₂		1,363	1,271	En ₇₀		
10	1,387	FO ₆₆	–	1,402	An ₆₀	–	–	1,282	En ₇₀		
11	1,365	FO ₆₄	–	1,389	An ₅₃	–	–	1,285	En ₆₉		
12	1,350	FO ₆₂	–	1,391	An ₅₀	–	–	1,277	En ₆₈		
13	1,363	FO ₆₃	–	1,397	An ₅₅	–	–	1,271	En ₆₈		
14	1,300	FO ₅₈	–	1,386	An ₄₂	(An ₅₈₋₄₂)	–	1,255	En ₆₅	(En ₅₁)	1,321 K
15	1,227	FO ₄₈	present	1,349	An ₃₃	(An ₅₂₋₄₁)	–	1,210	En ₅₉		
16	1,272	FO ₄₆	(FO ₂₀₋₁₂)	1,374	An ₃₇		1,238	1,215	En ₅₆		1,309
17	1,248	FO ₄₅	(FO ₁₃₋₉)	1,364	An ₃₃		–	1,205	En ₅₆		1,281
18	1,143	FO ₃₉	(FO ₃₃₋₉)	1,297	An ₁₉	(An ₃₁)	1,198	1,145	En ₅₅		1,154

^a Temperature derived from one-phase magnetites and ilmenites

^b Predicted equilibration temperatures from observed phenocryst compositions

known composition with water undersaturated liquids at low pressures (less than 10 kbars).

Conclusions

We have presented a new regular solution model for the free energy of mixing of natural silicate liquids. This represents a significant improvement over previous attempts (Ghiorso and Carmichael 1980) in that: 1) the model is calibrated from an experimental database of equilibrated liquid and solid compositions as a function of temperature, pressure and *oxygen fugacity*, 2) the liquid compositions span the compositional spectrum of basic lavas, the solids include a wide variety of igneous minerals and the component space is not restricted to a subset of natural liquids, and 3) the regression techniques used in the model calibration procedure incorporate numerical algorithms that insure that the values of the model parameters will be stable to minor fluctuations caused by experimental uncertainty in the database variables.

The model fits the experimental data to the level of uncertainty in the thermodynamic constants used in constructing the regression equations (± 500 cal). Though predominantly designed to treat anhydrous liquids, modifications to strict regular solution theory (Eqs. (A3-15) and (A3-16) in Appendix 3) allow additional model parameters to be extracted that adequately express (± 700 cal) experimental data on the solubility of H_2O in a number of liquids of basaltic to granitic compositions with up to 10 wt. % water. Solid/liquid equilibria in water-bearing siliceous lavas have also been modelled with more limited success.

The regular solution free energy of mixing model has numerous applications. It can be used as a solid/liquid geothermometer in calculating temperatures as a function of pressure and oxygen fugacity for the solid phases: olivine, plagioclase, orthopyroxene, clinopyroxene, spinel, rhombohedral oxides (hematite-ilmenite-geikielite solid solutions), leucite, melilite and potassium feldspar. It provides a means of estimating the activity of any liquid component (such as silica) as a function of T , P , f_{O_2} and bulk composition, irrespective of the presence or absence of solid phases. Additionally, limiting law activity coefficients can be estimated for minor components in solid phases that coexist with the liquid. Examples are provided in the text regarding the activity coefficient of the $KAlSi_3O_8$ component in plagioclase and the partial molar excess free energy ($RT \ln \gamma$) of the Mn_2SiO_4 component in olivine.

The shape of the excess free energy of mixing surface is characterized by a single strongly asymmetric multicomponent saddle point with no internal minima or maxima. The excess free energy in the compositional region of natural silicate liquids is quite negative (< -10 kcal). However, because of its asymmetry when combined with the symmetric ideal free energy of mixing surface the overall topology suggests the existence of liquid immiscibility. Calculations of the compositions of coexisting immiscible liquids for a wide variety of igneous rock compositions suggest that an immiscible dome in T -composition space underlies basic lavas and encompasses the liquidus compositions of most tholeiites. Predicted elemental partitioning trends

between coexisting immiscible liquids is in agreement with experimental and field evidence with the exception of CaO and TiO_2 which are predicted to partition into the SiO_2 rich phase. Quantitative agreement between prediction and experiment is difficult to judge under the "solid absent" constraint imposed upon the calculations. More sophisticated calculations, modelling the crystallization sequences of natural liquids – including the effects of immiscibility, fractionation and assimilation, await the development of numerical techniques and computer software for minimizing the total Gibbs free energy of a multiphase solid/liquid system subject to bulk composition constraints. Some results in this direction are presented, including the calculation of saturation compositions and temperatures for a suite of four experimentally investigated mid-ocean ridge basalts and for the Thingmuli volcanic series, but further work is needed to include the precipitation of spinels and Ca-rich pyroxenes.

Improvements to the solution model itself await the construction of a more extensive database for hydrous silicate liquids. In particular, coexisting solid/liquid compositions for water-undersaturated natural liquids, equilibrated at controlled oxygen fugacities, are badly needed. Though uncertainties in available anhydrous solid/liquid experimental data need to be reduced, particularly through interlab calibration of microprobe standards, a real need for better thermodynamic data on silicate liquids is obvious. Basic work on the compositional dependence of heat capacity and compressibility will test the validity of the regular solution approximation itself and better data on enthalpies of fusion will prevent the solution parameters from having to compensate for gross inconsistencies in the standard state chemical potentials of the liquid components. Such inconsistencies are currently thought to distort the topology of the free energy of mixing surface.

We have written a computer program (in FORTRAN IV) to perform all of the applications discussed in this paper. These include geothermometry, the calculation of liquid solution properties (e.g. activity of silica), the determination of the existence of two-phase immiscibility and the calculation of the compositions of these coexisting immiscible liquids, and liquid/solid solubility calculations including the prediction of the solid composition which would coexist with a given liquid, at equilibrium, at a specific T , P and f_{O_2} . A listing of the program is available from the first author. Copies on tape can also be provided at cost.

Appendix 1. Activity/composition relations in the solids

In the following summary of activity/composition relations adopted for the solid phases the notation a_i^j denotes the activity of the i^{th} solid component in the j^{th} mineral phase, γ_i^j the activity coefficient of the i^{th} atom on the j^{th} site, X_i^j the site mole fraction of the i^{th} atom on the j^{th} site, n_i^j the number of i atoms in the mineral formula per j^{th} site, n_i the number of i atoms in the mineral formula, R the gas constant in cal/bar-K and T the absolute temperature.

Olivine

The sub-regular solution model of Wood and Kleppa (1981) for the system Mg_2SiO_4 (forsterite)– Fe_2SiO_4 (fayalite) was used to extract the following expressions:

$$a_{\text{Mg}_2\text{SiO}_4}^{\text{Olivine}} = (X_{\text{Mg}}^{\text{Oct}} \gamma_{\text{Mg}}^{\text{Oct}})^2, \quad (\text{A1-1a})$$

$$a_{\text{Fe}_2\text{SiO}_4}^{\text{Olivine}} = (X_{\text{Fe}}^{\text{Oct}} \gamma_{\text{Fe}}^{\text{Oct}})^2 \quad (\text{A1-1b})$$

where

$$\gamma_{\text{Mg}}^{\text{Oct}} = \exp[2,000(1 - X_{\text{Mg}}^{\text{Oct}})(1 - X_{\text{Mg}}^{\text{Oct}})^2]/(RT) \quad (\text{A1-2a})$$

and

$$\gamma_{\text{Fe}}^{\text{Oct}} = \exp[1,000(1 + 2 X_{\text{Fe}}^{\text{Oct}})(1 - X_{\text{Fe}}^{\text{Oct}})^2]/(RT). \quad (\text{A1-2b})$$

Equation (A1-1) and (A1-2) demonstrate significant deviations from ideality for the Fe rich olivines over the temperature range of interest in this study.

Plagioclase

Solid-solution in the system $\text{NaAlSi}_3\text{O}_8$ (albite)– $\text{CaAl}_2\text{Si}_2\text{O}_8$ (anorthite) was taken to be ideal (Kerrick and Darken 1975):

$$a_{\text{NaAlSi}_3\text{O}_8}^{\text{Plagioclase}} = X_{\text{Na}}^A, \quad (\text{A1-3a})$$

$$a_{\text{CaAl}_2\text{Si}_2\text{O}_8}^{\text{Plagioclase}} = X_{\text{Ca}}^A. \quad (\text{A1-3b})$$

Recent work by Newton et al. (1980) on the excess enthalpy of mixing of plagioclase suggests the following expressions

$$a_{\text{NaAlSi}_3\text{O}_8}^{\text{Plag}} = X_{\text{Na}}^A (2 - X_{\text{Na}}^A) \exp[X_{\text{Ca}}^{2,A} (6,746 - 9,442 X_{\text{Na}}^A) / RT], \quad (\text{A1-4a})$$

$$a_{\text{CaAl}_2\text{Si}_2\text{O}_8}^{\text{Plag}} = \frac{1}{4} X_{\text{Ca}}^A (1 + X_{\text{Ca}}^A)^2 \exp[X_{\text{Na}}^{2,A} (2,025 + 9,442 X_{\text{Ca}}^A) / RT] \quad (\text{A1-4b})$$

which incorporate ideal entropy terms that account for the Al-avoidance model of high-temperature plagioclase. Calculations comparing the activity model posed by Eq. (A1-4) with that of (A1-3) as a function of temperatures and bulk composition demonstrate that deviations from ideality over the temperature/plagioclase composition range appropriate to this study are small (generally <5 mol %). In addition work by Henry et al. (1982) shows that the excess enthalpy of mixing demanded by Eq. (A1-4) necessitates an empirical “regular” excess entropy term in the liquid in order to satisfactorily compute the albite-anorthite binary liquidus loop. It is pointed out by these authors, however, that Bowen (1913) also computed the Ab–An loop, in agreement with experiment, assuming ideal mixing in both liquid and solid, though utilizing “fortuitously erroneous” enthalpies of fusion. As the liquid solution model adopted in this study allows extreme flexibility in our choice of enthalpies of fusion (through interdependencies with binary interaction parameters), but makes no provision for excess entropy terms of the form indicated by Henry et al. (1982), we have elected to adopt the Kerrick and Darken (1975) model in treating plagioclase solid solution.

Potassium feldspar

Consistent with our treatment of plagioclase, an ideal solution model was adopted for the activity of KAlSi_3O_8 (High sanidine) in potassium feldspar:

$$a_{\text{KAlSi}_3\text{O}_8}^{\text{Potassium Feld}} = X_{\text{K}}^A. \quad (\text{A1-5})$$

Orthopyroxene

Ghiorso and Carmichael (1980) adopted an ideal site mixing model for the orthopyroxene system MgSiO_3 (enstatite)– FeSiO_3 (ferrosilite) based upon Wood (1976) and Newton's (1976) treatment of diopside. They write:

$$a_{\text{MgSiO}_3}^{\text{Orthopyroxene}} = (X_{\text{Mg}}^{M1} X_{\text{Mg}}^{M2})^{1/2}, \quad (\text{A1-5a})$$

$$a_{\text{FeSiO}_3}^{\text{Orthopyroxene}} = (X_{\text{Fe}}^{M1} X_{\text{Fe}}^{M2})^{1/2} \quad (\text{A1-5b})$$

where

$$X_{\text{Mg}}^{M1} = n_{\text{Mg}}^{M1} / (n_{\text{Cr}} + \frac{1}{2} n_{\text{Al}} + n_{\text{Ti}} + n_{\text{Mg}}^{M1} + n_{\text{Fe}}^{M1}),$$

$$X_{\text{Mg}}^{M2} = n_{\text{Mg}}^{M2} / (n_{\text{Ca}} + n_{\text{Mn}} + n_{\text{Na}} + n_{\text{Mg}}^{M2} + n_{\text{Fe}}^{M2}),$$

$$X_{\text{Fe}}^{M1} = n_{\text{Fe}}^{M1} / (n_{\text{Cr}} + \frac{1}{2} n_{\text{Al}} + n_{\text{Ti}} + n_{\text{Mg}}^{M1} + n_{\text{Fe}}^{M1}),$$

$$X_{\text{Fe}}^{M2} = n_{\text{Fe}}^{M2} / (n_{\text{Ca}} + n_{\text{Mn}} + n_{\text{Na}} + n_{\text{Mg}}^{M2} + n_{\text{Fe}}^{M2}),$$

$$n_{\text{Mg}}^{M1} = \frac{R'}{2} (n_{\text{Ca}} + n_{\text{Mn}} + n_{\text{Na}} + n_{\text{Mg}} + n_{\text{Fe}} - n_{\text{Cr}} - n_{\text{Ti}} - \frac{1}{2} n_{\text{Al}}),$$

$$n_{\text{Mg}}^{M2} = n_{\text{Mg}} - n_{\text{Mg}}^{M1},$$

$$n_{\text{Fe}}^{M1} = n_{\text{Mg}}^{M1} \left(\frac{1}{R'} - 1 \right),$$

$$n_{\text{Fe}}^{M2} = n_{\text{Fe}} - n_{\text{Fe}}^{M1}$$

and

$$R' = n_{\text{Mg}} / (n_{\text{Mg}} + n_{\text{Fe}}).$$

Equations (A1-5) are consistent with the more elaborate treatment of Sack (1980) at the pyroxene equilibration temperatures appropriate to this study.

Clinopyroxene

The ideal site mixing model of Wood (1976) and Newton (1976) was used, modified to account for ferric iron-titanium coupling by calculating the amount of ferric iron in the analysis using the empirical relations of Sack (1982b). The activities of the end-member components $\text{CaMgSi}_2\text{O}_6$ (diopside) and $\text{CaFeSi}_2\text{O}_6$ (hedenbergite) were determined in the clinopyroxene. If Y_i denotes the number of i cations in the clinopyroxene formula calculated on a 4 cation basis, and if

$$M = (Y_{\text{Al}} - 2Y_{\text{Ti}} + Y_{\text{Na}} - Y_{\text{Cr}})$$

we have

$$Y_{\text{Fe}^{+++}} = 0.04M \quad \text{for } 0 \leq M < 0.05$$

$$Y_{\text{Fe}^{+++}} = 0.02 + 0.054(M - 0.05) \quad \text{for } 0.05 \leq M < 0.10$$

$$Y_{\text{Fe}^{+++}} = 0.0047 + 0.096(M - 0.10) \quad \text{for } 0.10 \leq M < 0.15$$

$$Y_{\text{Fe}^{+++}} = 0.0095 + 0.017(M - 0.15) \quad \text{for } 0.15 \leq M < 0.20$$

$$Y_{\text{Fe}^{+++}} = 0.018 + 0.24(M - 0.20) \quad \text{for } 0.20 \leq M < 0.25$$

$$Y_{\text{Fe}^{+++}} = 0.03 + 0.036(M - 0.25) \quad \text{for } 0.25 \leq M < 0.30$$

$$Y_{\text{Fe}^{+++}} = 0.048 + 0.48(M - 0.30) \quad \text{for } 0.30 \leq M < 0.35$$

and

$$Y_{\text{Fe}^{+++}} = M - 0.278 \quad 0.35 \leq M$$

$$Y_{\text{Fe}^{++}} = Y_{\text{Fe}} - Y_{\text{Fe}^{+++}}$$

From which it follows

$$a_{\text{CaMgSi}_2\text{O}_6}^{\text{Clinopyroxene}} = Y_{\text{Ca}} \frac{Y_{\text{Mg}}}{Y_{\text{Mg}} + Y_{\text{Fe}^{++}}} \cdot R', \quad (\text{A1-6a})$$

$$a_{\text{CaFe}^{++}\text{Si}_2\text{O}_6}^{\text{Clinopyroxene}} = Y_{\text{Ca}} \frac{Y_{\text{Fe}^{++}}}{Y_{\text{Mg}} + Y_{\text{Fe}^{++}}} \cdot R' \quad (\text{A1-6b})$$

where

$$R' = \frac{\frac{1}{2}(Y_{Mn} + Y_{Na} + Y_{Ca} + Y_{Fe^{+++}} + Y_{Mg})}{\left[\frac{1}{2}(Y_{Mn} + Y_{Na} + Y_{Ca} + Y_{Fe^{+++}} + Y_{Mg} + Y_{Ti} + Y_{Cr} + Y_{Ni} + Y_{Al/2})\right]^2}$$

Leucite

An ideal solution model was adopted:

$$a_{KAlSi_2O_6}^{Leucite} = X_K^A \quad (A1-7)$$

Melilite

Charlu et al. (1981) report a free energy of mixing for end-member akermanite ($Ca_2MgSi_2O_7$) and gehlenite ($Ca_2Al_2SiO_7$) in the melilite solid solution series:

$$\Delta G^{mix} = \Delta H^{ex} - T(S^{conf} - 2R X_{Ca_2MgSi_2O_7}^{Melilite} \ln 2)$$

where the excess enthalpy of mixing is given by the sub-regular solution expression

$$\Delta H^{ex} = 5,805(1 - X_{Ak}^{ML})(X_{Ak}^{ML})^2 + 120(X_{Ak}^{ML})(1 - X_{Ak}^{ML})^2 \quad (\text{cals})$$

and the configurational entropy by

$$S^{conf} = -R \left[X_{Ak}^{ML} \ln X_{Ak}^{ML} + X_{Ak}^{ML} \ln \left(\frac{X_{Ak}^{ML} + 2}{2} \right) + (2 - X_{Ak}^{ML}) \ln \left(\frac{2 - X_{Ak}^{ML}}{2} \right) + (1 - X_{Ak}^{ML}) \ln(1 - X_{Ak}^{ML}) \right]$$

We have calculated the quantity X_{Ak}^{ML} by assuming that Na, K, Sr and Ba are contained on the Ca sites, Mg, Fe^{++} , Mn, Ni and Co preferentially occupy the T1 site, the remainder being filled by Al with excess Al, Si, Ti, Fe^{+++} and Cr divided equally between the T2 and T3 sites. Thus

$$X = X_{Ca_2MgSi_2O_7}^{Melilite} = n_{Mg} / (n_{Mg} + \frac{1}{2}n_{Al} + n_{Fe^{++}} + \frac{1}{2}n_{Ti} + \frac{1}{2}n_{Fe^{+++}} + \frac{1}{2}n_{Cr} + n_{Mn} + n_{Ni} + n_{Co})$$

From the free energy of mixing one can show:

$$a_{Ca_2MgSi_2O_7}^{Melilite} = X(4 - X^2) \cdot \exp \left[-2(1 - X) + \frac{2X(1 - X)}{(X + 2)} + 11,610X(X - 1)^2/RT + 120(1 - 2X)(1 - X)^2/RT \right] \quad (A1-8)$$

Equation (A1-8) was adopted for the Mg-rich component of the melilites of this study.

Spinel

The activity/composition relations of Sack (1982a, expressions provided in Table II) were used to calculate the activities of Fe_3O_4 (magnetite), $MgAl_2O_4$ (spinel), Fe_2TiO_4 (ulvospinel), Mg_2TiO_4 and $FeAl_2O_4$ (hercynite) in the spinel phase. The relevant expressions for the activities are based upon a "Temkin" type model for the configurational entropy with a third degree Taylor's series expansion to describe the excess gibbs free energy of mixing. These are provided here in their explicit form: Let

$$X_1 \equiv X_{Fe(Al)_2O_4}^{spinel} = 1 - X_{Cr^{+3}}^{oct} - 2X_{Ti}^{oct} - X_{Mg}^{tet} - 2X_{Mg}^{oct} - X_{Fe^{+3}}^{tet}$$

$$X_2 \equiv X_{Mg(Al)_2O_4}^{spinel} = X_{Mg}^{tet} + 2X_{Mg}^{oct}$$

$$X_3 \equiv X_{Fe(Cr)_2O_4}^{spinel} = X_{Cr^{+3}}^{oct}$$

$$X_4 \equiv X_{Fe(Fe, Ti)_2O_4}^{spinel} = 2X_{Ti}^{oct}$$

and

$$X_5 \equiv X_{Fe^{+3}(Fe^{+3}, Fe^{+2})_2O_4}^{spinel} = X_{Fe^{+3}}^{tet}$$

where Fe^{+2} and Mg are assumed to be randomly distributed over tetrahedral and octahedral sites.

Then

$$a_{FeAl_2O_4}^{spinel} = (1 + X_4)(1 - X_2 + X_4)(1 - X_5)(1 - X_3 - X_4 - X_5)^2 \cdot \exp \left([(9,490 - 3.92T)X_2X_3 - 5,300X_2X_4 - (7,200 - 1.30T)X_2X_5 - 1,800X_2X_4(1 - 2X_4) + [(4,600 + 4,500(1 - X_3)]X_3^2 + [12,400 + 8,400(1 - X_4)]X_4^2 + [14,000 - 1,600(1 - X_5)]X_5^2 + 11,050X_3X_4 + 11,850X_3X_5 + 23,600X_4X_5]/RT \right) \quad (A1-9a)$$

$$a_{MgAl_2O_4}^{spinel} = X_2(1 - X_5)(1 - X_3 - X_4 - X_5)^2/(1 + X_4) \cdot \exp \left([(9,490 - 3.92T)(1 - X_2)X_3 + 5,300(1 - X_2)X_4 + (7,200 - 1.30T)(1 - X_2)X_5 + 1,800X_4[X_2X_4 + (1 - X_2)(1 - X_4)] + [4,600 + 4,500(1 - X_3)]X_3^2 + [12,400 + 8,400(1 - X_4)]X_4^2 + [14,000 - 1,600(1 - X_5)]X_5^2 + 11,050X_3X_4 + 11,850X_3X_5 + 23,600X_4X_5]/RT \right) \quad (A1-9b)$$

$$a_{Fe_2TiO_4}^{spinel} = (1 - X_2 + X_4)^2(1 - X_5)(X_4 + X_5)X_4/(1 - X_4)^2 \cdot \exp \left(-(9,490 - 3.92T)X_2X_3 + 5,300X_2(1 - X_4) - (7,200 - 1.30T)X_2X_5 + 1,800X_2(1 - X_4)(1 - 2X_4) + [4,600 + 4,500(1 - X_3)]X_3^2 + [16,600 - 8,400X_4](1 - X_4)^2 + [14,000 - 1,600(1 - X_5)]X_5^2 - 11,050X_3(1 - X_4) + 11,850X_3X_5 - 23,600(1 - X_4)X_5]/RT \right) \quad (A1-9c)$$

$$a_{Mg(Mg, Ti)_2O_4}^{spinel} = X_2^2(1 - X_5)(X_4 + X_5)X_4/(1 + X_4)^2 \cdot \exp \left((9,490 - 3.92T)(2 - X_2)X_3 - 5,400(2 - X_2)(1 - X_4) + (7,200 - 1.30T)(2 - X_2)X_5 + 1,800(1 - X_4)(X_2 + 2X_4 - 2X_2X_4) + [4,600 + 4,500(1 - X_3)](X_3)^2 + [16,600 + 8,400X_4](1 - X_4)^2 + [14,000 - 1,600(1 - X_5)]X_5^2 - 12,650X_3(1 - X_4) + 11,850X_3X_5 - 23,600(1 - X_4)X_5]/RT \right) \quad (A1-9d)$$

$$a_{Fe_3O_4}^{spinel} = (1 - X_2 + X_4)(X_4 + X_5)X_5^2/(1 + X_4) \cdot \exp \left(-(9,490 - 3.92T)X_2X_3 - 5,400X_2X_4 + (7,200 - 1.30T)X_2(1 - X_5) - 1,800X_2X_4(1 - 2X_4) + [4,600 + 4,500(1 - X_3)]X_3^2 + [12,400 + 8,400(1 - X_4)]X_4^2 + [13,200 + 1,600X_5](1 - X_5)^2 + 11,050X_3X_4 - 11,850X_3(1 - X_5) - 23,600X_4(1 - X_5)]/RT \right) \quad (A1-9e)$$

Rhombohedral oxides

The asymmetric ternary solution parameters of Anderson and Lindsley (1981, Table 1) were used to compute activity-composition relations in the system Fe_2O_3 (hematite)– FeTiO_3 (ilmenite)– MgTiO_3 (geikielite). If Y_i represents the number of cations on a two cation basis, adopting

$$X_{\text{Fe}_2\text{O}_3}^{\text{rhom}} = \frac{1}{2} Y_{\text{Fe}^{++}},$$

$$X_{\text{FeTiO}_3}^{\text{rhom}} = Y_{\text{Fe}^{++}},$$

$$X_{\text{MgTiO}_3}^{\text{rhom}} = Y_{\text{Mg}}$$

then from the expressions for the activity coefficients provided by Anderson and Lindsley (1981):

$$a_{\text{Fe}_2\text{O}_3}^{\text{rhom}} = \gamma_{\text{Fe}_2\text{O}_3}^{\text{rhom}} X_{\text{Fe}_2\text{O}_3}^{\text{rhom}}, \quad (\text{A1-10a})$$

$$a_{\text{FeTiO}_3}^{\text{rhom}} = \gamma_{\text{FeTiO}_3}^{\text{rhom}} X_{\text{FeTiO}_3}^{\text{rhom}}, \quad (\text{A1-10b})$$

$$a_{\text{MgTiO}_3}^{\text{rhom}} = \gamma_{\text{MgTiO}_3}^{\text{rhom}} X_{\text{MgTiO}_3}^{\text{rhom}} \quad (\text{A1-10c})$$

Quartz

The quartz activity was taken to be the mole fraction of SiO_2 :

$$a_{\text{SiO}_2}^{\text{quartz}} = X_{\text{SiO}_2}^{\text{quartz}}. \quad (\text{A1-11})$$

Appendix 2. Thermodynamic data and methods of calculation

In this appendix we present thermodynamic data, equations and relevant assumptions used in evaluating equilibrium constants, K , for reactions discussed in the text of the form:

$$M = \sum_i \nu_i C_i \quad (\text{A2-1})$$

(end-member component of a mineral solid solution) (liquid components used to describe composition of the silicate liquids).

The ν_i 's in Eq. (A2-1) are the stoichiometric numbers of each of the C_i components in the formula of M . The law of mass action for reaction (A2-1) can be written:

$$\begin{aligned} RT \ln K &= -\Delta G_{T,P}^{\text{reaction}} \\ &= -\left(\sum_i \nu_i \Delta G_{T,P}^{\text{app},i} - \Delta G_{T,P}^{\text{app},M} \right) \end{aligned} \quad (\text{A2-2})$$

where $\Delta G_{T,P}^{\text{app},i}$ and $\Delta G_{T,P}^{\text{app},M}$ refer to the apparent Gibbs free energies of formation at the equilibrium temperature (T) and pressure (P) of the i^{th} liquid component and the solid component respectively. For the solid phase we have adopted an expression for the heat capacity of the form:

$$C_p^s = a^s + b^s T + c^s/T^2 + d^s/T^{1/2} \quad (\text{A2-3})$$

which permits the evaluation of $\Delta G_{T,P}^{\text{app},M}$:

$$\Delta G_{T,P}^{\text{app},M} = \Delta H_{T,P}^{\text{app},M} - TS_{T,P}^M + \int_{P_r}^P V_T^M(P) dP \quad (\text{A2-4})$$

where

$$\begin{aligned} \Delta H_{T,P}^{\text{app},M} &= \Delta H_{T_r,P_r}^f + a^s(T - T_r) + \frac{b^s}{2}(T^2 - T_r^2) \\ &\quad - c^s(1/T - 1/T_r) + 2d^s(T^{1/2} - T_r^{1/2}), \end{aligned} \quad (\text{A2-5})$$

$$\begin{aligned} S_{T_r,P_r}^M &= S_{T_r,P_r}^M + a^s \ln(T/T_r) + b^s(T - T_r) \\ &\quad - c^s/2(1/T^2 - 1/T_r^2) - 2d^s(1/T^{1/2} - 1/T_r^{1/2}), \end{aligned} \quad (\text{A2-6})$$

and

$$\begin{aligned} \int_{P_r}^P V_T^s(P) dP &= V_{T_r,P_r}^s \frac{1}{\beta} (1 - \exp(-\beta(P - P_r))) \quad \text{if } \beta > 0 \\ &= V_{T_r,P_r}^s (P - P_r) \quad \text{if } \beta = 0 \end{aligned} \quad (\text{A2-7})$$

with

$$V_{T_r,P_r}^s = V_{P_r,T_r}^s \exp[\alpha_a^s(T - T_r) + \alpha_b^s/2(T^2 - T_r^2)]. \quad (\text{A2-8})$$

In Eqs. (A2-4) through (A2-8) H denotes enthalpy; S , entropy; V , volume; β the compressibility $\left[-1/V \left(\frac{\partial V}{\partial P} \right)_T \right]$; and α the thermal coefficient of expansion $\left[1/V \left(\frac{\partial V}{\partial T} \right)_P \right]$ which we express as:

$$\alpha = \alpha_a + \alpha_b T. \quad (\text{A2-9})$$

The superscript, f , denotes formation from the elements and the quantities T_r and P_r the reference temperatures and pressures, respectively, which we have chosen to be 298.15 K and 1.013 bars. The data and their sources for the evaluation of Eqs. (A2-4)–(A2-9) for all the solid phase components considered in this study are compiled in Tables (A2-1) and (A2-2). These have been selected to be most applicable to the temperature/pressure range of interest. Preference has been given to calorimetrically determined quantities. Internal consistency has been achieved by adjusting the $\Delta H_{T_r,P_r}^f$ as indicated in Table (A2-1). The method involved will be discussed below.

Each $\Delta G_{T,P}^{\text{app},i}$ of Eq. (A2-2) has been computed from:

$$\Delta G_{T,P}^{\text{app},i} = \Delta H_{T_r,P_r}^{\text{app},i} - TS_{T_r,P_r}^{\text{app},i} + \int_{P_r}^P V_T^i(P) dP \quad (\text{A2-10})$$

where

$$\begin{aligned} \Delta H_{T_r,P_r}^{\text{app},i} &= \Delta H_{T_r,P_r}^{f,i(s)} + a^{i(s)}(T_m^i - T_r) + \frac{b^{i(s)}}{2}(T_m^{2i} - T_r^2) \\ &\quad - c^{i(s)}(1/T_m^i - 1/T_r) + 2d^{i(s)}(T_m^{1/2} - T_r^{1/2}) \\ &\quad + \Delta H_{T_m^i,P_r}^{\text{fusion},i} + C_p^i(T - T_m^i), \end{aligned} \quad (\text{A2-11})$$

$$\begin{aligned} S_{T_r,P_r}^i &= S_{T_r,P_r}^{i(s)} + a^{i(s)} \ln(T_m^i/T_r) + b^{i(s)}(T_m^i - T_r) \\ &\quad - c^{i(s)}/2(1/T_m^{i2} - 1/T_r^2) - 2d^{i(s)}(1/T_m^{1/2} - 1/T_r^{1/2}) \\ &\quad + \Delta S_{T_m^i,P_r}^{\text{fusion},i} + C_p^i \ln(T/T_m^i) \end{aligned} \quad (\text{A2-12})$$

and

$$\begin{aligned} \int_{P_r}^P V_T^i(P) dP &= V_{P_r,T}^i \left[(P - P_r) - \frac{1.0 \times 10^{-6}}{0.7551 + 2.76 V_{P_r,T}^i/n_i} \right. \\ &\quad \cdot \left. \left[\frac{1}{2}(P^2 - P_r^2) - \frac{1.0 \times 10^{-6}}{0.7551 + 2.76 V_{P_r,T}^i/n_i} \frac{1}{2} P^2 \right] \right. \\ &\quad \left. \cdot \frac{1}{6}(P^3 - P_r^3) \right] \end{aligned} \quad (\text{A2-13})$$

with

$$V_{P_r,T}^i = V_{0K}^i + V_a^i T + V_b^i T^2 \quad (\text{A2-14})$$

except for

$$\int_{P_r}^P V_T^{\text{SiO}_2}(P) dP = V_{P_r,T}^{\text{SiO}_2}(P - 1) - 4.204 \times 10^{-6}(P^2 - P_r^2). \quad (\text{A2-15})$$

Table A2-1. Enthalpies of formation: solid phases

	$\Delta H_f^{(s, 298.1 \text{ bar})}$ cal/s	ref	+/-	Adjusted $\Delta H_f^{(s, 298.1 \text{ bar})}$ cal/s	Δ
Forsterite	- 518731	(1)	317	- 518350	- 381
Fayalite	- 353576	(1)	576	- 352370	-1206
Tephroite	- 413020	(1)	760	- 413020	
Albite	- 937916	(1)	870	- 938700	784
Anorthite	-1014110	(1)	747	-1013700	- 410
Sanidine	- 946358	(1)	805	- 945800	- 558
Enstatite	- 369921	(1)	290	- 369640	- 281
Ferrosilite	- 284734	(10, 2)		- 283920	- 814
Diopside	- 767390	(1)	2180	- 765570	-1820
Hedenbergite	- 678496	(6)		- 680490	1994
Leucite	- 730826	(1, 2)	658	- 728830	-1996
Akermanite	- 926511	(1)	676	- 927430	919
Magnetite	- 284927	(1, 2)	500	- 284630	- 297
Spinel	- 549551	(1)	179	- 551400	1849
Hercynite	- 470000	(1)	2032	- 468730	-1270
Ulvospinel	- 356758	(11)		- 358160	1402
Di-Mg-Titanate	- 517300	(8)	1500	- 513440	-3860
Hematite	- 194334	(1, 2)	300	- 194330	-4
Ilmenite	- 295560	(1)	380	- 296700	1140
Magnesiotitanate	- 375850	(8)	1500	- 375580	- 270
β -quartz	- 220772	(1, 2)	239	- 218140	-2632

- (1) Robie et al. 1978
- (2) Entropy consistent with metastable high T form. C_p extrapolated to 298 K. Tabulation of data in this manner alleviates need to compute low T phase transitions below working temperatures
- (3) $/T$. C_p for high T form stable above T (K)
- (4) Refitted to Meyer-Kelley form to increase extrapolative stability
- (5) Ghiorso and Carmichael 1980
- (6) Helgeson et al. 1978
- (7) Kelley 1960
- (8) Stull and Prophet 1971
- (9) Calculated from $\rho=3.895$ g/cc and MW=120.22 g/mol
- (10) Estimated from the log K for the reaction $\text{Fe}_2\text{SiO}_4(\text{fa}) + \text{SiO}_2(\beta\text{-qtz}) \rightleftharpoons 2\text{FeSiO}_3(\text{ferrosilite})$ reported in Carmichael and Ghiorso (in prep.) and the data reported above for β -quartz and fayalite. $\text{Log } K = 0.2070 - 205.1/T$
- (11) Carmichael and Ghiorso, in prep. $V_{\text{ferrosilite}} = 0.77862 + 3.0567 \times 10^{-5} T + 6.3138 \times 10^{-10} T^2$; T in K
- (12) Ghiorso et al. 1979
- (13) Birch 1966
- (14) Skinner 1966 (refitted)
- (15) Chase et al. 1974

Table A2-2. Thermodynamic data: solid phases

	$S_{298}^{(s)}$	$V_{298}^{(s)}$	$\alpha^{(s)}$ K^{-1}					
	cal/K-mol	ref	cal/bar-mol					
			$a \times 10^5$					
			$bT \times 10^8$					
Forsterite	Mg_2SiO_4	22.75	(1)	1.0466	(1)	2.1171	2.5000	(14)
Fayalite	Fe_2SiO_4	35.45	(1)	1.1088	(1)	2.6634	0.5000	(14)
Tephroite	Mn_2SiO_4	39.01	(1)	1.1618	(1)			
Albite	$\text{NaAlSi}_3\text{O}_8$	54.11	(1)	2.4003	(1)	1.4378	1.8750	(14)
Anorthite	$\text{CaAl}_2\text{Si}_2\text{O}_8$	47.63	(1)	2.4089	(1)	-0.14630	2.0000	(14)
Sanidine	KAlSi_3O_8	55.66	(1)	2.6064	(1)			
Enstatite	MgSiO_3	16.22	(1)	0.75220	(1)	2.2269	1.0000	(14)
Ferrosilite	FeSiO_3	23.66	(10,2)	0.78779	(11)	3.9258	0.080608	(11)
Diopside	$\text{CaMgSi}_2\text{O}_6$	34.20	(1)	1.5796	(1)	2.1269	1.0000	(14)
Hedenbergite	$\text{CaFeSi}_2\text{O}_6$	40.70	(6)	1.6533	(6)			
Leucite	KAlSi_2O_6	34.16	(1, 2)	2.1126	(1)			
Akermanite	$\text{Ca}_2\text{MgSi}_2\text{O}_7$	50.03	(1)	2.2182	(1)			
Magnetite	Fe_3O_4	-12.34	(1, 2)	1.0641	(1)			
Spinel	MgAl_2O_4	19.27	(1)	0.97395	(1)			
Hercynite	FeAl_2O_4	25.40	(1)	0.97395	(1)			
Ulvospinel	Fe_2TiO_4	40.36	(1)	1.1327	(11)			
Di-mg titanate	Mg_2TiO_4	27.51	(8)					
Hematite	Fe_2O_3	30.37	(1, 2)	0.72360	(1)			
Ilmenite	FeTiO_3	25.30	(1)	0.75740	(1)			
Magnesiotitanate	MgTiO_3	17.82	(8)					
β -quartz	SiO_2	8.925	(1, 2)	0.57926	(12)	-3.8564	3.8518	(12)

References as on Table A2-1.

Table A2-3. Enthalpies of formation

	$\Delta H_f^{(s, 298, 1 \text{ bar})}$ cal/s reported	ref	+/-	Adjusted $\Delta H_f^{(s, 298, 1 \text{ bar})}$ cal/s	Δ
Si ₄ O ₈	- 865704	(2, 1)	2000	- 867448	1744
Ti ₄ O ₈	- 903204	(1)	2000	- 909543	6339
Al _{1.6/3} O ₈	- 1067995	(1)	803	- 1069406	1411
Fe _{1.6/3} O ₈	- 518224	(2, 1)	800	- 519023	799
Cr _{1.6/3} O ₈	- 723200	(1)	5333	- 723200	-
Fe ₄ Si ₂ O ₈	- 707152	(1)	1152	- 704730	-2422
Mn ₄ Si ₂ O ₈	- 826038	(1)	1520	- 826038	-
Mg ₄ Si ₂ O ₈	- 1037462	(1)	634	- 1036701	- 761
Ca ₄ Si ₂ O ₈	- 1110620	(2, 1)	1540	- 1109070	- 1550
Na _{1.6/3} Si _{8/3} O ₈	- 988667	(8)	2667	- 987623	- 1044
K _{1.6/3} Si _{8/3} O ₈	- 986667	(15)	5333	- 990064	3397
P _{1.6/5} O ₈	- 575488	(1)	1606	- 575488	-
Sr ₈ O ₈	- 1129048	(1)	1759	- 1129048	-

References as on Table A2-1

The notation for Eqs. (A2-10) to (A2-15) is identical to that of Eqs. (A2-4) to (A2-9). In addition T_m^i denotes the temperature of melting (fusion) of the i (s) solid going to the i^{th} liquid. The i (s) solids were selected to be the stable form (minerals if possible) at T_r , P_r here 298.15 K and 1.013 bars. Equation (A2-13) is the integrated form of

$$V_T^i(P) = V_{T_r, P_r}^i \left(1 - \frac{1.0 \times 10^{-6}}{0.7551 + 2.76 V_{P_r, T_r}^i / n_i} \right) \cdot \left[P - \frac{1.0 \times 10^{-6}}{0.7551 + 2.76 V_{P_r, T_r}^i / n_i} \frac{1}{2} P^2 \right] \quad (\text{A2-15})$$

where n_i is the number of atoms in the formula unit of the i^{th} component. Equation (A2-15) was calibrated by examining the pressure dependence of liquid volumes deduced from an examination of available fusion curves.

The data and their sources for the evaluation of Eqs. (A2-10)–(A2-15) for all the liquid components considered in this study are compiled in Tables (A2-3) through (A2-5). The

criteria used in selecting entries for Tables (A2-3) and (A2-4) are identical to those for the solid components of the mineral phases, discussed above. The enthalpies of formation have been adjusted to achieve internal consistency as described below. The thermodynamic data for the liquids (Table A2-5) are much more poorly known; in particular high uncertainties exist in entropies and hence enthalpies of fusion ($\Delta H_{T_m, P_r}^{\text{fusion}, i} = T_m^i \Delta S_{T_m, P_r}^{\text{fusion}, i}$). The data of Table (A2-5) are consistent with available fusion curves for naturally occurring silicates (see Ghiorso and Carmichael 1980). Fortunately, the sensitivity of the results of the present modelling to large uncertainties in the liquid thermodynamic properties is small. These uncertainties translate directly into the interaction parameters (Table A4-3) extracted from the experimental data. This allows the magnitude of the individual interaction parameters to vary monotonically with changes in the enthalpies of fusion while altering the overall solution model but slightly. Thus attempts to render the data of Table (A2-5) internally consistent by adjusting $\Delta S_{T_m, P_r}^{\text{fusion}}$ proved irresolvable.

$\beta^{(s)} \text{ bars}^{-1}$		$Cp^{(s)} \text{ Cals/K-mol}$				ref
$\times 10^6$	ref	a	$b \times 10^3 T$	$c \times 10^{-5} / T^2$	d/\sqrt{T}	
0.79	(13)	54.489	0.81594	- 2.1366	-416.97	(1)
0.91	(13)	36.510	9.3600	- 6.7000		(6)
		39.255	3.7477	- 9.1147		(1, 4)
1.48	(5)	67.329	8.9172	- 20.354		(1, 4)
1.50	(13)	63.311	14.794	- 15.440		(6)
1.82	(13)	65.908	10.209	- 19.324		(1, 4)
1.01	(13)	49.130	- 3.0583	2.8504	- 549.16	(1)
1.00	(11)	21.000	9.0000			(6, 3/413)
1.07	(13)	52.870	7.8400	- 15.700		(6)
		54.810	8.1700	- 15.010		(6)
		46.958	6.6123	29.304		(1, 3/955)
		60.090	11.400	- 11.400		(6)
0.56	(13)	23.141	12.604	134.83		(1, 3/848)
0.41	(13)	53.277	1.4643	- 4.0289	- 370.75	(1)
0.41	(assumed = to spinel)	53.788	2.6660	- 2.1705	- 369.41	(1, spinel-MgO + FeO)
		33.340	15.080	- 3.4000		(7)
		36.380	8.1730	- 7.2577		(8, fitted)
0.60	(13)	- 261.88	65.170	- 244.72	8116.6	(1, 3/950)
0.56	(13)	- 0.71451	15.547	- 12.203	579.97	(1)
		28.280	3.2900	- 6.6047		(8, fitted)
0.92887	(12, 1000 K)	14.084	2.3975			(12, 3/848)

Table A2-4. Thermodynamic properties: units: cal/K-mol

	$S_{298}^{(s)}$		$C_p^{(s)}$				
			a	$b \times 10^3 T$	$c \times 10^{-5}/T^2$	d/\sqrt{T}	
Si ₄ O ₈ (cristobalite)	48.61	(2, 1)	69.556	1.2432	-39.503	0.0	(1,3/523)
Ti ₄ O ₈ (rutile)	48.08	(1)	60.304	10.810	-9.4289	-5.3692	(1)
Al _{16/3} O ₈ (α -corundum)	32.45	(1)	100.293	0.45827	-12.090	-629.73	(1)
Fe _{16/3} O ₈ (hematite)	80.99	(2, 1)	-698.32	173.79	-65.259	21644.0	(1, 3/950)
Cr _{16/3} O ₈ (eskolaitite)	51.73	(1)	75.856	0.60525	-9.1899	-2.1698	(1)
Fe ₄ Si ₂ O ₈ (fayalite)	70.90	(1)	73.020	18.720	-1.3400	0.0	(2)
Mn ₄ Si ₂ O ₈ (tephroite)	78.02	(1)	78.510	7.4953	-18.229	0.0	(1, 4)
Mg ₄ Si ₂ O ₈ (forsterite)	45.50	(1)	108.977	1.6319	-4.2733	-833.94	(1)
Ca ₄ Si ₂ O ₈ (β -larnite)	36.44	(1, 2)	98.000	0.0	0.0	0.0	(1, 3/1800)
Na _{16/3} Si _{8/3} O ₈	72.56	(4)	83.040	25.600	-17.253	0.0	(7)
K _{16/3} Si _{8/3} O ₈	93.15	(4)	79.280	44.933	-9.5467	0.0	(7)
P _{16/5} O ₈	44.18	(1)	13.400	86.402	0.0	0.0	(1)
Sr ₈ O ₈	106.16	(1)	106.44	10.443	-5.3164	-289.14	(1)

Sources: As on Table A2-1

Table A2-5. Thermodynamic properties

	T_m (K)		ΔS_f		C_p^l	V^l				
			[cal/mol-K]			a cal/mol-bar	$b \times 10^4$ cal/mol-bar-K			
Si ₄ O ₈ (cristobalite)	1,996	(3)	3.908	(3)	83.16	(2)	2.604	(1)	-0.1294	(1)
Ti ₄ O ₈ (rutile)	2,143	(4)	39.20	(4)	106.96	(2)	1.202	(1)	5.740	(1)
Al _{16/3} O ₈ (α -corundum)	2,327	(5)	32.08	(5)	65.71	(2)	1.767	(1)	3.397	(1)
Fe _{16/3} O ₈ (hematite)	1,895	(3)	34.80	(11)	122.27	(12)	2.173	(1)	3.659	(1)
Cr _{16/3} O ₈ (eskolaitite)	2,603	(6)	31.76	(6)	100.00	(6)	1.854	(9)		
Fe ₄ Si ₂ O ₈ (fayalite)	1,490	(3)	29.57	(3)	114.60	(2)	1.920	(1)	2.834	(1)
Mn ₄ Si ₂ O ₈ (tephroite)	1,620	(3)	26.46	(3)	116.20	(3)	2.584	(9)		
Mg ₄ Si ₂ O ₈ (forsterite)	2,163	(10)	37.61	(10)	128.06	(2)	2.238	(1)	0.8797	(1)
Ca ₄ Si ₂ O ₈ (β -larnite)	2,403	(1)	20.81	(12)	118.96	(2)	1.859	(1)	5.923	(1)
Na _{16/3} Si _{8/3} O ₈	1,362	(4)	24.24	(4)	113.01	(2)	2.859	(1)	4.170	(1)
K _{16/3} Si _{8/3} O ₈	1,249	(4)	25.62	(4)	114.67	(2)	3.456	(1)	7.138	(1)
P _{16/5} O ₈	853	(8)	10.68	(8)	93.60	(2)	2.272	(9)		
Sr ₈ O ₈	2,938	(3)	49.02	(3)	128.00	(6)	3.955	(9)		

- (1) Regressed from data in Table 3 of Nelson and Carmichael 1979 and Table 3 of Mo et al. 1982, $V^{\text{mixing}} = 0$
- (2) Carmichael et al. 1977
- (3) Robie et al. 1978
- (4) Stull and Prophet 1971
- (5) Chase et al. 1974
- (6) Chase et al. 1975
- (7) Chase et al. 1978
- (8) Extracted from Hill et al. (1944) through application of freezing point depression equation
- (9) V^l assumed equal to V^s at 298.15 K, 1 bar. Data from Robie et al. 1978
- (10) Ghiorsio and Carmichael 1980
- (11) Estimated from ΔS_f of FeO, Wustite and Magnetite reported by Robie et al. 1978, by plotting $\Delta S_f/g\text{-atom}$ against the Fe/O ratio in the solid and extrapolating to Fe₂O₃ with a straight line
- (12) Estimated

Internal consistency of enthalpies of formation

The enthalpies of formation ($\Delta H_{T_r, P_r}^f, M$ and $\Delta H_{T_r, P_r}^{f, (s)}$) of Tables (A2-1) and (A2-3) were adjusted (generally within their uncertainty, as indicated) for internal consistency between the thermodynamic and experimental data and the solution model. This was performed by forcing the *average* deviation of each solid component - liquid equilibria from the modelled free energy surface to zero using the following method. For any M (Eq. A2-1) used in calibrating the model the left-hand side of Eq. (A2-2) can be predicted from the experimentally determined composition of the solid solution involving M

and its coexisting liquid, the activity/composition relations of Appendix 1 and the interaction parameters of Table (A4-3) - see Eq. (17) of the text. Let us call this predicted quantity $RT \ln K'$ which is just a measure, in calories, of the deviation of this particular experimental result from the calibrated solution model. In the vernacular of least squares it represents a residual. Now if the solution model works equally well, on average, in predicting liquid/solid equilibria for any M (that is the residuals are randomly distributed about the data base) then the quantity

$$RT \ln K - RT \ln K' \quad (\text{A2-16})$$

should on average be zero for any M . It must by definition be zero for the sum of all M 's used to calibrate the model (i.e. the sum of the positive must equal the sum of the negative residuals). We have attributed average deviations of the form of Eq. (A2-16) to inconsistencies amongst the thermodynamic data with the largest uncertainties, that is the reported enthalpies of formation of Tables (A2-1) and (A2-3). Let the average deviation due to individual residuals of the form (A2-16) for the M^{th} solid component be denoted: ΔH_M^{err} , then from Eq. (A2-2) we may write a statement like

$$\Delta H_M^{\text{err}} = \sum_i v_i \Delta H_{T_r, P_r}^{\text{corr}, f, i} - \Delta H_{T_r, P_r}^{\text{corr}, f, M} \quad (\text{A2-17})$$

for each of the M solid components. Inspection of Table (A2-1) will reveal that 20 statements of Eq. (A2-17) can be constructed from the residuals of a least squares calibration of the solution model. These 20 equations involve 29 variables ($20 \Delta H_{T_r, P_r}^{\text{corr}, f, M}$ and $9 \Delta H_{T_r, P_r}^{\text{corr}, f, i}$). In addition coexistence between orthopyroxene and olivine in some experimental charges provided two more statements like Eq. (A2-17) involving $\Delta H_{T_r, P_r}^{\text{corr}, f, \text{Si}_2\text{O}_6}$, $\Delta H_{T_r, P_r}^{\text{corr}, f, \text{enstatite}}$, $\Delta H_{T_r, P_r}^{\text{corr}, f, \text{forsterite}}$, $\Delta H_{T_r, P_r}^{\text{err}}$, $\Delta H_{T_r, P_r}^{\text{corr}, f, \text{ferrosillite}}$, $\Delta H_{T_r, P_r}^{\text{corr}, f, \text{fayalite}}$ and $\Delta H_{T_r, P_r}^{\text{err}}$. These last two equations, when satisfied exactly and coupled with those already mentioned define an under-determined least squares problem involving 20 equations and 27 unknowns. After each least squares calibration of the solution model we determined a solution to this under-determined system using the computer code LSEQIEQ (Ghiorso 1983) and adjusted the enthalpies of formation accordingly:

$$\Delta H_{T_r, P_r}^{f, \text{new}} = \Delta H_{T_r, P_r}^{f, \text{old}} + \Delta H_{T_r, P_r}^{\text{corr}, f}$$

The process of model calibration with subsequent adjustment of enthalpies of formation was repeated until the average residual for each solid component (ΔH_M^{err}) remained unchanged (and in all cases was less than 100 cal). The adjusted enthalpies of formation reported in Tables (A2-1) and (A2-3) reflect this condition. It is encouraging to note that the majority of these adjustments (column labeled Δ) are within the indicated two standard deviation reported uncertainty. Exceptions probably reflect inappropriate experimental data or activity/composition relations for the solids.

Appendix 3. Modifications for hydrous liquids

In modelling activity/composition relations in hydrous liquids we have entertained the possibility that H_2O does not behave as a regular solution component (as there is no experimental evidence to suggest this). We must therefore modify Eq. (8) to have the form

$$G^{(\text{liquid})} = \sum_{i=1}^n \mu_i^0 n_i + NRT \sum_{i=1}^n X_i \ln X_i + N/2 \sum_{i=1}^n \sum_{j=1}^n W_{ij} X_i X_j + Nf(X_w) \quad (\text{A3-1})$$

where $f(X_w)$ is some, yet to be specified, function of the mole fraction of H_2O (X_w) and represents the potential departure of hydrous liquids from strictly regular solutions. From Eqs. (A3-1), (2), (3) and (4) it follows that

$$G^{\text{excess}} = N/2 \sum_{i=1}^n \sum_{j=1}^n W_{ij} X_i X_j + Nf(X_w) \quad (\text{A3-2})$$

Differentiation of Eq. (A3-2) with respect to the number of moles of water in solution generates an equation for the partial molar excess free energy ($RT \ln \gamma_w$) of water dissolved in a silicate liquid (where $W_{\text{H}_2\text{O}, i}$ is written W_{wi}):

$$RT \ln \gamma_w = \left(\frac{\partial G^{\text{excess}}}{\partial n_w} \right)_{T, P, \text{other } n_i} = \sum_{i=1}^n W_{wi} X_i - \frac{1}{2} \sum_{i=1}^n \sum_{j=1}^n W_{ij} X_i X_j + N \left(\frac{\partial f(X_w)}{\partial n_w} \right)_{T, P, \text{other } n_i} + f(X_w) \quad (\text{A3-3})$$

If we let

$$C' = \exp \left[\sum_{i=1}^n W_{wi} X_i - \frac{1}{2} \sum_{i=1}^n \sum_{j=1}^n W_{ij} X_i X_j \right] / RT \quad (\text{A3-4})$$

then

$$\gamma_w = C' \exp \left[N \left(\frac{\partial f(X_w)}{\partial n_w} \right)_{T, P, \text{other } n_i} + f(X_w) \right] / RT \quad (\text{A3-5})$$

Finally we have

$$a_w = \gamma_w X_w \quad (\text{A3-6})$$

The solubility data of Hamilton et al. (1964) has suggested to many authors that at low water contents the activity of water is best represented by

$$a_w = C'' X_w^2 \quad (\text{A3-7})$$

where we have C'' as a constant slope, thus:

$$\gamma_w = C'' X_w \quad (\text{A3-8})$$

At higher water contents, however, it appears that C'' is a slowly varying function of water mole fraction. Nicholls (1980) has developed equations similar to (A3-1) through (A3-8) and proceeded to describe water solubility in magmas by defining a C'' in terms of regular solution theory and *anhydrous* bulk rock composition. This has met with considerable success in reproducing the solubility measurements of water in several silicate melts (Nicholls 1980, Table 2). Recently Stolper (1982a and b) has pointed out that the dissociation of H_2O into hydroxyl groups in silicate liquids, a structural model which is consistent with Eq. (A3-7), does not accurately describe water solubility at high total water contents, and thus it follows that C'' itself in Eq. (A3-7) should be some function of X_w . Though it would be preferable to speciate dissolved water between molecular and hydroxyl units as Stolper suggests, in lieu of a more complete hydrous liquid database we have adopted the not inconsistent formulation that the C'' of Eq. (A3-7) be described by regular solution theory which *includes* component interaction terms for water (i.e. finite W_{wi} 's) and allows C'' to be a function of X_w . Departing now from the approach of Nicholls (1980) and combining Eqs. (A3-5) and (A3-7):

$$C'' X_w = C' \exp \left\{ \left[N \left(\frac{\partial f(X_w)}{\partial n_w} \right)_{T, P, \text{other } n_i} + f(X_w) \right] / RT \right\} \quad (\text{A3-9})$$

We now let $C'' = C' C'''$ where C''' is an arbitrary constant or at most a function only of X_w , and Eq. (A3-9) becomes

$$RT \ln X_w C''' = N \left(\frac{\partial f(X_w)}{\partial n_w} \right)_{T, P, \text{other } n_i} + f(X_w) = \left(\frac{\partial Nf(X_w)}{\partial n_w} \right)_{T, P, \text{other } n_i} \quad (\text{A3-10})$$

Thus:

$$Nf(X_w) = RT \int_0^{n_w} \ln X_w dn_w + RT \int_0^{n_w} \ln C''' dn_w \quad \text{at constant } T, P, n_j \neq n_w \quad (\text{A3-11})$$

The first integral in Eq. (A3-11) can be readily evaluated to yield:

$$\begin{aligned} Nf(X_w) &= RT[n_w \ln n_w - n_w - N \ln N + N \\ &\quad + (N - n_w) \ln(N - n_w) - (N - n_w)] \\ &\quad + RT \int_0^{n_w} \ln C''' dn_w \end{aligned}$$

or

$$\begin{aligned} f(X_w) &= RT[X_w \ln X_w + (1 - X_w) \ln(1 - X_w)] \\ &\quad + RT/N \int_0^{n_w} \ln C''' dn_w. \end{aligned} \quad (\text{A3-12})$$

Substituting Eq. (A3-12) into Eq. (A3-3) we have for the partial molar excess free energy of water in a hydrous silicate melt:

$$\begin{aligned} RT \ln \gamma_w &= \sum_{i=1}^n W_{wi} X_i - \frac{1}{2} \sum_{i=1}^n \sum_{j=1}^n W_{ij} X_i X_j \\ &\quad + RT \ln C''' X_w. \end{aligned} \quad (\text{A3-13})$$

Differentiation of Eq. (A3-2), with Eq. (A3-12) substituted in for $f(X_w)$, with respect to n_k (where $k \neq w$) yields the partial molar excess free energy for an anhydrous component in a hydrous liquid (to be compared with Eq. 10):

$$\begin{aligned} RT \ln a_k &= RT \ln X_k + RT \ln \gamma_k, \\ RT \ln \gamma_k &= \sum_{i=1}^n W_{ki} X_i - \frac{1}{2} \sum_{i=1}^n \sum_{j=1}^n W_{ij} X_i X_j \\ &\quad + RT \ln(1 - X_w) - RT/N^2 \int_0^{n_w} \ln C''' dn_w \\ &\quad + RT/N \left(\frac{\partial}{\partial n_k} \left[\int_0^{n_w} \ln C''' dn_w \right] \right)_{T,P,n_j \neq n_w}. \end{aligned} \quad (\text{A3-14})$$

For our purposes we have chosen to set C''' equal to unity, and hence for hydrous liquids the relevant activity composition relations are:

$$RT \ln \gamma_w = \sum_{i=1}^n W_{wi} X_i - \frac{1}{2} \sum_{i=1}^n \sum_{j=1}^n W_{ij} X_i X_j + RT \ln X_w \quad (\text{A3-15})$$

and

$$\begin{aligned} RT \ln \gamma_k &= \sum_{i=1}^n W_{ki} X_i - \frac{1}{2} \sum_{i=1}^n \sum_{j=1}^n W_{ij} X_i X_j \\ &\quad + RT \ln(1 - X_w). \end{aligned} \quad (\text{A3-16})$$

In order to compute hydrous-liquid/solid phase stability or water solubility using Eq. (17) we need additional thermodynamic data not provided in Appendix 2 on the standard state properties of water. The chemical potential of the supercritical fluid at the temperatures and pressures of interest were computed from data in Robie et al. (1978) using the interpolation equations of Nicholls (1980). Similarly, the pressure dependence of the chemical potential of dissolved H_2O has been obtained from Nicholls (1980, Eq. 13). The paucity of available data does not warrant a more elaborate treatment than do adopt an expression of the form

$$(A/T + B) \cdot RT = \mu_{1 \text{ bar}, T}^0 \quad (\text{A3-17})$$

to describe the 1 bar temperature dependence of the standard state chemical potential of dissolved H_2O (Nicholls 1980). The best value for B extracted from the water solubility data by Nicholls (1980) is 18.3527. We have adopted this number

but determined independently a value for A (essentially the average enthalpy term) as part of the hydrous interaction parameter calibration procedure (see Appendix 4), to allow for greater flexibility in fitting the data. Our value of $-38,304.7$ is just outside of two standard deviations of Nicholls's $-34,345.9$.

Equations (A3-15) and (A3-16) encapsulate our descriptions of activity/composition relations in hydrous silicate liquids.

Appendix 4. Construction of the regression equations and the estimation of the binary interaction parameters

From the considerations detailed above and the experimental database it is a straight forward matter to construct the quantities found on the left hand side of Eq. (17). Let us label this quantity using the scalar variable b . The chemical reactions corresponding to Eq. (17) for the various liquid/solid equilibria considered in this study are provided in Table A4-1. We have also indicated in Table A4-1 the coefficients (v_i 's in Eq. 17) which proceed the mole fractions and interaction parameters on the right hand side of Eq. (17). In addition, the sum of the v_i 's is provided for each solid/liquid equilibria. With the coefficients of Table A4-1 Eq. (17) can be written for any solid/liquid equilibria with only the W_{ij} 's remaining as unknowns. To see how these W_{ij} 's can be best approximated from the database we must restate Eq. (17) with our definition for b

$$b = \sum_{i=1}^n v_i \sum_{j=1}^n W_{ij} X_j - \frac{1}{2} \sum_{i=1}^n v_i \sum_{j=1}^n \sum_{k=1}^n W_{jk} X_j X_k \quad (17')$$

into vector notation. Let X^T define a row vector of mole fractions of length n (i.e. $X^T = [X_1 X_2 X_3 \dots X_n]$), the T means transpose, that is X without the T is a vertical or column vector), δ_i^T defines a row vector of n -zero entries except for the i th place which contains a one (i.e. $\delta_2^T = [0 \ 1 \ 0 \ 0 \dots 0]$, with n entries) and let W define a symmetric matrix of interaction parameters:

$$W = \begin{bmatrix} W_{11} & W_{12} & W_{13} & \dots & W_{1n} \\ W_{21} & W_{22} & W_{23} & \dots & W_{2n} \\ \vdots & \vdots & \vdots & \ddots & \vdots \\ \vdots & \vdots & \vdots & \ddots & \vdots \\ W_{n1} & W_{n2} & W_{n3} & \dots & W_{nn} \end{bmatrix} \quad (\text{A4-1})$$

where as before $W_{ij} = W_{ji}$, and $W_{ii} = 0$. With these definitions Eq. (17') can be written

$$b = \sum_{i=1}^n v_i \delta_i^T W X - \sum_{i=1}^n v_i \frac{1}{2} X^T W X \quad (\text{A4-2})$$

where it should be appreciated that we are dealing with mixed scalar (v_i), vector (δ_i , X), matrix (W) multiplication. For convenience we will define the vector

$$V^T = \sum_{i=1}^n v_i \delta_i^T \quad (\text{A4-3})$$

and the scalar

$$v = \sum_{i=1}^n v_i$$

to write Eq. (A4-2) in the form

$$b = V^T W X - \frac{1}{2} v X^T W X$$

or

$$b = (V^T - v/2 X^T) W X. \quad (\text{A4-4})$$

Table A4-1. Coefficients for the liquid/solid equilibria

<i>l</i>	Reaction	Si_4O_8	Ti_4O_8	$\text{Al}_{16/3}\text{O}_8$	$\text{Fe}_{16/3}\text{O}_8$	$\text{Fe}_4\text{Si}_2\text{O}_8$	$\text{Mn}_4\text{Si}_2\text{O}_8$	$\text{Mg}_4\text{Si}_2\text{O}_8$	$\text{Ca}_4\text{Si}_2\text{O}_8$	$\text{Na}_{16/3}\text{Si}_8/3\text{O}_8$	$\text{K}_{16/3}\text{Si}_8/3\text{O}_8$	H_2O	$-\sum_k \nu_{lk}$
Clinopyroxene													
CATS	$\text{CaAl}_2\text{SiO}_6 = 1/4\text{Ca}_4\text{Si}_4\text{O}_8 + 3/8\text{Al}_{16/3}\text{O}_8 + 1/8\text{Si}_4\text{O}_8$	0.125		0.375					0.25				-0.75
Diopside	$\text{CaMgSi}_2\text{O}_6 = 1/4\text{Ca}_4\text{Si}_4\text{O}_8 + 1/4\text{Mg}_4\text{Si}_2\text{O}_8 + 1/4\text{Si}_4\text{O}_8$	0.25						0.25	0.25				-0.75
Hedenbergite	$\text{CaFeSi}_2\text{O}_6 = 1/4\text{Ca}_4\text{Si}_4\text{O}_8 + 1/4\text{Fe}_4\text{Si}_2\text{O}_8 + 1/4\text{Si}_4\text{O}_8$	0.25				0.25			0.25				-0.75
Jaderte	$\text{NaAlSi}_2\text{O}_6 = 3/16\text{Na}_{16/3}\text{Si}_8/3\text{O}_8 + 3/16\text{Al}_{16/3}\text{O}_8 + 3/8\text{Si}_4\text{O}_8$	0.375		0.1875						0.1875			-0.75
Wollastonite	$\text{CaSiO}_3 = 1/4\text{Ca}_4\text{Si}_4\text{O}_8 + 1/8\text{Si}_4\text{O}_8$	0.125							0.25				-0.375
Feldspar													
Albite	$\text{NaAlSi}_3\text{O}_8 = 3/16\text{Na}_{16/3}\text{Si}_8/3\text{O}_8 + 3/16\text{Al}_{16/3}\text{O}_8 + 5/8\text{Si}_4\text{O}_8$	0.625		0.1875					0.25	0.1875			-1.00
Anorthite	$\text{CaAl}_2\text{Si}_2\text{O}_8 = 1/4\text{Ca}_4\text{Si}_4\text{O}_8 + 3/8\text{Al}_{16/3}\text{O}_8 + 3/8\text{Si}_4\text{O}_8$	0.375		0.375					0.25				-1.00
Sandine	$\text{KAlSi}_3\text{O}_8 = 3/16\text{K}_{16/3}\text{Si}_8/3\text{O}_8 + 3/16\text{Al}_{16/3}\text{O}_8 + 5/8\text{Si}_4\text{O}_8$	0.625		0.1875							0.1875		-1.00
Feldspathoids													
Kalsilite	$\text{KAlSiO}_4 = 3/16\text{K}_{16/3}\text{Si}_8/3\text{O}_8 + 3/16\text{Al}_{16/3}\text{O}_8 + 1/8\text{Si}_4\text{O}_8$	0.125		0.1875							0.1875		-0.50
Leucite	$\text{KAlSi}_2\text{O}_6 = 3/16\text{K}_{16/3}\text{Si}_8/3\text{O}_8 + 3/16\text{Al}_{16/3}\text{O}_8 + 3/8\text{Si}_4\text{O}_8$	0.375		0.1875							0.1875		-0.75
Nepheline	$\text{NaAlSi}_3\text{O}_8 = 3/16\text{Na}_{16/3}\text{Si}_8/3\text{O}_8 + 3/16\text{Al}_{16/3}\text{O}_8 + 1/8\text{Si}_4\text{O}_8$	0.125		0.1875						0.1875			-0.50
Meltilite													
Akermanite	$\text{Ca}_2\text{MgSi}_2\text{O}_7 = 1/2\text{Ca}_4\text{Si}_4\text{O}_8 + 1/4\text{Mg}_4\text{Si}_2\text{O}_8 + 1/8\text{Si}_4\text{O}_8$	0.125		0.375				0.25	0.5				-0.875
Gehlenite	$\text{Ca}_2\text{Al}_2\text{SiO}_7 = 1/2\text{Ca}_4\text{Si}_4\text{O}_8 + 3/8\text{Al}_{16/3}\text{O}_8$	0.125		0.375				0.25	0.5				-0.875
Olivine													
Fayalite	$\text{Fe}_2\text{SiO}_4 = 1/2\text{Fe}_4\text{Si}_2\text{O}_8$					0.5							-0.5
Forsterite	$\text{Mg}_2\text{SiO}_4 = 1/2\text{Mg}_4\text{Si}_2\text{O}_8$						0.5						-0.5
Tephroite	$\text{Mn}_2\text{SiO}_4 = 1/2\text{Mn}_4\text{Si}_2\text{O}_8$							0.5					-0.5
Orthopyroxene													
Enstatite	$\text{MgSiO}_3 = 1/4\text{Mg}_4\text{Si}_2\text{O}_8 + 1/8\text{Si}_4\text{O}_8$	0.125						0.25					-0.375
Ferrosilite	$\text{FeSiO}_3 = 1/4\text{Fe}_4\text{Si}_2\text{O}_8 + 1/8\text{Si}_4\text{O}_8$	0.125				0.25							-0.375
Perovskite	$\text{CaTiO}_3 + 1/8\text{Si}_4\text{O}_8 = 1/4\text{Ca}_4\text{Si}_2\text{O}_8 + 1/4\text{Ti}_4\text{O}_8$	-0.125	0.25						0.25				-0.375
β -Quartz	$\text{SiO}_2 = 1/4\text{Si}_4\text{O}_8$	0.25											-0.25
Rhombohedral oxide													
Hematite	$\text{Fe}_2\text{O}_3 = 3/8\text{Fe}_{16/3}\text{O}_8$				0.375								-0.375
Ilmenite	$\text{FeTiO}_3 + 1/8\text{Si}_4\text{O}_8 = 1/4\text{Fe}_4\text{Si}_2\text{O}_8 + 1/4\text{Ti}_4\text{O}_8$	-0.125	0.25			0.25							-0.375
Gieckelite	$\text{MgTiO}_3 + 1/8\text{Si}_4\text{O}_8 = 1/4\text{Mg}_4\text{Si}_2\text{O}_8 + 1/4\text{Ti}_4\text{O}_8$	-0.125	0.25					0.25					-0.375
Spinel													
Magnetite	$\text{Fe}_3\text{O}_4 + 1/8\text{Si}_4\text{O}_8 = 1/4\text{Fe}_4\text{Si}_2\text{O}_8 + 3/8\text{Fe}_{16/3}\text{O}_8$	-0.125		0.375	0.25								-0.50
Spinel	$\text{MgAl}_2\text{O}_4 + 1/8\text{Si}_4\text{O}_8 = 1/4\text{Mg}_4\text{Si}_2\text{O}_8 + 3/8\text{Al}_{16/3}\text{O}_8$	-0.125		0.175				0.25					-0.50
Ulvospinel	$\text{Fe}_2\text{TiO}_4 + 1/4\text{Si}_4\text{O}_8 = 1/2\text{Fe}_4\text{Si}_2\text{O}_8 + 1/4\text{Ti}_4\text{O}_8$	-0.25	0.25		0.5								-0.50
Dt-Mg utanate	$\text{Mg}_7\text{TiO}_4 + 1/4\text{Si}_4\text{O}_8 = 1/2\text{Mg}_4\text{Si}_2\text{O}_8 + 1/4\text{Ti}_4\text{O}_8$	-0.25	0.25					0.5					-0.50
Herynyite	$\text{FeAl}_2\text{O}_4 + 1/4\text{Si}_4\text{O}_8 = 1/4\text{Fe}_4\text{Si}_2\text{O}_8 + 3/8\text{Al}_{16/3}\text{O}_8$	-0.125		0.375		0.25							-0.50

Let *l* range over all phase/component equilibrium pairs, and *k*, *i*, *j* over all *n* components. Thus (in general)

$$\sum_k \nu_{lk} \left(\sum_{i=1}^n W_{li} X_i - \frac{1}{2} \sum_{i=1}^n \sum_{j=1}^n W_{ij} X_i X_j \right) = -RT \ln \left(\prod_k (1 - X_{\text{H}_2\text{O}})^{\nu_{lk}} \right) + RT \ln K - RT \ln \left(\prod_k X_k^{\nu_{lk}} \right) + RT \ln (a_l^{\text{sil}})$$

Now the unknowns in Eq. (A4-4) are the elements of the matrix W . If these are to be approximated using some conventional technique like least squares, we must first arrange the elements of W into a vector.¹² To see this we employ matrix algebraic techniques which are discussed at length in Graham (1981). We define an operator $\text{vec}(\)$ which makes a matrix into a vector:

$$\text{vec}(W) = \begin{bmatrix} W_{11} \\ W_{21} \\ \vdots \\ W_{n1} \\ W_{12} \\ W_{22} \\ \vdots \\ W_{n2} \\ \vdots \\ W_{1n} \\ W_{2n} \\ \vdots \\ W_{nn} \end{bmatrix}$$

by stacking up the columns from left to right. In addition we will use the direct product operator¹³, \otimes , and an identity from Graham (1981) [$\text{vec}(PQR) = (R \otimes P) \text{vec}(Q)$] to operate on Eq. (A4-4):

$$\begin{aligned} \text{vec}(b) &= \text{vec}[(V^T - v/2X^T)WX] \\ b &= [X^T \otimes (V^T - v/2X^T)] \text{vec}(W) \end{aligned}$$

or simplifying

$$b = (X^T \otimes V^T - v/2X^T \otimes X^T) \text{vec}(W). \quad (\text{A4-5})$$

Equation (A4-5) is in a proper form for least squares. Notice that the dimensions of the matrices $X^T \otimes X^T$ and $X^T \otimes V^T$ are 1 by n^2 and the length of the vector $\text{vec}(W)$ is n^2 . Each solid/liquid equilibria yields one statement of Eq. (A4-5). In the experimental database defined above, let there be p such equilibria. The p statements of Eq. (A4-5) can be assembled, stacked one on top of each other, as:

$$\begin{aligned} b_1 &= (X_1^T \otimes V_1^T - v_1/2X_1^T \otimes X_1^T) \text{vec}(W) \\ b_2 &= (X_2^T \otimes V_2^T - v_2/2X_2^T \otimes X_2^T) \text{vec}(W) \\ &\vdots \\ b_p &= (X_p^T \otimes V_p^T - v_p/2X_p^T \otimes X_p^T) \text{vec}(W). \end{aligned} \quad (\text{A4-6})$$

If B denotes the p -vector of b_i 's and Γ the p by n^2 matrix of coefficients preceding the elements of $\text{vec}(W)$, then Eq. (A4-6) may be written:

- 12 In conventional least squares equations of the form $AX = B$ are solved, where X is a vector of unknown coefficients, B is a dependent variable vector, and A is a matrix of independent variables, one row of which corresponds to each observation
- 13 Consider two arbitrary matrices A and B . For convenience let

$$A = \begin{bmatrix} a_{11} & a_{12} \\ a_{21} & a_{22} \end{bmatrix} \quad \text{and} \quad B = \begin{bmatrix} b_{11} & b_{12} \\ b_{21} & b_{22} \end{bmatrix} \quad \text{then}$$

$$A \otimes B = \begin{bmatrix} a_{11}b_{11} & a_{11}b_{12} & a_{12}b_{11} & a_{12}b_{12} \\ a_{11}b_{21} & a_{11}b_{22} & a_{12}b_{21} & a_{12}b_{22} \\ a_{21}b_{11} & a_{21}b_{12} & a_{22}b_{11} & a_{22}b_{12} \\ a_{21}b_{21} & a_{21}b_{22} & a_{22}b_{21} & a_{22}b_{22} \end{bmatrix}$$

$$B = \Gamma \text{vec}(W). \quad (\text{A4-7})$$

This least squares problem, subject to the constraints $W_{ij} = W_{ji}$ and $W_{ii} = 0$ is the basis upon which the binary interaction parameters are calibrated from the experimental/thermodynamic database. The solution of Eq. (A4-7) for $\text{vec}(W)$ could not be effected using conventional least squares techniques and necessitated the development of new computer software (Ghiorso 1983) whose numerical algorithms are rooted in generalized inverse theory (Lawson and Hanson 1974). In order to appreciate why this is so we first must comment upon data uncertainties and their effect on the numerical stability of the matrix Γ .

Several constituents of the experimental liquids vary so slightly in their abundances between samples or so infrequently have non-zero abundances that we have opted not to include interaction parameters involving them in the model. These components were treated as ideal diluents and will be referred to as inactive. They are designated as the unstarred components of Table 4. Of the active component set, H_2O occurs so infrequently in the database that the anhydrous and hydrous interaction parameters were calibrated separately. Under these conditions no solid/anhydrous-liquid pair was seen to control the solution excess terms of $\text{Fe}_{1.6/3}\text{O}_8$ or $\text{Mn}_4\text{Si}_2\text{O}_8$. The latter component, though generally of finite concentration, varies but little in abundance throughout the dataset, while the former unfortunately assumes small values that are generally uncertain by the amount present. This fact can be easily demonstrated by propagating uncertainties through the equations of Sack et al. (1981). A general error propagation analysis was undertaken and the results indicate that the average uncertainty in the elements of the matrix Γ is on the order of 1-5% (with the exception of ferric iron, which is much larger). These stem largely from analytical uncertainties in composition (determined by electron microprobe). Uncertainties in the vector B arise from 1) the thermodynamic data of Appendix 2, 2) the activity/composition relations of Appendix 1, and 3) the analytical uncertainties in determining the compositions of both liquids and solids. Error analysis reveals that the major source of uncertainty lies in enthalpy values for both the liquid and solid. We have attempted to eliminate the latter by generating an internally consistent set of solid enthalpy of formation data for the phases concerned. The details are presented in Appendix 2. Uncertainties in the enthalpies of the liquid components are a consequence of imprecisely known enthalpies of fusion. Fortunately, however, large inconsistencies amongst the adopted enthalpies of fusion translate linearly into the interaction parameters. Computer experiment has shown that the shape of the free energy of mixing surface is distorted to account for these inconsistencies. Some of the difficulties with the surface shape (i.e. immiscibility) which are discussed in the text probably stem from this source of uncertainty. Values for the enthalpies of fusion cannot be extracted from the database however, since large variations in their magnitude do not substantially alter the quality of the fit. Another source of uncertainty in B arises when the poorly known concentrations of trace constituents are used to define activities of end-member components and hence statements of Eqs. (17) or (A4-5). To alleviate this difficulty we have adopted a set of exclusion criteria that rejects a solid/liquid equilibria from contributing to Eq. (A4-7) if the concentration of any element defining the end-member component's activity for that solid phase drops below a certain tolerance. These tolerances are provided in Table A4-2. These carefully chosen exclusion criteria limited the compositional uncertainties inherent in the elements of the vector B .

In a least squares problem uncertainties in data can translate into erroneous and wildly unstable values for the coefficients of the solution vector. These effects can be minimized if some provision is made in computing the least

Table A4-2. Wt% concentration for exclusion (<constraints)

Forsterite	MgO <1
Fayalite	FeO <1
Albite	Na ₂ O <1
Anorthite	CaO <1
Sanidine	K ₂ O <1
Enstatite	MgO <1
Ferrosilite	FeO <1
Diopside	MgO <1
Hedenbergite	FeO <1
Leucite	none
Akermanite	MgO <1
Spinel	MgO <1 or Al ₂ O ₃ <5
Hercynite	FeO <1 or Al ₂ O ₃ <5
Ulvospinel	FeO <1/2 or TiO ₂ <3
Di-Mg Titanate	MgO <1/2 or TiO ₂ <3
Ilmenite	none
Geikielite	MgO <2
Quartz	none

squares solution that recognizes the cause of this instability. This in fact ends up being an attempt to extract the "true" number of independent variables the problem contains. This number is referred to as the pseudorank of the least squares problem. One either states the answer in the reduced number of variables, thereby offering a solution in fewer variables than the proposed model, or by determining the linear dependencies amongst the variables, computes a solution vector whose coefficients are linearly related. The former approach has given rise to the technique of stepwise regression and was used by Ghiorso and Carmichael (1980) to solve their least squares problem and extract values of the W_{ij} . Because, in stepwise regression, there is little control on the order of the coefficients extracted, dubious numerical significance may be placed upon interaction parameters which have little compositional significance. We believe this underlies the failure of the Ghiorso and Carmichael (1980) equations to adequately express the details of liquid immiscibility and solid/liquid equilibria amongst phases other than olivine and plagioclase. The failure lies, as one might suspect, in extrapolating the shape of the free energy surface and defining its derivatives into compositional volumes outside the database. For these reasons, in the present treatment, we have utilized the computer code LSEQIEQ (Ghiorso 1983) to extract a pseudorank based upon data uncertainty and solve Eq. (A4-5) in a least squares sense (subject to $W_{ij}=W_{ji}$ and $W_{ii}=0$) to generate a complete set of interaction parameters which exhibit linear dependencies. Assuming a 1% uncertainty in the elements of F a pseudorank of 26 was determined (26 of the interaction parameters are truly independent) at the 1% level and the 45

linearly dependent anhydrous coefficients of Table A4-3 were extracted from the anhydrous database. Before discussing the quality of the anhydrous data fit we will justify the problem pseudorank on more theoretical grounds.

The solution to the least squares problem suggested by Eq. (A4-7), namely finding numerical values for the coefficients of $\text{vec}(W)$ such that the norm of the vector $B - \Gamma \text{vec}(W)$ is minimized is given by:

$$\Gamma^T B = \Gamma^T \Gamma \text{vec}(W)$$

subject to

$$W_{ij} = W_{ji} \quad \text{and} \quad W_{ii} = 0.$$

The pseudorank, or number of linearly independent interaction parameters, is identical to the minimum of the number of linearly independent rows or columns of the n^2 by n^2 square matrix $\Gamma^T \Gamma$. The matrix $\Gamma^T \Gamma$ can be written as:

$$\Gamma^T \Gamma = \sum_{i=1}^p [(X_i \otimes V_i - v_i/2 X_i \otimes X_i) \cdot (X_i^T \otimes V_i^T - v_i/2 X_i^T \otimes X_i^T)]$$

which reduces to

$$\Gamma^T \Gamma = \sum_{i=1}^p X_i X_i^T \otimes [(V_i - v_i/2 X_i)(V_i^T - v_i/2 X_i^T)]. \quad (\text{A4-8})$$

Now the number of independent rows/columns in the inner product n by n matrix $X_i X_i^T$ cannot be greater than 1, i.e. just the number that exist in the vector X . The same can be said for the inner product matrix $(V_i - v_i/2 X_i)(V_i^T - v_i/2 X_i^T)$. Thus the direct product

$$X_i X_i^T \otimes [(V_i - v_i/2 X_i)(V_i^T - v_i/2 X_i^T)]$$

though a matrix of dimensions n^2 by n^2 possesses no more than one independent row/column. Clearly then, the number of independent rows/columns in $\Gamma^T \Gamma$ can be no greater than the minimum value of p or n^2 . As there are far more experiments than variables the pseudorank can at most be n^2 . With the equality constraints ($W_{ij}=W_{ji}$, $W_{ii}=0$) it is easy to show that this reduces to the product $n(n-1)/2$. The number of "active" components (Table 4) is ten and the maximum possible pseudorank is 45.

Now suppose the experimental results used to calibrate the W_{ij} 's of Eq. (A4-5) were sufficiently similar to be identical within analytical uncertainty, i.e. suppose 1,000 experiments were performed on the same liquid at the same T , P and f_{O_2} , all crystallizing one phase, say olivine. Then the pseudorank of $\Gamma^T \Gamma$ would be one. One variable, and only one variable,

Table A4-3. Regression Coefficients (W_{ij})

	Si ₄ O ₈	Ti ₄ O ₈	Al _{16/3} O ₈	Fe _{16/3} O ₈	Fe ₄ Si ₂ O ₈	Mn ₄ Si ₂ O ₈	Mg ₄ Si ₂ O ₈	Ca ₄ Si ₂ O ₈	Na _{16/3} Si _{8/3} O ₈	K _{16/3} Si _{8/3} O ₈
Si ₄ O ₈										
Ti ₄ O ₈	-29364.5									
Al _{16/3} O ₈	-78563.2	-67349.7								
Fe _{16/3} O ₈	2637.93	-6821.82	1240.32							
Fe ₄ Si ₂ O ₈	-9630.14	-4594.59	-59528.6	4524.46						
Mn ₄ Si ₂ O ₈	5525.36	-2043.20	-1917.75	212.196	-703.340					
Mg ₄ Si ₂ O ₈	-30353.6	12673.6	-48674.8	-1277.03	-57925.8	-2810.10				
Ca ₄ Si ₂ O ₈	-64068.1	-102442	-98428.3	1519.81	-59355.5	699.123	-78924.5			
Na _{16/3} Si _{8/3} O ₈	-73758.3	-101074	-135615	-3717.38	-36966.2	780.150	-92611.4	-62779.9		
K _{16/3} Si _{8/3} O ₈	-87596.4	-40700.7	-175326	283.726	-84579.5	-60.7241	-45162.9	-27908.0	-18129.7	
H ₂ O	-411.866	-196.101	-71216.2	-103024	7930.96	309.614	-20259.7	-38502.1	-49213.2	-23295.7

Standard state enthalpy of dissolved H₂O: -76121.4. Units are calories

Table A4-4. Regression Statistics

<i>Anhydrous (step 1)</i> (45 variables, 1160 cases)				<i>Hydrous (step 2)</i> (11 variables, 80 cases)			
A) Unbounded ANOVA (full rank)				A) Unbounded ANOVA (full rank)			
	Sum of Squares	Degrees of Freedom	F	Sum of Squares	Degrees of Freedom	F	
regression	3.11693×10^{11}	45	25177	1.39604×10^{11}	11	19790	
residuals	3.06473×10^8	1114		4.36089×10^7	68		
Multiple correlation coefficient: 0.99951				Multiple correlation coefficient: 0.99984			
Residual norm: 17506.4; Standard error: 525				Residual norm: 6603.70; Standard error: 738			
Absolute value of the minimum tolerance used for inclusion: 0.0375 (1% of $\ A\ $)				Absolute value of the minimum tolerance used for inclusion: 0.0242 (0.5% of $\ A\ $)			
Pseudorank: 26; Residual norm: 7315.2				Pseudorank: 10; Residual norm: 2453.8			
B) Unbounded Anova (rank deficient)				B) Unbounded Anova (rank deficient)			
	Sum of Squares	Degrees of Freedom	F	Sum of squares	Degrees of Freedom	F	
regression	3.11639×10^{11}	26	37724	1.39598×10^{11}	10	19408	
residuals	3.59986×10^8	1133		4.96300×10^7	69		
Multiple correlation coefficient: 0.99884				Multiple correlation coefficient: 0.99964			
Residual norm: 18973.3; Standard error: 557				Residual norm: 7044.9; Standard error: 788			
No Equality constraints				45 equality constraints (anhydrous coefficients)			
All variables bounded within the inclusive range -500,000 to 500,000 cal.				All variables bounded within the inclusive range -500,000 to 500,000 cal.			
Residual norm due to bounding: 0.0				Residual norm due to bounding: 0.0			
C) Bounded Anova (rank deficient) {see B above}				C) Bounded Anova (rank deficient) {see B above}			

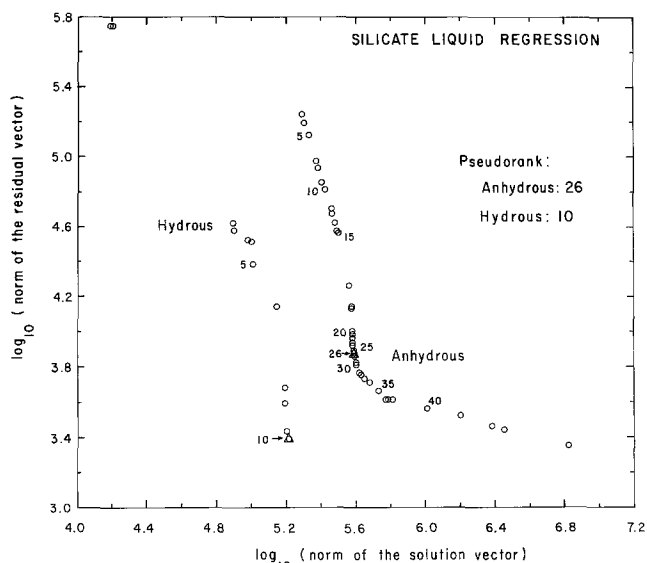


Fig. A4-1. Rank deficiency displayed by the least squares problem defined by Eq. (A4-7). The intermittently labeled points correspond to the number of orthogonal axes used in the construction of the solution vector. The optimal number (the effective pseudorank) is chosen such that the residual and solution vector norms are simultaneously minimized, thus satisfying the objective of least squares while simultaneously insuring parameter stability with respect to minor perturbations in the database. A pseudorank of 26 (triangle) was chosen for the anhydrous database and a pseudorank of 10 was selected for the hydrous database. A physical explanation for this rank deficiency is suggested in the text

would describe the database. Though this is an extreme example, it emphasizes the need to utilize experimental data on widely different liquid compositions involving diverse solid phases. We do not believe our deficient pseudorank results substantially from this experimental multiplicity.

Instead let us consider the case where not all the compositional variables (elements of X) are linearly independent. Let's label this number m , and note that $m \leq n$. Then from Eq. (A4-8) with each inner product now possessing no more than m independent terms, the pseudorank of $\Gamma^T \Gamma$ becomes at most m^2 , and with $W_{ij} = W_{ji}$ and $W_{ii} = 0$, $m(m-1)/2$. We have already discussed the large uncertainties associated with the ferric iron component concentrations and the relatively constant and unconstrained values for the manganese component. Both components were left in the active set because of strong potential for interaction with the other components in the liquid, yet they probably should not be treated as "truly" independent compositional variables when uncertainties are taken into account. Removing them, m becomes 8, and the predicted pseudorank of $\Gamma^T \Gamma$ becomes 28. This is in excellent agreement with that derived using the program of Ghiorso (1983) and assuming a 1% data uncertainty. The whole problem is best visualized in Fig. A4-1. Here we have plotted the norm of the residual vector (the square root of the sum of the squares of the actual values of b , Eq. (A4-4), minus the predicted ones using the least squares estimates of the interaction parameters) against the norm of the solution vector (the square root of the sum of the squares of the unique elements of $\text{vec}(W)$) as a function of proposed pseudorank. The object of such a diagram is to demonstrate the appropriate problem pseudorank such that the residual norm is minimized without making the solution vector norm too large (Lawson and Hanson 1974). This insures that the interaction parameters remain within bounds and are not subject to wild fluctuations with minor changes in the database. The best choice for the anhydrous database is clearly somewhere around a pseudorank of 28 as was suggested above. By assuming a 1% uncertainty in the elements of Γ we have achieved an optimal least squares solution to Eq. (A4-5) which should ensure numerical stability when the model is extrapolated throughout the compositional range of natural liquids.

Table A4-4 displays statistics necessary to evaluate the quality of the overall anhydrous data fit. The high multiple correlation coefficient and total F substantiate the validity of

the mathematical model for the free energy of mixing (Eq. 7). The standard error in predicting the value of b in Eq. (A4-4) is 587 cal and is equivalent to the calculated uncertainties in b (largely from the $RT\ln K$ contribution) due to the thermodynamic database. The regular solution model therefore fits the anhydrous experimental database to within the accuracy of measurement.

Table A4-4 also lists statistics pertaining to regression of the "hydrous" database. In constructing Eq. (A4-5) for hydrous liquids, terms like $RT\ln X_w$ and $RT\ln(1 - X_w)$ (cf. Eqs. (A3-15) and (A3-16)) were added to the dependent variable, b (Eq. A4-5), and the regression carried out fixing the anhydrous interaction parameters to the values shown in Table A4-3. By simultaneously extracting an enthalpy for dissolved H_2O , this became an eleven variable problem for which there were 80 experimental results. Using the software of Ghiorso (1983), a pseudorank of 10 was determined. This is demonstrated on Fig. A4-1 where the hydrous point that corresponds to a pseudorank of eleven would plot off scale to the right, but would insignificantly lower the residual norm. The hydrous interaction parameters so derived are provided in Table A4-3. The standard error of 788 cal given in Table A4-4 is due largely to the solid/liquid data and not the water solubility measurements. It is still small and of the order of magnitude of the uncertainties in the contributing thermodynamic data.

Acknowledgements. This paper benefited greatly due to a provoking discussion with J.B. Thompson and a thorough review by B. Wood. We are indebted to numerous people who have contributed much by way of experimental data, stimulating discussion and critical insight. In particular we would like to thank T. Grove, J. Stebbins, E. Stolper and D. Walker. W. Bryan and T. Grove generously allowed the use of their experimental results prior to publication. F. Bardsley assisted in the drafting of the figures and L. Criscenti assisted in typing the manuscript. This research was funded by grants from NSF (EAR 78-03642 and EAR 81-03344 to Carmichael) and by the Office of Energy Research, Office of Basic Energy Sciences, Division of Engineering, Mathematics and Geosciences, of the US Department of Energy, under contract W-7405-ENG-48. Computer time at the University of Washington was kindly provided by the College of Arts and Sciences.

References

- Adamkovicova K, Kosa L, Proks I (1980) The heat of fusion of calcium silicate. *Inst Inorg Chem, Slovak Acad Sci Silikaty (Prague)* 24:193-201
- Anderson DJ, Lindsley DH (1981) A valid Margules formulation for an asymmetric ternary solution: revision of the olivine-ilmenite thermometer, with applications. *Geochim Cosmochim Acta* 45:847-854
- Barron LM (1972) Thermodynamic multicomponent silicate equilibrium phase calculations. *Am Mineral* 57:809-823
- Barron, L.M. (1978) The geometry of multicomponent exsolution. *Am J Sci* 278:1269-1306
- Barron LM (1981) The calculated geometry of silicate liquid immiscibility. *Geochim Cosmochim Acta* 45:495-512
- Bender JF, Hodges FN, Bence AE (1978) Petrogenesis of basalts from the project FAMOUS area: experimental study from 0 to 15 kbars. *Earth Planet Sci Lett* 41:277-302
- Beswick AE, Carmichael ISE (1978) Constraints on Mantle source compositions imposed by phosphorus and the rare-earth elements. *Contrib Mineral Petrol* 67:317-330
- Birch, F. (1966) Compressibility; elastic constants. In: *Handbook of Physical Constants* (SP Clark Jr, ed). *Geol Soc Am Mem* 97:97-173
- Bottinga Y, Richet P (1978) Thermodynamics of liquid silicates; a preliminary report. *Earth Planet Sci Lett* 40:382-400
- Bottinga Y, Weill DF, Richet P (1981) Thermodynamic modeling of silicate melts. In: *Thermodynamics of Minerals and Melts* (RC Newton, A Navrotsky, BJ Wood, eds) pp 207-245 New York: Springer-Verlag
- Bowen NL (1913) The melting phenomena of the plagioclase feldspars. *Am J Sci*, 4th series 40:161-185
- Bowen NL, Schairer JF (1935) The system, MgO-FeO-SiO₂. *Am J Sci* 29:151-217
- Bowen NL, Schairer JF, Posnjak E (1933) The system CaO-FeO-SiO₂. *Am Jour Sci* 26:193-284
- Brown FH (1971) Volcanic petrology of Recent volcanic rocks in the Lake Rudolf region, Kenya. Unpublished Ph. D. thesis, University of California, Berkeley
- Brown FH, Carmichael ISE (1969) The Quaternary volcanoes of the Lake Rudolf region: I. The basanite-tephrite series of the Korath Range. *Lithos* 2:239-260
- Brown FH, Carmichael ISE (1971) The Quaternary volcanoes of the Lake Rudolf region: II. The lavas of North Island, South Island, and the Barrier. *Lithos* 4:305-323
- Burnham CW (1974) NaAlSi₃O₈-H₂O solutions: a thermodynamic model for hydrous magmas. *Bull Soc Fr Mineral Cristallogr* 97:223-230
- Burnham CW (1975a) Water and magmas; a mixing model. *Geochim Cosmochim Acta* 39:1077-1084
- Burnham CW (1975b) Thermodynamics of melting in experimental silicate-volatile systems. *Fortschr Miner* 52:101-118
- Burnham CW (1979) The importance of volatile constituents. In: *The Evolution of the Igneous Rocks - Fiftieth Anniversary Perspectives* (HS Yoder, Jr, ed) pp 439-482 New Jersey: Princeton University Press
- Burnham CW (1981) The nature of multicomponent aluminosilicate melts. In: *Chemistry and Geochemistry of Solutions at High Temperatures and Pressures* (DT Rickard, FE Wickman, eds). *Phys Chem Earth* 13/14:197-229
- Burnham CW, Jahns RH (1962) A method for determining the solubility of water in silicate liquids. *Am J Sci* 260:721-745
- Carmichael ISE (1960) The pyroxenes and olivines from some Tertiary acid glasses. *J Petrol* 1:309-336
- Carmichael ISE (1962) Pantelleritic liquids and their phenocrysts. *Mineral Mag* 33:86-113
- Carmichael ISE (1964) The petrology of Thingmuli, a Tertiary volcano in eastern Iceland. *J Petrol* 5:435-460
- Carmichael ISE (1967a) The iron-titanium oxides of silicic volcanic rocks and their associated ferromagnesian silicates. *Contrib Mineral Petrol* 14:36-64
- Carmichael ISE (1967b) The mineralogy of Thingmuli, a Tertiary volcano in Eastern Iceland. *Am Mineral* 52:1815-1841
- Carmichael ISE, Ghiorso MS (in prep) Intensive variables in siliceous magmas.
- Carmichael ISE, Nicholls J, Spera FJ, Wood BJ, Nelson SA (1977) High-temperature properties of silicate liquids: applications to the equilibration and ascent of basic magma. *Phil Trans R Soc Lond A* 286:373-431
- Carstens H (1979) Liquid immiscibility in basic alkaline magmas. *Chem Geol* 27:297-307
- Charlu TV, Newton RC, Kleppa OJ (1981) Thermochemistry of synthetic Ca₂Al₂SiO₇ (gehlenite) - Ca₂MgSi₂O₇ (akermanite) melilites. *Geochim Cosmochim Acta* 45:1609-1617
- Chase MW Jr, Curnutt JL, McDonald RA, Syverud AN (1978) JANAF Thermochemical Tables, 1978 Supplement. *J Phys Chem Ref Data* 7:793-940
- Chase MW, Curnutt JL, Prophet H, McDonald RA, Syverud AN (1975) JANAF Thermochemical Tables, 1975 Supplement. *J Phys Chem Ref Data* 4:1-175
- Chase MW, Curnutt JL, Hu AT, Prophet H, Syverud AN, Walker LC (1974) JANAF Thermochemical Tables, 1974 Supplement. *J Phys Chem Ref Data* 3:311-480
- Clark SP (1966) High Pressure Phase Equilibria. In: *Handbook of Physical Constants* (SP Clark Jr, ed.). *Geol Soc Am Mem* 97:345-370
- Drake MJ (1972) The distribution of major and trace elements

- between plagioclase feldspar and magmatic silicate liquid: an experimental study. Unpublished Ph. D. thesis, University of Oregon
- Eggler DH (1972) Water saturated and undersaturated melting relations in a Paricutin andesite and an estimate of water content in the natural magma. *Contrib Mineral Petrol* 34:261–271
- Flanigan FJ, Kazdan JL (1971) *Calculus Two: Linear and Nonlinear Functions*, pp 443. New Jersey: Prentice-Hall, Inc.
- French WJ (1971) The correlation between “Anhydrous” Crystallization temperatures and rock composition. *Contrib Mineral Petrol* 31:154–158
- French WJ, Cameron EP (1981) Calculation of the temperatures of crystallization of silicates from basaltic melts. *Mineral Mag* 44:19–26
- Gaskell DR (1982) The densities and structures of silicate melts. In: *Advances in Physical Geochemistry* (Vol. II) (S.K. Saxena, ed) pp 153–171 New York: Springer-Verlag
- Ghiorso MS (1983) LSEQIEQ: A FORTRAN IV subroutine package for the analysis of multiple linear regression problems with possibly deficient pseudorank and linear equality and inequality constraints. *Computers and Geosciences* 9:391–416
- Ghiorso MS, Carmichael ISE (1980) A regular solution model for met-aluminous silicate liquids: Applications to geothermometry, immiscibility, and the source regions of basic magma. *Contrib Mineral Petrol* 71:323–342
- Ghiorso MS, Carmichael ISE Density calculations for silicate liquids. I. Revised method for aluminosilicate compositions by Bottinga, Weill, and Richet: A commentary, *Geochim Cosmochim Acta* (submitted)
- Ghiorso MS, Carmichael ISE, Moret LK (1979) Inverted high-temperature quartz. Unit cell parameters and properties of the α - β inversion. *Contrib Mineral Petrol* 68:307–323
- Gill PE, Murray W (eds) (1974) *Numerical methods for constrained optimization*, pp 283. New York: Academic Press Inc.
- Graham A (1981) *Kronecker Products and Matrix Calculus with Applications*, pp 130. New York: John Wiley and Sons
- Green DH, Hiberson WO, Jaques AL (1979) Petrogenesis of mid-ocean ridge basalts. In: *The Earth: Its Origin, Structure and Evolution* (MW McElhinny ed.) Acad Press
- Grove TL, Bryan WB (1983) Fractionation of pyroxene-phyric MORB at low pressures: An experimental study. *Contrib Mineral Petrol* (in press)
- Grove TL, Gerlach DC, Sando TW (1982) Origin of calc-alkaline series lavas at Medicine Lake volcano by fractionation, assimilation and mixing. *Contrib Mineral Petrol* 80:160–182
- Hamilton DL, Burnham CW, Osborn EF (1964) The solubility of water and effects of oxygen fugacity and water content on crystallization in mafic magmas. *J Petrol* 5:21–39
- Helgeson HC, Delaney JM, Nesbitt HW, Bird DK (1978) Summary and critique of the thermodynamic properties of rock-forming minerals. *Am J Sci* 278–229
- Helz RT (1973) Phase relations of basalts in their melting range at $P_{\text{H}_2\text{O}} = 5$ kbar as a function of oxygen fugacity. Part I. Mafic Phases. *J Petrol* 14:249–302
- Henry DJ, Navrotsky A, Zimmerman HD (1982) Thermodynamics of plagioclase melt equilibria in the system albite-anorthite-diopside. *Geochim Cosmochim Acta* 46:381–391
- Hess PC (1971) Polymer model of silicate melts. *Geochim Cosmochim Acta* 35:289–306
- Hess PC (1980) Polymerization model for silicate melts. In: *Physics of Magmatic Processes* (RB Hargraves, ed) pp 3–48 Princeton, New Jersey: Princeton Univ Press
- Hildreth EW (1977) The magma chamber of the Bishop Tuff: gradients in temperature, pressure, and composition. Unpublished Ph. D. thesis, University of California, Berkeley
- Hill WL, Faust GT, Reynolds DS (1944) The binary system $\text{P}_2\text{O}_5 - 2 \text{CaO} \cdot \text{P}_2\text{O}_5$. *Am J Sci*, 242 (part I), 457–477
- Hon R, Henry DJ, Navrotsky A, Weill DF (1981) A thermochemical calculation of the pyroxene saturation surface in the system diopside-albite-anorthite. *Geochim Cosmochim Acta* 45:157–161
- Hostetler CJ, Drake MJ (1980) Predicting major element mineral/melt equilibria: A statistical approach. *J Geophys Res* 85:3789–3796
- Kelley KK (1960) Contributions to the data on theoretical metallurgy: part 13, High temperature heat content, heat capacity and entropy data for the elements and inorganic compounds. *US Bur Mines Bull* 584, pp 232
- Kerrick DM, Darken LS (1975) Statistical thermodynamic models for ideal oxide and silicate solid solutions, with applications to plagioclase. *Geochim Cosmochim Acta* 39:1431–1442
- Khitarov NI, Kadik AA (1973) Water and carbon dioxide in magmatic melts and peculiarities of the melting process. *Contrib Mineral Petrol* 41:205–215
- Khitarov NI, Lebedev EB, Regartan EV, Arseneva RV (1959) Solubility of water in basaltic and granitic melts. *Geochemistry* 5:479–492
- King EG, Orr RL, Bonnicksen KR (1954) Low temperature heat capacity, entropy at 298.16° K and high temperature heat content of sphene (CaTiSiO_5). *J Am Chem* 76:4320–4321
- Kosa L, Adamkovicova K, Proks I (1981) Determining the heat of incongruent decomposition of merwinite. *Inst Inorg Chem, Slovak Acad Sci, Silikaty* (Prague) 25(3):199–208
- Lawson CL, Hanson RJ (1974) *Solving Least Squares Problems*, pp 340. New Jersey: Prentice-Hall Inc.
- Leeman WP (1974) Experimental determination of partitioning of divalent cations between olivine and basaltic liquid. Part II. Unpublished Ph. D. thesis, University of Oregon
- Longhi J, Walker D, Hays JF (1978) The distribution of Fe and Mg between olivine and lunar basaltic liquid. *Geochim Cosmochim Acta* 42:1545–1558
- Luhr JF, Carmichael ISE (1980) The Colima Volcanic Complex, Mexico. I. Post-Caldera andesites from Volcán Colima. *Contrib Mineral Petrol* 71:343–372
- Mahood GA (1981) Chemical evolution of a Pleistocene rhyolitic center: Sierra La Primavera, Jalisco, Mexico. *Contrib Mineral Petrol* 77:129–149
- Masson CR (1968) Ionic equilibria in liquid silicates. *J Am Ceram Soc*, 51:134–143
- Meijering JL (1950) Segregation in regular ternary solutions. Part I. *Philips Res Rep* 5:333–356
- Meijering JL (1951) Segregation in regular ternary solutions. Part II. *Philips Res Rep* 6:183–210
- Meyer HOA, Boyd FR (1972) Composition and origin of crystalline inclusions in natural diamonds. *Geochim Cosmochim Acta* 36:1255–1273
- Mo X, Carmichael ISE, Rivers M, Stebbins J (1982) The partial molar volume of Fe_2O_3 in multicomponent silicate liquids and the pressure dependence of oxygen fugacity in magmas. *Mineral Mag* 45:237–245
- Morse SA (1980) *Basalts and Phase Diagrams*, pp 493. Heidelberg: Springer-Verlag
- Mukherjee A, Bhattacharya A (1980) High-pressure silicate liquidus data: Retrieval of partial molar enthalpy and partial molar entropy of mixing, a test of the regular solution formulation, and comments on the P–T modelling of ascending magmas. *Earth Planet Sci Lett* 49:231–236
- Mysen BO, Kushiro I (1977) Compositional variations of coexisting phases with degree of melting of peridotite in the upper mantle. *Am Mineral* 62:843–856
- Mysen BO, Virgo D, Seifert FA (1982) The structure of silicate melts: Implications for chemical and physical properties of natural magma. *Rev Geophys and Space Phys* 20:353–383
- Nelson SA, Carmichael ISE (1979) Partial molar volumes of oxide components in silicate liquids. *Contrib Mineral Petrol* 71:117–124
- Nesbitt HW, Fleet ME (1981) An ion-association model for $\text{PbO} - \text{SiO}_2$ melts: Interpretation of thermochemical, conductivity, and density data. *Geochim Cosmochim Acta* 45:235–244
- Newton KC (1976) Thermochemistry of garnets and aluminous pyroxenes in the CMAS system. In: *Thermodynamics in Geology* (DC Fraser, ed), pp 29–56. Holland: D Reidel 1976

- Newton RC, Charlu TV, Kleppa OJ (1980) Thermochemistry of the high structural state plagioclases. *Geochim Cosmochim Acta* 44:933–941
- Nicholls J (1976) The activities of components in natural silicate melts. In: *Thermodynamics in Geology* (DC Fraser, ed), pp 327–348. Holland: D Reidel
- Nicholls J (1980) A simple thermodynamic model for estimating the solubility of H₂O in magmas. *Contrib Mineral Petrol* 74:211–220
- Nicholls J, Carmichael ISE (1972) The equilibrium temperature and pressure of various lava types with spinel- and garnet-peridotite. *Am Mineral* 57:941–959
- Nisbet EG, Bickle MJ, Martin A (1977) The mafic and ultramafic lavas of the Belingwe Greenstone Belt, Rhodesia. *J Petrol* 18:521–566
- Orr RL (1953) High temperature heat contents of magnesium orthosilicate and ferrous orthosilicate. *J Am Chem Soc* 75:528–529
- Oxtoby S, Hamilton DL Calculation of the solubility of water in granitic melts. In: *Progress in Experimental Petrology* (W.S. Mackenzie ed) Natural Environment Research Council, Great Britain, 4th Progress Report, 37–40
- Parlett BN (1980) The Symmetric Eigenvalue Problem, pp 348. New Jersey: Prentice-Hall, Inc
- Philpotts AR (1976) Silicate liquid immiscibility: its probable extent and petrogenetic significance. *Am J Sci* 276:1147–1177
- Philpotts AR (1979) Silicate liquid immiscibility in tholeiitic basalts. *J Petrol* 20:99–118
- Philpotts AR (1982) Compositions of immiscible liquids in volcanic rocks. *Contrib Mineral Petrol* 80:201–218
- Pitzer KS (1981) Characteristics of very concentrated aqueous solutions. In: *Chemistry and Geochemistry of solutions at High Temperatures and Pressures* (Rickard DT, Wickman FE, eds) *Phys Chem Earth* 13/14:249–272
- Rammensee W, Fraser DG (1982) Determination of activities in silicate melts by Knudsen cell mass spectrometry – I. The system NaAlSi₃O₈–KAlSi₃O₈. *Geochim Cosmochim Acta* 46:2269–2278
- Reed MH (1982) Calculation of multicomponent chemical equilibria and reaction processes in systems involving minerals, gases and an aqueous phase. *Geochim Cosmochim Acta* 46:513–528
- Rivers ML, Ghiorsio MS (1980) Free energy minimization in multicomponent systems: Applications to silicate liquid immiscibility. *GSA Abstr with Progr* 12: no. 7, 511
- Robie RA, Hemingway BS, Fisher JR (1978) Thermodynamic properties of minerals and related substances at 298.15 K and 1 bar (10⁵ Pascals) pressure and at higher temperatures. *US Geol Surv Bull* 1452:pp 456
- Roedder E (1979) Silicate liquid immiscibility in magmas. In: *The Evolution of the Igneous Rocks-Fiftieth Anniversary Perspectives* (Yoder HS, ed), pp 15–58. New Jersey: Princeton University Press
- Roeder PL (1974) Activity of iron and olivine solubility in basaltic liquids. *Earth Planet Sci Lett* 23:397–410
- Sack RO (1980) Some constraints on the thermodynamic mixing properties of Fe–Mg orthopyroxenes and olivines. *Contrib Mineral Petrol* 71:257–269
- Sack RO (1982a) Spinels as petrogenetic indicators: activity-composition relations at low pressures. *Contrib Mineral Petrol* 79:169–186
- Sack RO (1982b) Fe²⁺–Mg²⁺ and TiAl₂–MgSi₂ exchange rate between clinopyroxenes and silicate melts. *GSA Abstr with Progr* 14: no. 7, 606
- Sack RO, Carmichael ISE, Rivers M, Ghiorsio MS (1981) Ferric-ferrous equilibria in natural silicate liquids at 1 bar. *Contrib Mineral Petrol* 75:369–376
- Skinner BJ (1966) Thermal Expansion. In: *Handbook of Physical Constants* (Clark SP, ed) *Geol Soc Am Mem* 97:75–96
- Smith MP (1983) A feldspar-liquid geothermometer. *Geophys Res Lett* 10:193–195
- Stebbins JF, Carmichael ISE (1981a) Heats of fusion of diopside and sanidine and high pressure volume changes in aluminous silicate liquids. *GSA Abstr with Progr* 13: no 7, 560
- Stebbins JF, Carmichael ISE (1981b) The heat of fusion of fayalite: assessment of oxidation in calorimetric measurements. *EOS*, 62: no. 45, 1070
- Stebbins JF, Carmichael ISE, Weill DF (1980) High temperature heat contents, heat capacities, and solution properties of plagioclase composition liquids. *GSA Abstr with Progr* 12, no. 7, 528
- Stolper E (1980) A phase diagram for mid-ocean ridge basalts: Preliminary results and implications for petrogenesis. *Contrib Mineral Petrol* 74:13–27
- Stolper E (1982a) Water in silicate glasses: an infrared spectroscopic study. *Contrib Mineral Petrol* 81:1–17
- Stolper E (1982b) On the speciation of water in silicate melts. *Geochim Cosmochim Acta* 46:2609–2620
- Stull DR, Prophet H (1971) JANAF Thermochemical Tables, 2nd ed. *Nat Stand Ref Data Ser, Nat Bur Stand (US)*, 37: pp.1141
- Takahashi E (1978) Partitioning of Ni²⁺, Co²⁺, Fe²⁺, Mn²⁺, and Mg²⁺ between olivine and silicate melts: compositional dependence of partition coefficient. *Geochim Cosmochim Acta* 42:1829–1844
- Takahashi E (1980) Melting relations of an alkali-olivine basalt to 30 kbars, and their bearing on the origin of alkali basalt magmas. *Carnegie Inst Wash Ann Yearb* 79:271–276
- Thompson RN (1974) Primary basalts and magma genesis I. *Contrib Mineral Petrol* 45:317–341
- Thompson RN (1975) Primary basalts and magma genesis II. *Contrib Mineral Petrol* 52:213–232
- Toop GW, Samis CS (1962) Activities of ions in silicate melts. *Trans Metall Soc AIME*, 224:878–887
- Visser W, Koster van Groos AF (1979) Effects of P₂O₅ and TiO₂ on liquid-liquid equilibria in the system K₂O–FeO–Al₂O₃–SiO₂. *Am J Sci* 279:970–988
- Walker D, Mullins O Jr (1981) Surface tension of natural silicate melts from 1,200°–1,500° C and implications for melt structure. *Contrib Mineral Petrol* 76:455–462
- Walker D, Shibata T, Delong SE (1979) Abyssal tholeiites from the oceanographer fracture zone. II. Phase equilibria and mixing. *Contrib Mineral Petrol* 70:111–125
- Weill DF, Hon R, Navrotsky A (1980a) The igneous system CaMgSi₂O₆–CaAl₂Si₂O₈–NaAlSi₃O₈: variations on a classic theme by Bowen. In: *Physics of Magmatic Processes* (RB Hargraves, ed), pp 49–92. New Jersey: Princeton University Press
- Weill DF, Stebbins JF, Hon R, Carmichael ISE (1980b) The enthalpy of fusion of anorthite. *Contrib. Mineral. Petrol.* 74, 95–102
- Wood BJ (1976) Experimental determination of mixing properties of solid solutions with particular reference to garnet and clinopyroxene solutions. In: *Thermodynamics in Geology*, (Fraser DC, ed), pp 11–28. Holland: D Reidel
- Wood BJ, Kleppa OJ (1981) Thermochemistry of forsterite-fayalite olivine solutions. *Geochim Cosmochim Acta* 45:529–534
- Wood MI, Hess PC (1980) The structural role of Al₂O₃ and TiO₂ in immiscible liquids in the system SiO₂–MgO–CaO–FeO–TiO₂–Al₂O₃. *Contrib Mineral Petrol* 72:319–328

Received November 2, 1982; Accepted June 16, 1983